





**Aquaculture** 

Aquaculture 270 (2007) 249-258

www.elsevier.com/locate/aqua-online

## Classification of differentiating oocytes during ovarian cycle in the giant freshwater prawn, *Macrobrachium rosenbergii* de man

Prasert Meeratana a,\*, Prasert Sobhon b

<sup>a</sup> Department of Medical Sciences, Faculty of Science, Burapha University, Chonburi, 20131, Thailand
 <sup>b</sup> Department of Anatomy, Faculty of Science, Mahidol University, Rama 6 Rd., Bangkok, 10400, Thailand

Received 9 August 2006; received in revised form 1 March 2007; accepted 7 March 2007

#### Abstract

Based on the light microscopic observations of cells' sizes, chromatin patterns, amount of lipid droplets and yolk granules, the female germ cells could be classified into four different phases, which include 1) oogonia (Oog), 2) primary oocytes (pOc), 3) secondary oocytes (sOc), and 4) mature oocyte (mOc). Oog are small oval-shaped cells with irregular-shaped nuclei sizing 4–6 μm in diameter. They rest on the connective tissue germinal cord at the tip of each ovarian pouch (lobule). Oogonia increase their number through mitotic division, and the daughter cells move into ovarian pouch where they undergo first meiotic division to become primary oocytes, which have various steps of 1st meiotic prophase accumulating at the innermost zone of the ovarian pouch. The primary oocytes are small oval-shaped cells (8.5–10 μm in diameter) with large nuclei containing chromatin in various states of condensation that finally transform into chromatids. Their nuclei are surrounded by thin rim of faint blue-stained cytoplasm. The secondary oocytes derived from 2nd meiosis and comprise five steps: Oc1 and Oc2, classified as previtellogenic oocytes, Oc3 and Oc4, classified as vitellogenic oocytes, and mature oocyte (mOc) The zones of ovarian pouch are defined based on the accumulation of various steps of developing oocytes, namely, oogenic, previtellogenic, vitellogenic and mature zones, respectively. The ovarian cycle is divided into five stages based on the number and types of oocytes present in each stage. Stage 0 and I are spawn and spent stages. Stage II and III are proliferative and premature stages, while stage IV is mature stage. During ovarian stage I, each ovarian pouch contains primarily oogonia, primary oocytes, Oc1 and a few Oc2. In stage II, the pouch contains mainly Oc2 and Oc3, while in stage III the predominant cells are Oc4. Mature oocytes appear synchronously, in stage IV. The ovulating mature oocytes pass through the thin disrupted wall of ovarian pouch into subcapsular space, that leads into the oviduct situated on the ventro-lateral side of the ovarian lobe. At spawning, the ovarian pouches break down and only connective sheaths and hemolymph sinuses remain. The germinal cords and islets of oogonia remain in the central area of stage 0 ovary. The ovarian capsule, including the muscular layer, becomes attenuated as the ovary progresses from stage 0 to IV. The hemolymph vessels become highly convoluted in the central area of the ovary, and they branch radially into smaller hemolymph sinuses around each oogenic pouch. © 2007 Elsevier B.V. All rights reserved.

Keywords: Differentiating oocytes; Ovarian pouch; Ovarian cycle; Macrobrachium rosenbergii

E-mail address: g3936465@yahoo.com (P. Meeratana).

### 1. Introduction

The gonads of female crustaceans undergo a sequence of morphological transformation during each reproductive cycle. Such changes exhibit a number and classes of oocytes that are undergoing various steps of cellular differentiation. The cycle of ovarian and oocyte

<sup>\*</sup> Corresponding author. Tel.: +66 2 745900x3167; fax: +66 2

development in Macrobrachium rosenbergii have been studied by a few groups of investigators (O'Donovan et al., 1984; Charniaux-Cotton, 1985; Chang and Shih, 1995). In 1984, O'Donovan et al. divided the developing ovary of M. rosenbergii during intermolt period into six stages based on timing of embryogenesis, premating molt and oviposition, while the developing oocytes were divided into five stages based on size, yolk accumulation and follicular cell stage. The steps of oogenesis were also classified according to the accumulation of a yolk protein, vitellogenin, into previtellogenic and vitellogenic stages (Charniaux-Cotton, 1985). Recently, Chang and Shih (1995) classified five stages of ovarian cycle according to the changes in gross morphology and coloration as observed through the carapace, in correlation with oocytes' diameters. However, detailed classification and variation in oocyte numbers and steps remaining in each stage of the ovarian cycle are still not clearly defined. In the present study we attempted to identify all steps of differentiating oocytes and their accumulation pattern in various stages of each ovarian cycle.

### 2. Materials and methods

### 2.1. Experimental animals

Adult females, M. rosenbergii, weighing 35–40 gm were obtained from a commercial farm in Panasnikom district of Chonburi province, Thailand. The stages of ovarian development were determined by visual observation through the carapace as ordinarily used in hatcheries (O'Donovan et al., 1984; Charniaux-Cotton, 1985; Chang and Shih, 1995). The animals were kept in in-door concrete tanks, each with 1.5 m in diameter and 1 m in height, containing 0.80 m water with adequate aeration, and 20% of water volume changed daily. The prawns were acclimated under the light-dark cycle of 12:12 for two weeks before the experiment. The water temperature was maintained at 27-28 °C. Commercial prawn feed was provided daily at 3% of the body weight. To allow mating, blue-claw males were stocked in the same tank at the ratio of 1 male to 5 females. The prawns were anesthetized by placing on ice and the ovaries were dissected out and cut into small blocks about 1 mm<sup>3</sup> size. They were immediately washed in isotonic physiological saline (IPS) (Meeratana et al., 2006), and fixed in Davidson's fixative for 72 h.

### 2.2. Tissue preparation for histological observation

The ovarian tissue blocks were dehydrated through a series of increasing concentrations of ethanol, cleared in xylene, infiltrated with liquid paraffin at 58 °C, and finally embedded in paraffin blocks. The blocks were trimmed and sectioned at  $5-7~\mu m$  thick and stained with Harris' Hematoxylin and counter-stained with Eosin (H&E stain). Periodic Acid Schiff (PAS) was also used to stain ovarian sections for determining the presence of carbohydrate components in the ovarian structures and oocytes. Mallory stain was used to outline the connective tissue scaffolds.

### 3. Results

### 3.1. Histology of the developing ovary and oviduct

The ovary of the mature giant freshwater prawn has two lobes situated underneath the carapace dorsal to the hepatopancreas and ventral to the heart. Histologically, the developing ovary is invested by ovarian capsule made of fibromuscular tissue. Parts of the capsule extended as sheet-like structures into the interior of the ovary. These sheets divide the ovarian tissue of each lobe into cone-shaped ovarian pouches or lobules, each containing various steps of oocytes according to the stages of ovarian development. The core of each ovarian lobe contains the main convoluted hemolymph vessel surrounded by connective and muscular tissues. This hemolymph vessel branches radially into hemolymph sinuses, which pass into trabeculae to form a network around each pouch, and finally drained into the subcapsular hemolymph sinus (Fig. 1A–C).

The oviduct is a delicate translucent fibromuscular sac continuing from the ovarian capsule on ventrolateral side of each ovarian lobe (Fig. 1D). Its luminal surface is lined by a simple cuboidal epithelium resting on the basement membrane (Fig. 1E). The cuboidal epithelial cells possess prominent spherical nuclei with granular heterochromatin, which are centrally located. Proximally, the lining of the oviduct is thickened as it becomes stratified cuboidal epithelium, which is also folded. Numerous long fibrillar network of mucin-like coating appears on the surface of apical epithelial cells (Fig. 1F). Transitions to low cuboidal and squamous type epithelium occur gradually towards the distal part of the oviduct (Fig. 1G). Connective tissue and smooth muscle lie underneath the basement membrane of the epithelium.

Within 48 h after spawning, the ovarian tissue appears loose, and contains large subcapsular space and dilated hemolymph sinuses. The germinal cords holding germinal cells appear in the central area of the ovary (Fig. 2A, B). Islets of new clones of growing oocytes are

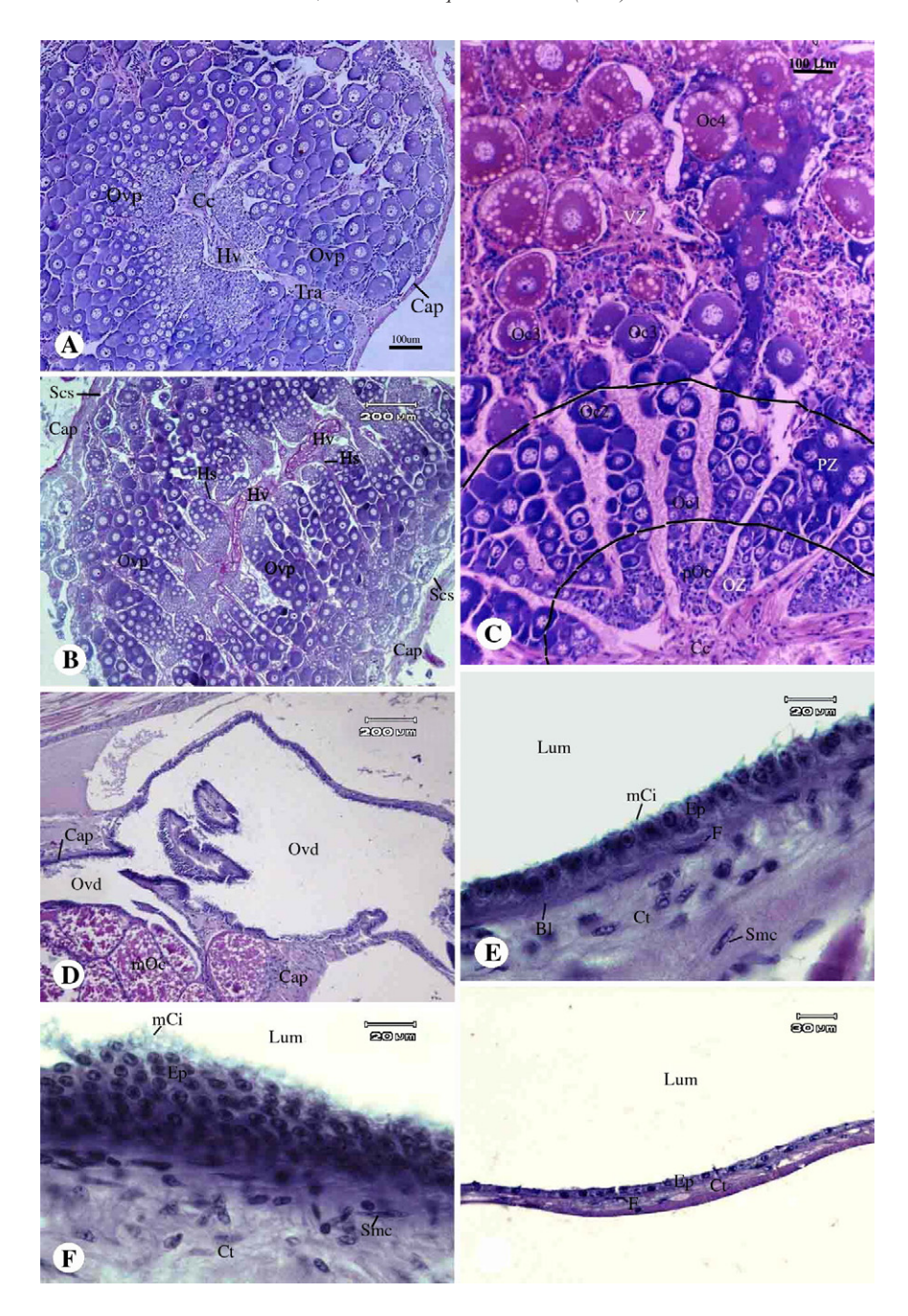


Fig. 1. Light micrographs of paraffin sections stained with PAS, showing the general histology of giant freshwater prawn ovary. A, B. Cross and longitudinal sections of stage II ovaries, showing fibromuscular ovarian capsule (Cap), trabeculae (Tra), ovarian pouches (Ovp), central ovarian core (Cg), hemolymph vessel (Hv), hemolymph sinuses (Hs), and subcapsular space (Scs). C. Cross section of stage III ovary: oogenic zone (OZ) containing primary oocytes (pOc), previtellogenic zone (PZ) containing previtellogenic oocytes (Oc1, Oc2), vitellogenic zone (VZ) containing vitellogenic oocytes (Oc3, Oc4). D. The fully mature ovary in premating broodstock showing oviduct (Ovd) and fibromuscular ovarian capsule (Cap). E. The proximal and middle parts of oviductal wall are lined by simple cuboidal epithelium. Bl—basal lamina, Ct—loose connective tissue, Smc—smooth muscle cells, Ep—epithelium, mCi —Mucin-like coating, Lum—luminal surface. F. Tangential section of the epithelial lining of the proximal part of oviduct showing accumulation of mucin-like coating (mCi) on the luminal surface. The epithelial cells possess a prominent central spherical nuclei with granular heterochromatin. Ct—loose connective tissue, Smc—smooth muscle cells, Ep—epithelium, mc—mucin-like coating, Lum—luminal surface. G. Transition of epithelial lining from simple cuboidal to simple squamous on the distal part of the oviduct.

clearly visible among the germinal cords. Based on the number and steps of differentiating oocytes the growing ovarian pouches can be divided into four zones: oogenic, previtellogenic, vitellogenic and mature zones. The oogenic zone is the inner most region facing the central ovarian core. This zone contains dividing oogonia and primary oocytes, which predominate in ovarian stage I (Fig. 2C). The previtellogenic zone is located next to the oogenic zone and contains previtellogenic secondary oocytes (Oc1 and Oc2). This zone predominates in the ovarian stage II (Fig. 1A, B, D). The vitellogenic zone is located in peripheral area of the

ovary and contains vitellogenic secondary oocytes (Oc3 and Oc4). This zone predominates in stage III ovary (Figs. 1C, 2E). In ovarian stage IV, the maturation zone contains fully mature oocytes (mOc) which are distinguished by deep acidophilic (reddish) stain, and the zone expands throughout the ovarian tissue of mature ovary (Fig. 2F).

The follicular cells are classified into two types. Type I follicular cells (Fc1) exhibits ellipsoid shape, and surround Oc2, Oc3 and Oc4. They become more elongated and flattened around the mOc stage, and exhibit prominent spindle-shaped nuclei with deeply

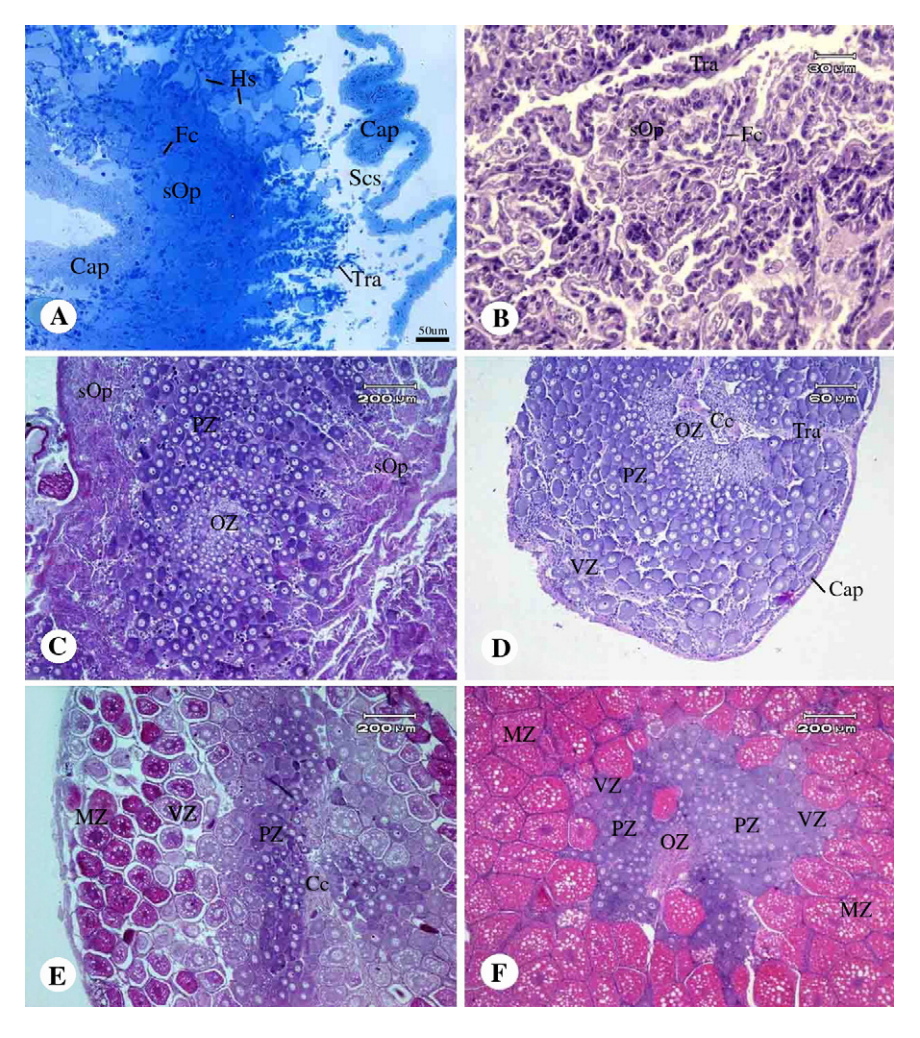


Fig. 2. Light micrographs of semithin section stained with toludine blue (A) and paraffin sections stained with H&E (B–F), showing different ovarian stages. A, B. The ovary following spawn (stage 0): Ovp—ovarian pouch, sOp—spent ovarian pouch, Scs—subcapsular space, Hs—hemolymph sinus, Tra—trabeculae, Fc—follicular cells, Cap—fibromuscular ovarian capsule. Stage I (spent) at 2 days after spawning: Oz—oogenic zone, Pz—previtellogenic zone, sOp—spent ovarian pouch. Stage II (proliferation) ovary: The oocytes in this ovarian stage advance to early vitellogenic oocytes(Oc3). This stage occurs about one week following spent period. Cap—fibromuscular ovarian capsule. Stage III (premature) ovary containing mainly Oc4. Cc—central ovarian core, PZ—previtellogenic zone, VZ—vitellogenic zone, MZ—mature zone. F. The ovarian stage IV (mature) is mostly occupied by the fully mature oocytes appearing in deep eosinophilia in the maturation zone (MZ). Islets of primary and previtellogenic oocytes still remain in the central ovarian core (Cc). This stage of ovary usually occurs at 3 to 8 weeks after spawn period.

stained chromatin. Fc1 adhere closely to oocytes' surface (Fig. 3E). Type II follicular cells (Fc2) first appear during Oc2 step. They exhibit less change in shape and size from Oc2 to Oc4 steps. Fc2 have lighter stained and more ovoid nuclei, and they form an outer layer next to Fc1 (Figs. 3E, F, 4D–F). They proliferate and aggregate in the spaces between oocytes during Oc3 and Oc4 steps. During the mOc step, the nuclei of both types of follicular cells are quite similar. However, the Fc1 nucleus is more flattened into spindle shape and the Fc2 nucleoplasm becomes darker.

### 3.2. Steps of differentiating oocytes

### 3.2.1. Oogonia (Oog)

The Oog are located in the germinal epithelium that lies along the trabeculae and connective tissue scaffold. The Oog is an ovoid cell that contains an irregularly shaped nucleus (4–6  $\mu$ m in diameter) with deep bluestained heterochromatin. It is notable that the nucleolus is not noticeable in this stage (Fig. 3A–C), while the cytoplasm is stained faint blue with H&E. Oog are frequently seen in groups, each with 2–4 cells in a row at the tip of the ovarian pouch. The Oog are dividing

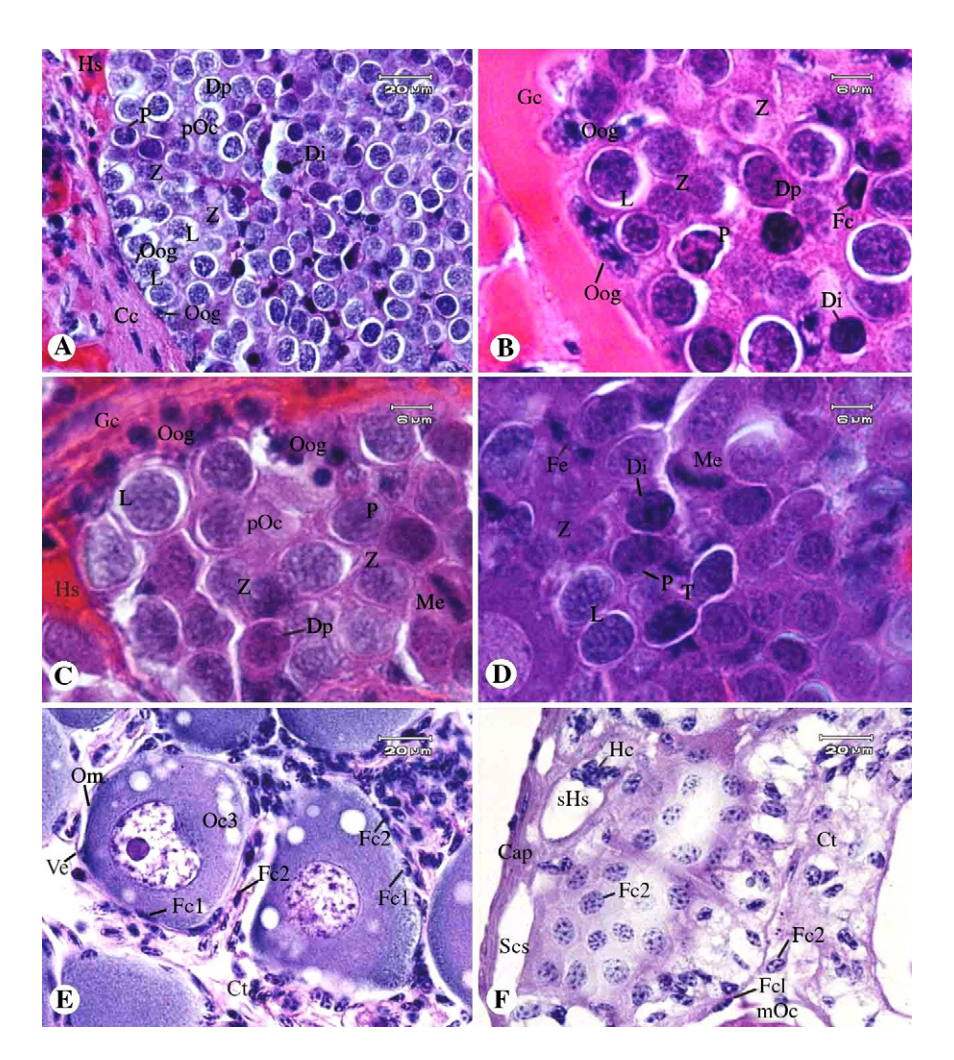


Fig. 3. Light micrographs of paraffin section stained with PAS, showing various stages of developing germ cells and oocytes. Oog (oogonia) aggregate at the tip of the ovarian pouch near the central ovarian core (Cc). All stages of primary oocytes including leptotene (L), zygotene (Z), pachytene (P), diplotene (Dp) and diakinesis (Di) of 1st meiotic prophase are also present. Higher magnification of A showing oogonia appearing in rows of 2–4 cells on the connective tissue trabeculae of an ovarian pouch. C, D. Primary oocytes in various prophase I stage including metaphase (Me) and telophase (T) of 1st meiotic prophase. Follicular cells (Fc) during Oc3 and Oc4 stages that surround the oocytes. Tangential section of mature oocyte (mOc) in ovarian stage IV, showing extremely thin follicular cells around its surface. Other abbreviations: Cap—ovarian capsule, Fc1— type I follicular cell, Fc2— type II follicular cell, Gc— germinal cord, Hc—hemocytes, N— nucleus, No— nucleolus, Om—oocyte membrane, Scs—subcapsular space, sHs—subcapsular hemolymph sinus.

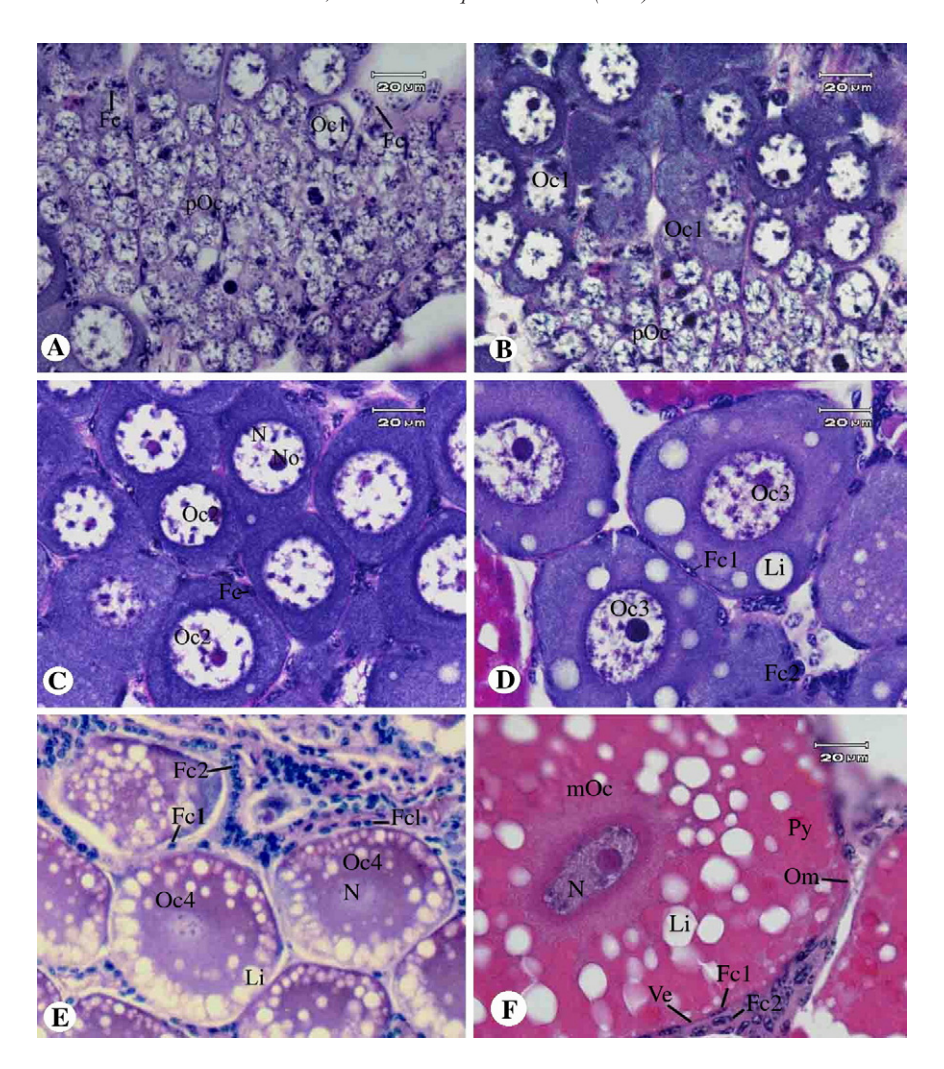


Fig. 4. Micrographs of the developing oocytes taken from paraffin sections stained with H&E, showing different steps of oocytes from primary oocyte (pOc) to mature oocyte (mOc). Primary oocytes (pOc) at the tip of an ovarian pouch. Fc—follicular cell. Early previtellogenic oocyte (Oc1). N—nuclei. Late previtellogenic oocyte (Oc2). Follicular cells with ovoid profile appear more distinct. No—nucleolus. Early vitellogenic oocyte (Oc3) containing lipid droplet (Li). Two types of follicular cells, type I (Fc1) and type II (Fc II), could be identified at this stage. Late vitellogenic oocyte (Oc4). Follicular cells with elongated shape are prominent. F. Mature oocyte (mOc) containing proteinatious yolk plaques (Py). Type I follicular cell is more flattened and in close apposition to the oocyte surface, while type II is more prominent and more frequently seen. The vitelline envelope (Ve) appears as a very thin line closes to the oocyte membrane (Om).

mitotically, and their daughter cells progress into the pouch and increase in size while entering the 1st meiosis.

### 3.2.2. Primary oocyte (pOc)

Primary oocytes accumulate at the oogenic zone next to the germinal cord, at the tip of a conical-shaped ovarian pouch. These cells are undergoing 1st meiosis, and are characterized by the nuclei containing dense small cords of heterochromatin with variable sizes which are intertwined within the nuclear boundaries. Primary oocytes appear in various steps of prophase, including leptotene, zygotene, pachytene, diplotene, diakinesis, metaphase and telophase (Fig. 3A–D). Their

very thin rim of cytoplasm appear blue with H&E stain, and their sizes range from  $8.5{\text -}10~\mu m$  in diameter. The oogonia and pOc are predominantly in the ovarian stage I (Fig. 2C).

### 3.2.3. Secondary oocytes (sOc)

This phase of developing oocytes is undergoing 2nd meiosis and they are classified into five steps, which include Oc1, Oc2, Oc3, Oc4, and mOc.

### 3.2.4. Early previtellogenic oocyte (Oc1)

Oc1 is characterized by a substantial increase in size (ranging from  $10-30~\mu m$  in diameter) when compared

to the primary oocytes. The cytoplasm is large and appears deep blue with H&E stain. The nucleus is characterized by the presence of the intensely blue-stained small blocks of heterochromatin, while the rest of the nucleoplasm appears very light. The nucleolus is small and not always clearly visible. Oc1 occupy a zone external to the oogonia and primary oocytes, which is termed previtellogenic zone (Fig. 4B). They are surrounded by spindle-shaped follicular cells.

### 3.2.5. Late previtellogenic oocyte (Oc2)

Oc2 is characterized by the increase in cell size (ranging from 30–100 µm in diameter) and the decrease of nucleo-cytoplasmic ratio. The cytoplasm is enlarged and exhibits more intensely blue staining with H&E. The nucleus is characterized by the presence of dense blocks of heterochromatin scattering throughout. The centrally located nucleolus becomes prominent with densely packed materials. The follicular cells surrounding Oc2 are more elongated as well as increased in number and size (Fig. 4C). Oc2, like Oc1, are located in the previtellogenic zone next to the oogenic zone of the developing ovary, and this zone occupies most of the oogenic pouch in the ovarian stage II (Fig. 2D).

### 3.2.6. Early vitellogenic oocyte (Oc3)

Oc3 is characterized by the decrease of bluish stain (basophilia) and the increase of reddish stain (eosinophilia) in the cytoplasm. The cytoplasm also contains some lipid droplets, which are distributed randomly at the periphery (Figs. 3E and 4D). The cell size is about 100 to 200 µm in diameter. The round nucleus is enlarged and still centrally located, and exhibits numerous and variable size heterochromatin blocks scattering throughout. This step of oocyte has increasing number of type II follicular cells with oval nuclei. Meanwhile, type I follicular cells are tightly adhered to the surface of each oocyte and remain unchanged from their previous stage.

### 3.2.7. Late vitellogenic oocyte (Oc4)

Oc4 displays violet-stained acidophilic cytoplasm with increasing amount of lipid droplets and reddish protein-aceous yolk plaques. The acidophilia at the periphery is more intense in comparison to the area surrounding nucleus. The cell size ranges from 150–250 µm in diameter. At this stage of oocyte, the lipid droplets apparently increase in size and become located along the cytoplasmic rim. The follicular cells type I and II are more apparent and more elongated in shape (Fig 4E). Oc4 and Oc3 are located in the vitellogenic zone peripheral to the previtellogenic zone of the developing ovary, and this

zone occupies most of the oogenic pouch in the ovarian stage III (Fig. 2E).

### 3.2.8. Mature oocyte (mOc)

The mOc is characterized by a remarkable increase in cell size, more than ten times the early previtellogenic oocytes. Most of them are around 300–550 µm in diameter and have a hexagonal shape. The cytoplasm becomes highly acidophilic and filled with large lipid droplets and proteinaceous yolk plaques. Accumulation of a deep purple-stained material could be noticed underneath the perivitelline space. The nucleus contains almost entirely euchromatin and a prominent nucleolus (Fig. 4F). The nuclear membrane is not apparent and frequently disappears, which may be the result from germinal vesicle breakdown. Type I and type II follicular cells surrounding mOc are fully elongated, and they are tightly attached to the cell surface. Unlike *Penaeus* shrimp, no cortical rod is observed in mature oocytes.

### 3.3. Stages of the ovarian cycle

Histologically, the ovarian cycle could be classified into five stages: stage 0 (spawn), I (spent), II (proliferative), III (premature) and IV (mature), respectively.

In stage 0, the ovary right after spawning appears loose and empty. It contains collapsed ovarian pouches with only strands of follicular cells and connective tissue remaining. Most of the follicular cells return to their original ovoid shape. The main hemolymph vessel in the central ovarian area is still present and appears intact. However, the small hemolymph sinuses are dispersed throughout ovarian tissue, but their boundaries are not clearly defined. Groups of oogonia at the central ovarian core are frequently seen. Thickening and folding of the ovarian capsule is apparent around the ovary (Fig. 2A, B).

During stage I (spent), the ovary is filled with primary oocytes occupying the oogenic zone, and previtellogenic oocytes (Oc1 to Oc2) occupying the previtellogenic zone. Follicular cells are rarely seen at this stage of the oocytes. The hemolymph vessels and sinuses reconvert to the more intact form (Fig. 2C).

In stage II (proliferative), the ovary exhibits faint orange color. The oocytes are mainly the late previtellogenic (Oc2) and the early vitellogenesis (Oc3) steps. The division between oogenic and previtellogenic zone becomes clearly visible. Follicular cells increase in number and become more apparent (Fig. 2D).

In stage III (premature), the ovary is bright orange in color and increases in size. Most of the oocytes are in late vitellogenesis (Oc4). The follicular cells elongate to spindle shape and are less frequently seen (Fig. 2E).

In stage IV (mature), the ovary appears in deep orange color and it size increases remarkably when compared to earlier stages. The ovary contains mostly mature oocytes (mOc), while islets of oogonia and primary oocytes are frequently seen in the central ovarian core, and other oocytes (Oc1–Oc4) are absent. Follicular cells are decreasing in number, while those remaining appear as thin spindle shapes closely surrounding each oocyte (Fig. 2F). The ovarian capsule and trabeculae are very thin and the ovarian pouch boundaries are hardly discernible. The oviducts are seen on the ventro-lateral side of each ovarian lobe. Their walls continue with the extremely thin ovarian capsule (Fig. 1D).

### 4. Discussion

### 4.1. General histology and origin of oogonia

The capsule of the ovary is made of relatively thick connective and muscular tissues. In turn, the capsule forms trabecular sheets, from which the germinal cells appear to generate. The trabecular sheets divided the ovary into a number of conical-shaped ovarian lobules called ovarian pouches, which are similar in structure to ovarian subunits in *Penaeus vannamei* (Krol et al., 1992) and oogenic pouches in crayfish (Holdich, 2002) and freshwater crab Potamon dehaani (Ando and Makioka, 1999). Each ovarian pouch contains various stages of differentiating oocytes surrounded by follicular cells. The germinal cells, from which the oogonia are derived, aggregate at the tip of the ovarian pouch facing the central ovarian core. In lobster, Homarus americanus, the germinal cells aggregates between ovarian pouches and serve as oogonial reserve (Talbot, 1981). The oogonia undergo mitotic division with successive karvokinesis and incomplete cytokinesis within the germinal layer in the same way as reported in another species of crustacea, Eoleptestherita ticinensis (Scanabissi and Tommasini, 1990). The daughter oogonia then separate from the germinal cord and enter the oogenic zone, where they undergo 1st meiotic division. The aggregation of oogonia at the tip of the ovarian pouch is different from other decapods, and factors contributing to the migration and aggregation of oogonia at this location have not yet been elucidated. In any case, oocytes, which are their daughter cells, develop, enter the previtellogenic zone and move to periphery, while the ovarian pouches become expanded. Depending on ovarian stages, each ovarian pouch of M. rosenbergii may contain combinations of various steps of developing germ cells, including Oog, pOc, Oc1, Oc2, Oc3, Oc4 and mOc. Each step of developing oocytes is aggregated in the same zone. Thus the oocytes differentiate while they also move from the central core to the periphery of the ovary.

The central core of the ovary is made of connective and muscular tissues running along its longitudinal axis. The main hemolymph vessel is highly convoluted and runs within the central core. It branches radially, and the branches run in the trabeculae between ovarian pouches and terminate as hemolymph capillary plexus surrounding each pouch. Muscle cells in the capsule, trabeculae and central ovarian core are not striated type as reported in the lobster's, Homarus americanus ovary (Harrison and Humes, 1992; Talbot and Helluy, 1995). In this prawn, the ovarian muscle cells exhibit corkscrew nuclei and indistinct striation, thus resembling vertebrate smooth muscles. Such muscle cells are believed to be the contractile part that squeeze oocytes into the oviduct and broodchamber during oviposition. In crayfish, Procambarus paeninsulanus, such contraction of the ovarian muscle during oviposition is reportedly induced by prostaglandins (Spaziani et al., 1993). Unlike in Penaeus shrimps, the oviduct of this prawn is not present in the central ovarian core (Bell and Lightner, 1988). In stead the oviduct is the receptacle that is continuous with the subcapsular space lying underneath the capsule. Mature oocytes at periphery of the ovarian pouch move into the space and then pass into the oviduct, perhaps by contraction of the muscle cells as mentioned above.

### 4.2. Classification of differentiating oocytes

In this species, Oog differentiate into primary oocytes which enter 1st meiotic division within the oogenic zone. All steps of prophase I, including leptotene, zygotene, pachytene, diplotene, metaphase, and telophase could be observed in the oogenic zone. The previtellogenic and vitellogenic oocytes (Oc1, Oc2, Oc3 and Oc4) are, most likely secondary oocytes, undergoing differentiation during 2nd meiotic prophase. The differentiation process stops at mOc step, waiting for ovulation to occur. The developmental process of oocytes in the giant freshwater prawn is comparable to those reported in other crustaceans (Van Herp and Soyes, 1997), which is characterized by a long 1st meiotic prophase during which DNA replication and the first phase of cell division are taking place; and also relatively long period of 2nd meiotic prophase, during which the oocytes accumulate ribosomes, glycogen, lipid, yolk and mRNAs (Kleckner et al., 1994). The deposition of yolk in the Oc3 is slow while the oocytes undergo gradual increase in size. At this stage, yolk protein probably is produced endogenously (Van Herp, 1992; Tsutsui, 2000). In contrast, Oc4 and mOc rapidly increases in size and acidophilia due to accumulation of yolk protein which could be derived from extra-ovarian sources (Chang and Shih, 1995; Sagi et al., 1995). The hepatopancreas and adipose tissue were proposed as exogenous sources of yolk proteins (Lee and Chang, 1999; Tsutsui et al., 2000; Yang et al., 2000; Jasmani et al., 2004). Once the oocytes reach maturation they become highly enlarged, and they probably exert strong pressure in the ovary, so much that the thin connective tissue surrounding oogenic pouches are broken, allowing the oocytes to be released into the subcapsular space and pass into the oviduct.

### 4.3. Stages of the ovarian cycle

O'Donovan et al. (1984) divided developing ovary of the giant freshwater prawn during intermolt period in captivity, into six stages, while Damrongphol et al. (1991) proposed only four stages. More recently, Chang and Shih (1995) divided ovarian stages of this prawn, by observing the gross morphology and coloration through carapace, into five stages. Using histological criteria we also divide the ovarian cycle into five stages. The spawn ovary (stage 0) has enlarged in size more than the spent one (stage I). The stromal and connective tissues from collapsed and empty ovarian pouches become loosened and flaccid, while those of the spent ovary is firm and starts to have more oogonia and previtellogenic oocytes. The accumulation in significant numbers of previtellogenic oocytes (Oc1, Oc2) is the distinguishing characteristic of proliferative ovary (stage II). Progressive increase in size of premature (stage III) and mature (stage IV) ovaries is due to the increased numbers of vitellogenic oocytes (Oc3, Oc4, mOc), whose sizes are enlarged significantly due to the uptake of yolk protein from exogenous sources. The islets of oogonia and previtellogenic oocytes among fully mature oocytes in stage IV reflect the reserve capacity of the ovary of the multiple spawning species and it's readiness to start a new cycle.

### Acknowledgements

This research was supported by the grants from Thailand Research Fund (TRF) to P.M. and P.S., Burapha and Mahidol Universities, Thailand.

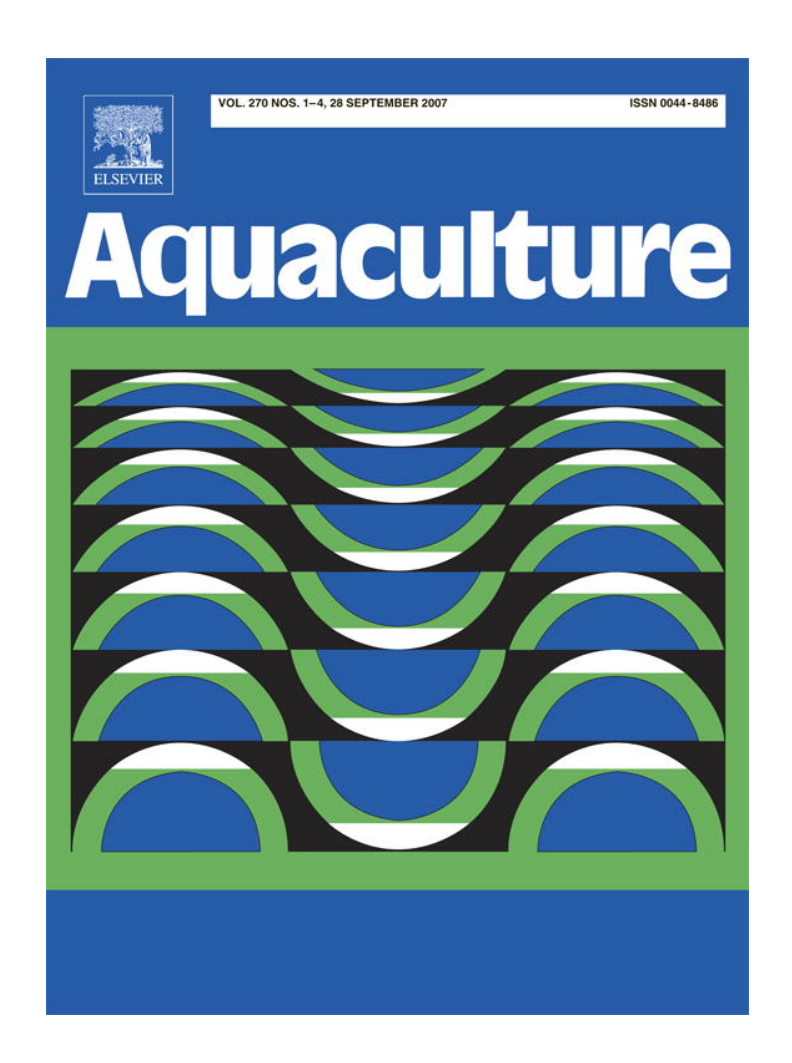
### References

Ando, H., Makioka, T., 1999. Structure of the ovary and mode of oogenesis in a freshwater crab *Potamon dehaani*. J. Morphol. 239, 107–114.

- Bell, T.A., Lightner, D.V., 1988. A Handbook of Normal Penaeid Shrimp Histology. World Aquaculture Society, Baton Rouge, LA.
- Chang, C.F., Shih, T.W., 1995. Reproductive cycle of ovarian development and vitellogenin profiles in the freshwater prawns, *Macrobrachium rosenbergii*. Invertebr. Reprod. Dev. 27, 11–20
- Charniaux-Cotton, H., 1985. Vitellogenesis and its control in malacostracan crustacea. Amer. Zool. 25, 197–206.
- Damrongphol, P., Eangchuan, N., Poolsanguan, B., 1991. Spawning cycle and oocyte maturation in laboratory maintained giant freshwater prawn (*Macrobrachium rosenbergii*). Aquaculture 95, 347–357.
- Harrison, F.W., Humes, A.G., 1992. Microscopic Anatomy of Invertebrates, vol. 9. John Wiley&Sons Inc., New York. 652pp.
- Holdich, D.M., 2002. Biology of Freshwater Crayfish. Blackwell Science, England. 702pp.
- Jasmani, S., Ohira, T., Jayasankar, V., Tsutsui, N., Aida, K., Wilder, M.N., 2004. Localization of vitellogenin mRNA expression and vitellogenin uptake during ovarian maturation in the giant freshwater prawn *Macrobrachiun rosenbergii*. J. Exp. Zool. A Comp. Exp. Biol. 301, 334–343.
- Kleckner, N., Szollosi, D., Wassarman, P., Willison, K., 1994. Germ cells and fertilization, In: Alberts, B., Bray, D., Lawis, J., Raff, M., Roberts, K., Watson, J.D. (Eds.), Molecular Biology of the Cell, 3rd ed. Garland Publishing Inc., New York, pp. 1011–1035.
- Krol, R.M., Hawkins, W.E., Overstreey, R.M., 1992. Reproductive components. In: Harrison, F.W., Humes, A.G. (Eds.), Microscopic Anatomy of Invertebrates, vol. 10. Wiley-Liss Inc., New York, pp. 295–343.
- Lee, F.Y., Chang, C.F., 1999. Hepatopancreas is the likely organ of vitellogenin synthesis in the freshwater prawn, *Macrobrachium* rosenbergii. J. Exp. Zool. 284, 798–806.
- Meeratana, Prasert, Withyachumnarnkul, Boonsirm, Damrongphol, Praneet, Wongprasert, Kanokphan, Seuseangthum, Anchalee, Sobhon, Prasert, 2006. Serotonin induces ovarian maturation in giant freshwater prawn broodstock, *Macrobrachium rosenbergii* de Man. Aquaculture 260, 315–325.
- O'Donovan, P., Abraham, M., Cohen, D., 1984. The ovarian cycle during the intermolt in ovigerous *Macrobrachium rosenbergii*. Aquaculture. 36, 347–358.
- Scanabissi, S.F., Tommasini, S., 1990. Origin and early development of female germ cells in *Eoleptestheria ticinensis* Balsamo-Crivelli, 1859 (Crustaeaa, Branchiopoda, Conchostraca). Mol. Reprod. Dev. 26, 47–52.
- Sagi, A., Soroka, Y., Snyr, E., Chomsky, O., Calderon, J., Milner, Y., 1995. Ovarian protein synthesis in the prawn *Macrobrachium rosenbergii*: does ovarian vitellin synthesis exist? Invertebr. Reprod. Dev. 27, 41–47.
- Spaziani, E.P., Hinsch, G.W., Edwards, S.C., 1993. Changes in prostaglandin E2 and F2 $\alpha$  during vitellogenesis in the Florida crayfish *Procambarus paeninsulanus*. J. Com. Physiol. B. 163, 541–545.
- Talbot, P., 1981. The ovary of the lobster, *Homarus americanus*.I. Architecture of mature ovary. J. Ultrastruct. Res. 76, 235–248.
- Tabolt, P., Helluy, S., 1995. Reproduction and embryonic development. In: Factor, J.R. (Ed.), Biology of the Lobster *Homarus americanus*. Academic press, San Diego, pp. 177–216.
- Tsutsui, N., 2000. Molecular characterization of a cDNA encoding vitellogenin and its expression in the hepatopancreas and ovary during vitellogenin synthesis in the kuruma prawn, *Penaeus japonicus*. Zool. Sci. 17, 651–660.

- Van Herp, F., 1992. Inhibiting and stimulating neuropeptides controlling reproduction in crustacea. Invertebr. Reprod. Dev. 22, 21–30.
- Van Herp, F., Soyes, D., 1997. Arthropoda–Crustacea. In: Adiyodi, K.G., Adiyodi, R.G., Adams, T.S. (Eds.), Reproductive Biology of Invertebrates, vol. VIII. John Wiley & Sons, New York, pp. 247–275.
- Yang, W.J., et al., 2000. Determination of amino acid sequence and site of mRNA expression of four vitellin in giant freshwater prawn, *Macrobrachium rosenbergii*. J. Exp. Zool. 287, 413–422.

Provided for non-commercial research and education use. Not for reproduction, distribution or commercial use.



This article was published in an Elsevier journal. The attached copy is furnished to the author for non-commercial research and education use, including for instruction at the author's institution, sharing with colleagues and providing to institution administration.

Other uses, including reproduction and distribution, or selling or licensing copies, or posting to personal, institutional or third party websites are prohibited.

In most cases authors are permitted to post their version of the article (e.g. in Word or Tex form) to their personal website or institutional repository. Authors requiring further information regarding Elsevier's archiving and manuscript policies are encouraged to visit:

http://www.elsevier.com/copyright



Available online at www.sciencedirect.com



**Aquaculture** 

Aquaculture 270 (2007) 289-298

www.elsevier.com/locate/aqua-online

# Biochemical characterization and physiological role of cortical rods in black tiger shrimp, *Penaeus monodon*

Hathairat Kruevaisayawan <sup>a,c</sup>, Rapeepun Vanichviriyakit <sup>a</sup>, Wattana Weerachatyanukul <sup>a,\*</sup>, Sirilug Magerd <sup>a</sup>, Boonsirm Withyachumnarnkul <sup>a,b</sup>, Prasert Sobhon <sup>a</sup>

<sup>a</sup> Department of Anatomy, Faculty of Science, Mahidol University, Rama VI Road, Bangkok 10400, Thailand
 <sup>b</sup> The Center of Excellence in Shrimp Biotechnology, Faculty of Science, Mahidol University, Bangkok 10400, Thailand
 <sup>c</sup> Department of Anatomy, Faculty of Medical Science, Naresuan University, Phitsanulok 65000, Thailand

Received 28 December 2006; received in revised form 15 March 2007; accepted 3 April 2007

### **Abstract**

Cortical rods (CRs), precursors of egg jelly investment in many penaeoid shrimp, are composed of different proportions of proteins and carbohydrates, the physiological role of which still requires extensive investigation. In this study, we demonstrated the biochemical properties of the CRs and their role in the induction of the acrosome reaction (AR). Profiles of the isolated CRs revealed a number of major protein bands ranging from 35 to 230 kDa. These CR proteins were extensively glycosylated and sulfated. Lectin-based carbohydrate analysis further revealed the highest reactivity of concanavalin A (Con A) among other lectins used. In addition, the selective interference of Con A binding with mannose but not glucose indicated that CR glycoproteins were of high-mannose type. Using immunoblotting with anti-CR antibody, we further demonstrated that part of egg water (EW, a natural AR inducer) was derived from miscible components of the CRs. Physiological tests of water-soluble CR (wsCR) revealed its high AR inducing competency comparable to that of EW, which was far superior to that of acid-urea treated CR (auCR). Furthermore, the wsCR-induced AR was selectively inhibited by Con A, suggesting the significance of the exposing mannose residues in regulating *P. monodon* sperm AR response.

© 2007 Elsevier B.V. All rights reserved.

Keywords: Cortical rod; Egg jelly; Carbohydrate; Acrosome reaction

### 1. Introduction

By the end of vitellogenesis in penaeiod shrimp, the developing eggs reach the final stage of oocyte maturation which is characterized by the appearance of rod-like bodies, called cortical rods (CRs), arranged radially around the periphery of the oocyte plasma

membranes (Anderson et al., 1984; Lynn and Clark, 1987; Pongtippatee-Taweepreda et al., 2004; Rankin and Davis, 1990; Yano, 1988). These CRs are located in the extracellular crypts formed by the invagination of the oolemma into the egg cortex. During spawning, CRs are released upon contact of the eggs with seawater and form a jelly investment around the eggs in many penaeiod shrimp species (Clark et al., 1990; Pongtippatee-Taweepreda et al., 2004; Rankin and Davis, 1990; Yano, 1995). Thereafter, the jelly substances gradually fall off from the spawned egg surface and become the

<sup>\*</sup> Corresponding author. Tel.: +66 02 201 5422; fax: +66 02 354 7168. *E-mail address:* scwwy@mahidol.ac.th (W. Weerachatyanukul).

flocculent materials referred to as "egg water" (EW), the property of which is recognized as a natural inducer of sperm acrosome reaction (AR) (Clark et al., 1990; Pillai and Clark, 1990). Biochemical characterization of the isolated CR from mature ovaries of *P. aztecus* has revealed that CRs contain approximately 25–30% carbohydrates and 70–75% proteins by weight (Lynn and Clark, 1987). Histochemical evidence in *P. monodon* has also consistently demonstrated that CRs are glycoprotein-based materials (Tan-Fermin and Pudadera, 1989). In *Sicyonia ingentis*, amino acid analysis of the crude CR proteins has indicated a predominance of aspartic acid and glycine with a relatively high ratio of cysteine (Lynn and Clark, 1987).

To date, many shrimp CR proteins have been characterized. In P. semisulcatus, one of the CR proteins has high sequence homology to insect peritrophins (intestinal chitin-binding proteins) (Elvin et al., 1996; Tellam et al., 1999), hence the term "shrimp ovarian peritrophin (SOP)" is introduced (Khayat et al., 2001; Avarre et al., 2001). The other protein termed "cortical rod protein (CRP)" is also biochemically characterized in Marsupenaeus japonicus (Kim et al., 2004; Kim et al., 2005). SOP and CRP share many common characteristics: 1) their mobility on SDS-PAGE (~33 kDa) is relatively similar; 2) both SOP and CRP are highly glycosylated; and importantly, 3) amino acid sequence of CRP shares the identities of 29 residues in the N-terminus to that of peritrophins or SOP, suggesting that these two proteins might be transcriptional products of the same gene. The other high molecular weight (>130 kDa) CR protein having sequence similarities to thrombospondin (TSP, the extracellular matrix protein in a cartilage oligomeric protein family) is characterized in M. japonicus and Fennerpenaeus chinensis and termed mjTSP and Fc-TSP, respectively (Sun et al., 2006; Yamano et al., 2004). Interestingly, the N-terminal domain of mjTSP peptide baring no significant homology to TSP family reveals a high sequence similarity to SOP (Yamano et al., 2004). These findings indicate that SOP is a considerably large extracellular protein family found in the CR glycoproteins. Nevertheless, the known functions of this insect peritrophin-related SOP as chitin-binding and antimicrobial proteins are not correlated to the fertilization-related function of egg jelly that is derived directly from the CRs. In this study, we therefore aimed to study the physiological significance of CR derived materials in regards to fertilization along with the biochemical characterization of the CR glycoprotein compositions.

### 2. Materials and methods

### 2.1. Sample preparation

### 2.1.1. Cortical rod isolation

Mature female shrimp containing fully mature ovaries were cold-anesthetized under ice. The carapace and shell were carefully dissected away and the mature ovaries (exhibiting dark green color on the dorsal region throughout the body length) were collected. Isolation of CRs was performed following the previously described protocol (Lynn and Clark, 1987). Briefly, pieces of ovaries were homogenized in the isolation medium (IM: 500 mM NaCl, 9 mM CaCl<sub>2</sub>, 14 mM KCl, 15 mM MgCl<sub>2</sub>, and 10 mM Tris, pH 7.6) containing 30% sucrose until no visible fragments were left in the suspension. This suspension was subjected to centrifugation (1000 ×g, 4 °C, 5 min). The pellet was resuspended in IM, and the suspension was overlaid onto 60% sucrose in IM and centrifuged (8000  $\times g$ , 4 °C, 60 min). The green supernatant containing chiefly yolk granules was discarded, while the white pellet containing mainly CRs was extensively washed (1000  $\times g$ , 4 °C, 5 min) with IM to get rid of contaminating yolk granules and used immediately or stored at -80 °C until use. Protein concentration was determined by Bradford's protein assay (Bradford, 1976) using Sigma Bradford reagents (Sigma, St. Louis, MO, USA).

To prepare the water-soluble materials of CRs (wsCR), isolated CRs were left overnight at 4 °C in IM solution. The suspension was centrifuged (1000  $\times g$ , 4 °C, 10 min) to pellet CR materials. The supernatant assigned as "wsCR" was collected and re-centrifuged  $(12,000 \times g, 4 \, ^{\circ}\text{C}, 15 \, \text{min})$  to eliminate contaminants. The insoluble CR materials in the pellet were further subjected to acid-urea treatment with 7 M urea in 0.1 N HCl (4 °C, overnight) followed by brief sonications at 100 W output (4×30 s). After centrifugation to pellet the remaining CR fragments, the supernatant was collected and designated as "acid-urea treated CRs (auCR)". Both wsCR and auCR were extensively dialysed against artificial seawater (ASW: 423 mM NaCl, 9 mM KCl, 9.3 mM CaCl<sub>2</sub>, 23 mM MgCl<sub>2</sub>, 9.3 mM MgSO<sub>4</sub>, 2.1 mM NaHCO<sub>3</sub>, pH 7.8) and the protein concentration was determined following the aforementioned method.

### 2.1.2. Collection of thelycal sperm and egg water

Since thelycal (T-) sperm have been known to possess higher fertilizing ability than spermatophoric sperm due to their higher maturation/capacitation status (Alfaro et al., 2003; Vanichviriyakit et al.,

2004), we thus used T-sperm for all the following experiments. To collect T-sperm, inseminated females were anesthetized under ice and the thelyca located at the 5th-pair walking legs were carefully removed and placed in calcium-free artificial seawater (CFASW: 423 mM NaCl, 9 mM KCl, 23 mM MgCl<sub>2</sub>, 9.3 mM MgSO<sub>4</sub>, 2.1 mM NaHCO<sub>3</sub>, pH 7.8). Subsequently, the sperm masses and contents inside the thelycum were physically isolated using dissecting forceps. T-sperm suspension was filtered through a 212- $\mu$ m-metal sieve (Endecotts, London, UK) to remove aggregates, washed (500 ×g, 5 min) and resuspended in CFASW at the final concentration of 1×10<sup>7</sup> sperm/ml before

Collection of egg water (EW) was carried out at the Bangkok Aquaculture Farm Company, Nakhon Si Thammarat, Thailand. Uninseminated mature females with mature ovaries were individually placed in a 500-l plastic tank. Upon spawning, the shrimp was held firmly over a 500-ml container and allowed to spawn their eggs into filtered seawater. After gentle swirling to settle the eggs to the bottom, seawater without spawned eggs was collected and assigned as "EW". This EW was centrifuged  $(12,000 \times g, 15 \text{ min}, 4 \, ^{\circ}\text{C})$  to remove particulates and kept in  $-80 \, ^{\circ}\text{C}$  until use. Protein concentration of the EW was determined by Bradford's protein assay.

### 2.2. Production of polyclonal antibody against CR proteins

Polyclonal antibody directed against the entire CR isolates was prepared in BALB/c mice according to the method described previously (Harlow and Lane, 1999). The animal handling procedures strictly followed the guidelines of The Animal Care Committee, Mahidol University. Briefly, the animals were given an intraperitoneal injection with  $\sim 2$  mg of the CR proteins emulsified with Freund's complete adjuvant (1:1, v/v). Booster injections with the same amount of immunogens mixed with Freund's incomplete adjuvant were administered 2 and 4 weeks after the first injection. One week after every immunization, the blood was collected for titer determination. The collected blood was allowed to clot (37 °C, 1 h) and the sera were obtained after centrifugation (3000 ×g, 10 min). These sera were further subjected to decomplimentation (56 °C, 1 h) prior to any applications. Titers of the antisera were checked by immunoblotting (see below). Antisera with titers >1:1000 were pooled and further subjected to ammonium sulfate precipitation and stored at -20 °C until use.

### 2.3. SDS-PAGE and detection of the sulfated glycans

Isolated CRs were homogenized in 10 mM PBS, pH 7.4 containing 2% SDS and sonicated at 100 W output (4×30 s). The non-solubilized fraction was discarded by centrifugation (12,000 ×g, 15 min, 4 °C). Approximately 20 μg of CR isolates, wsCR, auCR, or EW was solubilized in loading buffer and resolved by 10% SDS-PAGE under a reducing condition (Laemmli, 1970). The separated proteins on the gel were stained with 0.025% Coomassie Brilliant blue R 250. In order to analyze glycosulfated compositions in the CR glycoproteins, separated proteins on the duplicated gels were stained with periodic acid Schiff (PAS) or with 0.1% toluidine blue in 7% acetic acid and 20% methanol (Hirohashi and Vacquier, 2002).

### 2.4. Western immuno- and lectin blottings

For immunoblotting, approximately 3 µg of each sample was separated by 10% SDS-PAGE and was electrotransferred (Towbin et al., 1979) to a Hybond N-ECL 0.45 µm nitrocellulose membrane (Amersham Biosciences, UK). Non-specific binding of antibodies was blocked with 5% skim milk in Tris-buffered saline (TBS) containing 0.1% Tween 20 (TBS-T) (room temperature, 1 h). The transferred proteins were exposed to 1:1000 anti-CR antiserum (room temperature, 2 h) and subsequently to 1:2000 horse radish peroxidase (HRP)-conjugated goat anti-mouse IgG. Antigen-antibody complexes were visualized by an enhanced chemiluminescent method using ECL detection kit (Amersham Biosciences).

For lectin blotting (Bar-Nun and Gershoni, 1998), the transferred proteins were blocked with 4% bovine serum albumin (BSA) in TBS-T and further exposed to various biotinylated lectins (Vector laboratories, Burlingame, CA, USA) at a final concentration of 4 μg/ml (room temperature, 2 h). Lectins used in this study included concanavalin A (Con A), wheat germ agglutinin (WGA), Ricinus communis agglutinin I (RCA-I), Ulex europeaus agglutinin I (UEA-I) and Griffonia (bandeiraea) simplicifolia agglutinin I (BSL-I). After washing with TBS-T, the proteins were incubated with 1:5000 HRP-conjugated streptavidin and the lectin reactivity was detected by an enhanced chemiluminescent method as described above. In order to determine the binding specificity of biotinylated Con A (which was shown to be the major bound lectin to the CR glycoproteins: see Fig. 3) to either mannose or glucose residues, the final concentration of 0.4 M of these complimentary sugars

were added and pre-incubated (4 °C, 1 h) with Con A before exposing to the resolved CR proteins.

### 2.5. Enzyme-linked lectin assay (ELLA)

Quantitative analysis of lectin binding was performed using ELLA (Hirohashi and Lennarz, 2001). One hundred microlitres of 20 µg/ml CR proteins diluted in coating buffer, pH 9.0, were coated onto a 96-well plate at 4 °C for overnight. After extensive washes with TBS-T, the coated CR proteins were blocked with 3% BSA in TBS, washed and subsequently incubated in various concentrations (0.02-1 μg/ml) of biotinylated lectins in 1% BSA-TBS (room temperature, 1 h). After three washes with TBS-T, the proteins were exposed to HRP-conjugated streptavidin (1:5000 dilution, 1 h). Binding of lectins was detected by tetramethyl benzidine (TMB) peroxidase substrate (KPL, Gaithersburg, MD, USA). The reaction was stopped by adding 1 N HCl and the developing color was quantified at the wavelength of 450 nm using a VERSAmax microplate reader (Molecular Devices, Sunnyvale, CA, USA). Coated CR proteins exposed to HRP-conjugated streptavidin served as a blank control, the obtained value of which was used to eliminate the background staining of the experimental samples.

### 2.6. Induction of sperm acrosome reaction

To determine the possible physiological function of CR in an induction of sperm acrosome reaction (AR), isolated T-sperm were treated with 4–64 µg/ml of wsCR, auCR or EW for 5 min to initiate AR response. Treated sperm were fixed with 4% paraformaldehyde and the percentages of unreacted (with an intact long spike) and reacted (without the anterior spike) sperm (Vanichviriyakit et al., 2004) were scored under a phase contrast microscope. The percentage of spontaneous AR, as a control, was assessed from sperm treated with ASW. Approximately 200 sperm were counted for each data point. Each experiment was triplicated using different sperm samples.

To investigate the significance of specific sugar moieties of the CR glycoproteins in the AR induction, wsCR was pre-incubated with 50  $\mu$ g/ml of each the following: Con A, UEA-I, WGA, BSL-I and RCA-I or with the additional 100  $\mu$ g/ml Con A (the only lectin that showed inhibitory effect on the wsCR-induced AR: see Fig. 5B). These pre-incubated mixtures were then used to treat sperm and the assessment of the AR response was performed according to the aforemen-

tioned method. Sperm treated with 100  $\mu$ g/ml Con A served as a negative control.

### 3. Results

### 3.1. Profiles of the isolated CRs and their glycosulfated compositions

Protein profiles of the entire CR isolates determined by Coomassie blue staining were shown in Fig. 1. It was revealed that CRs consisted of a broad spectrum of the protein bands ranging from ~25 kDa to more than 200 kDa (Fig. 1, lane 2). Among these CR glycoproteins, the protein bands with  $M_r$  of 230, 180, 140, 100, 84, 80, 73, 58, 54, 50/51, 47, 44, 36 and 34 kDa (Fig. 1, lane 2) were intensely stained with Coomassie blue and considered as the major CR proteins. Some of these CR proteins with the  $M_{\rm r}$  of 230, 180, 140, 120, 47 and 36 kDa were also reactive with PAS (Fig. 1, lane 3, arrowheads). Notably, the 36 kDa protein band appeared to be more intensely reactive than the other PASpositive protein bands. This indicated that CR proteins were post-translationally modified by an extensive glycosylation. The details of sugar termini that were enriched in the CR glycoproteins were also studied and described below.

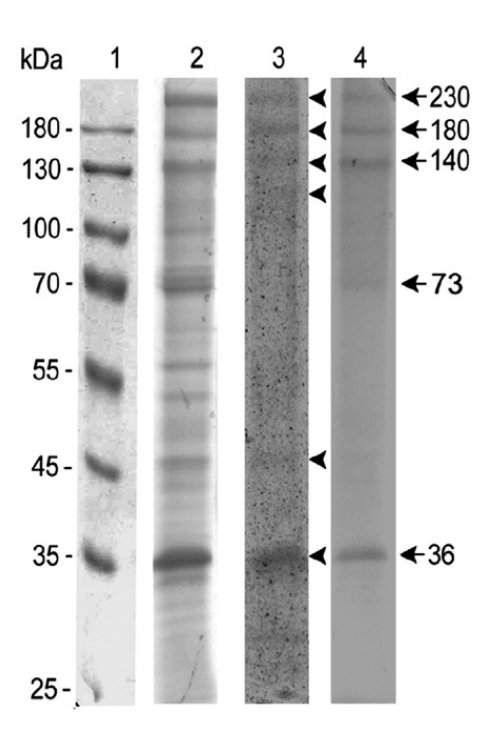


Fig. 1. Profiles of the isolated CR glyproteins subjected to Coomassie blue (lane 2), PAS (lane 3) and toluidine blue (lane 4) staining. Arrowheads and arrows indicate major bands of CR proteins that are intensely reactive with PAS and toluidine blue, respectively. Lane 1 = protein molecular weight marker.

We also investigated the sulfated moieties on the CR glycoproteins using metachromatic reaction of toluidine blue staining (Hirohashi and Vacquier, 2002). The result revealed that three slowly migrating (230, 180 and 140 kDa) and fast-medium migrating (36 and 73 kDa) CR glycoproteins showed the positive metachromatic reactivity, as visualized by a pinkish-purple staining on the protein bands (Fig. 1, lane 4, arrows). It was thus suggestive from this result that some CR glycosylated proteins were additionally sulfated at the *N*-linked sugar residues.

### 3.2. Determination of sugar moieties in the CR glycoproteins

To elucidate the specific types of sugar moieties that made up carbohydrate compositions of the CR glycoproteins, lectin blotting was performed with various biotinylated lectins. It was demonstrated that Con A (recognizing both mannose and glucose residues) appeared to have the broadest spectrum of reactivity (ranging from 28 to 180 kDa) and the highest reactive intensity with the isolated CR glycoproteins (Fig. 2A). To further rule out whether the reactivity of Con A indicated high-mannose or high-glucose type in the CR glycoproteins, a competitive assay of Con A binding with the complimentary sugars was performed. Inclusion of mannose monosaccharides into biotinylated Con

A showed a much pronounced inhibition of Con A binding to the resolved CRs than that of glucose (Fig. 2B), indicating the selective enrichment of mannose over glucose residues in the CR glycoproteins. Reactive intensity of other lectins (WGA, UEA-I, RCA-I and BSL-I), however, was to a lesser extent than that of Con A. Notably, among all lectins used, UEA-I was the only lectin that specifically recognized the ~36 kDa protein band, suggesting the selective modification of this 36-kDa protein with L-fucose residues (Fig. 2A, asterisk). A trace amount of reactivity was observed at the 180, 32 and 29 kDa protein bands in negative controls in which the biotinylated lectins were omitted.

We also investigated lectin reactivity on the wsCR and EW glycoproteins using Con A and RCA (as a representative of the four lectins having a minimal reactivity with the isolated CR glycoproteins). Reactivity of Con A on the wsCR samples was fairly different from the isolated CR samples (Fig. 2C). While wsCR protein bands ranging from 36 to 60 kDa were more prominently reactive (particularly the 60 kDa band) than those of the isolated CRs, the fast migrating wsCR proteins (27–33 kDa) were less reactive. This suggests that the intermediate migrating proteins (i.e., 36–60 kDa) in the CRs possess higher solubilizing property than the fast migrating ones, rendering them a higher proportion in the total wsCR proteins when compared to the total isolated CR proteins. Reactivity of Con A to the

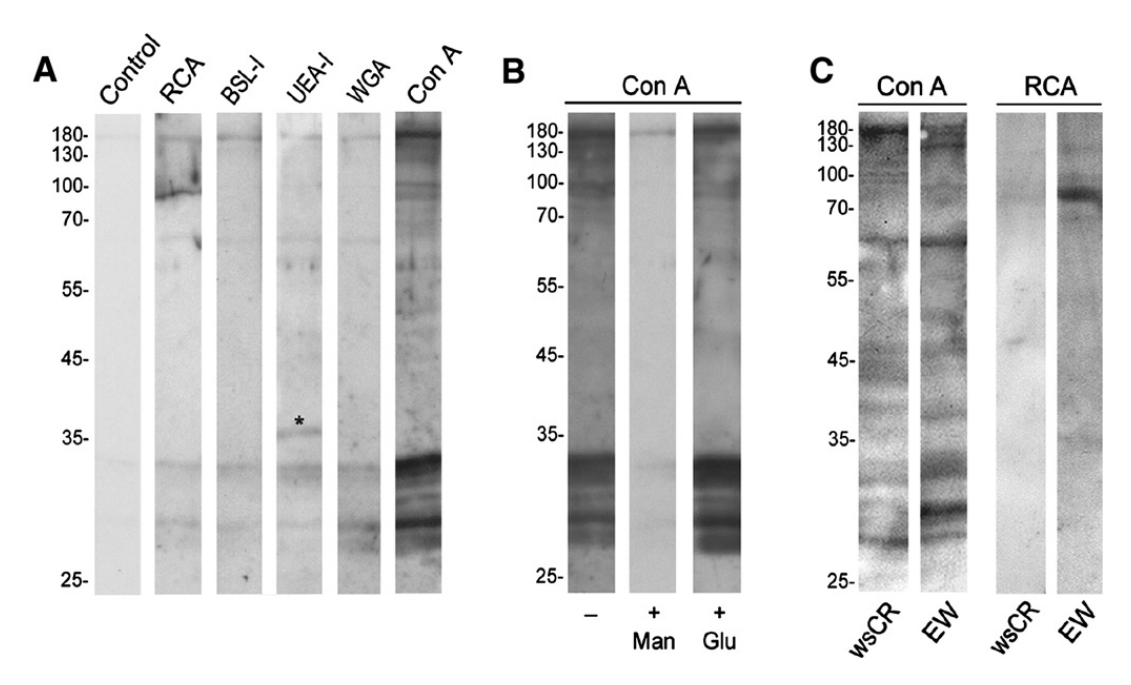


Fig. 2. Lectin blotting of the isolated CR, wsCR and EW glycoproteins. Panels A and C: The isolated CRs (panel A), wsCR and EW (panel C) were resolved by 12.5% SDS-PAGE and subjected to various biotinylated lectin staining. Types of lectins used are indicated on top of each lane. Control represents isolated CRs exposed to HRP-streptavidin. \*Indicates the specific reactivity of the 36-kDa CR protein band with UEA-I. Panel B: Competition assay of Con A binding to the isolated CR proteins with mannose (+Man) and glucose (+Glu) monosaccharides. Note the interference of mannose but not glucose with Con A binding.

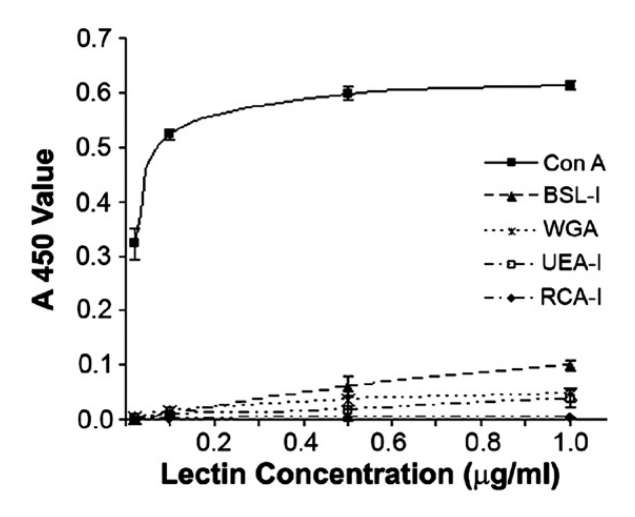


Fig. 3. Enzyme-linked lectin assay (ELLA) of the isolated CRs with various lectins. The CR proteins were coated onto micro-well plates and subsequently exposed to various concentrations of biotinylated lectins followed by TMB substrate. Bound lectins were measured as the absorbance of the developed color products at 450 nm (A450). The data were from four replicates and expressed as mean±S.D.

slow migrating proteins (100–180 kDa) was relatively similar in both samples. In EW, some common Con Areactive protein bands with wsCR could be observed, namely, the 180, 60, 47 and a set of 27–33 kDa proteins (Fig. 2C). However, it might not be able to claim at this state that these Con A-reactive proteins in EW were

parts of wsCR proteins. RCA was minimally reactive with soluble proteins in both wsCR and EW with the exception of the 84-kDa EW protein. Therefore, this RCA-reactive protein in EW should be derived from the alternative sources apart from the CRs.

Quantitative analysis of the individual sugar moiety in the isolated CR glycoproteins using ELLA (Fig. 3) generally supported the lectin blotting findings. It was found that the A450 value of Con A reactivity with the coated CR proteins was over 0.6. The binding level of Con A was concentration-dependent and the binding plateau was approached at the concentration of 0.5  $\mu$ g/ml. At this concentration, the reactivity of Con A was >10 folds higher than the other lectins. BSL-I, WGA and UEA-I at 0.5  $\mu$ g/ml revealed minimal reactivities with their A450 value ranging from 0.01 to 0.06 while RCA-I showed a negligible level of lectin reactivity.

### 3.3. Components of CRs that made up egg water

Two components of CRs, wsCR and auCR, were isolated and their protein profiles and physiological properties were compared with a natural AR inducer, EW. The protein pattern of wsCR was to some extent similar to that of EW. Both wsCR and EW shared at least 5 common protein bands including 230, 84, 73, 60 and 28 kDa (Fig. 4A). On the other hand, the pattern of

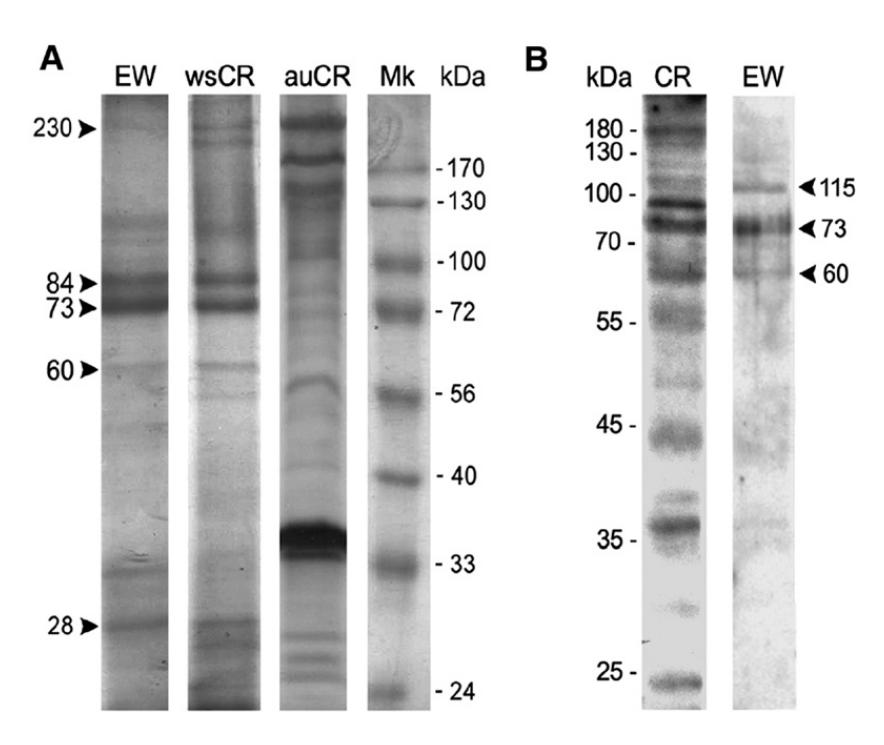
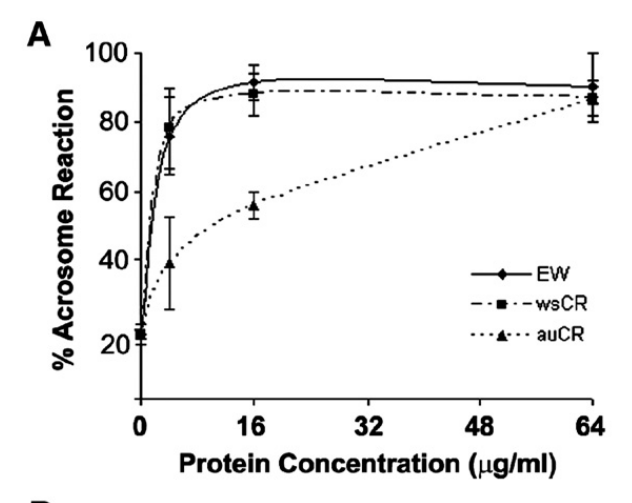


Fig. 4. Panel A: Protein profiles of two components of CRs, water-soluble (wsCR) and acid-urea treated (auCR), in comparison with that of egg water (EW). Arrowheads denote major CR glycoproteins that are resembled in both wsCR and EW. Panel B: Western immunoblotting of the isolated CRs and EW with anti-CR antibody. The immunoreactive protein bands of EW with the anti-CR antibody are indicated by arrowheads.



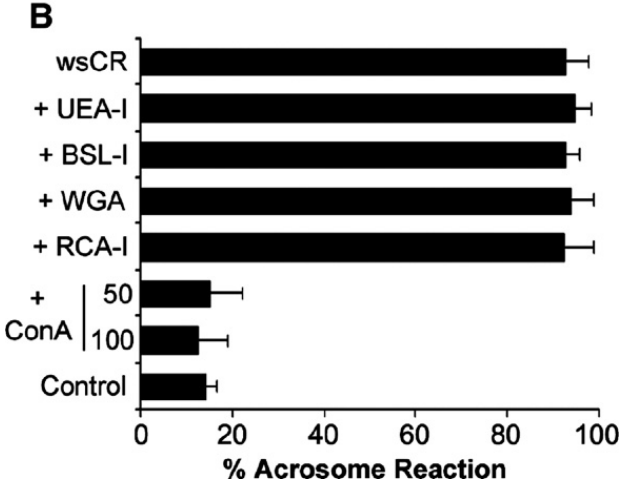


Fig. 5. Induction of the AR responses with various concentrations of EW, wsCR, and auCR (panel A) or with 16  $\mu g/ml$  wsCR in the presence of 50  $\mu g/ml$  of all studied lectins as well as in the presence of the additional 100  $\mu g/ml$  of Con A (panel B). Sperm exposed to 100  $\mu g/ml$  Con A (Control) served as a negative control for lectin competition assay. At least 200 sperm-cells were counted for each data point. Data were expressed as means  $\pm$  S.D. of four replicates performed on different sperm samples.

auCR containing many fast and slowly migrating proteins (Fig. 4A) drastically differed from those of EW and wsCR. The major protein bands of the auCR extracts were 36, 56 kDa and a set of slowly migrating proteins with the  $M_{\rm r} > 110$  kDa.

In order to detect the components of EW that were derived from part of CRs during egg spawning, Western immunoblotting using antibody against the entire CR proteins was performed. Fig. 4B revealed that anti-CR antibody reacting with a broad range of the isolated CR proteins (lane 1), immunoreacted with some EW proteins including the 115, 73 and 60 kDa bands (lane 2, arrowheads). This result suggested that at least three protein components of CRs were highly solubilized and were readily dispersed into seawater upon spawning to form part of EW ingredients.

3.4. Ability of CR glycoproteins in initiating sperm acrosome reaction

We further tested the physiological role of wsCR and auCR in initiating sperm AR response. The result in Fig. 5A demonstrated that wsCR was able to induce sperm AR in a comparable manner as with the ability of EW. The AR inducing ability of both EW and wsCR was relatively similar. The percentages of wsCR-induced AR were  $78.4\pm11.5$ ,  $88.0\pm6.1$  and  $86.9\pm4.9$  at 4, 16 and  $64~\mu g/ml$ , respectively. On the other hand, at the low concentrations of auCR (4 and  $16~\mu g/ml$ ), the AR response was far inferior to those initiated by the corresponding concentrations of wsCR and EW. However, with  $64~\mu g/ml$  auCR, sperm AR response approached the plateau of the AR induction ( $86.3\pm0.8\%$ ) which was comparable to that of wsCR ( $86.9\pm4.9\%$ ) or EW ( $90.1\pm9.9\%$ ).

When wsCR was pretreated with 50  $\mu$ g/ml of various lectins and tested for the ability to induce AR, it was found that Con A drastically inhibited the wsCR-induced AR to the background level (17.2 $\pm$ 9.2%) (Fig. 5B). Pretreatment of wsCR with 100  $\mu$ g/ml Con A slightly decreased the AR response to be 15.7 $\pm$ 1.0%. Percentage of the AR response inhibited by Con A was relatively comparable to that of negative control in which sperm were exposed to 100  $\mu$ g/ml Con A (13.3 $\pm$ 8.2%). Other lectins, in contrast, did not show any notable inhibitory effect on the wsCR-induced AR. The percentages of the AR responses were >90% when other lectins were included, similar to that observed for wsCR (Fig. 5B).

### 4. Discussion

In penaeiod shrimp including P. monodon, CR materials embedded in the egg's extracellular crypts have long been known to be glycoprotein-based constituents (Lynn and Clark, 1987; Tan-Fermin and Pudadera, 1989). Analysis of CR glycoproteins in kuruma prawn, M. japonicus has revealed five major glycoproteins with the apparent  $M_r$  of ~210, 150, 140, 130 and 30 kDa (Yamano et al., 2003). Based on the mobility on SDS-PAGE, the profile of the isolated CRs in P. monodon was also composed of many large (230, 180, 140 kDa), intermediate (73 and 58 kDa) and small (47 and 36 kDa) major glycoproteins. These CR glycoproteins represented extracellular matrices of the eggs which generally exhibited the bottle brush-like feature at the ultrastructural level in some shrimp species including S. ingentis (Clark et al., 1990) and P. monodon (Pongtippatee-Taweepreda et al., 2004). To date, the

characterization of these extracellular proteins in penaeiod shrimp has classified shrimp CR proteins into 2 major groups, SOP and TSP (Avarre et al., 2001; Khayat et al., 2001; Sun et al., 2006; Yamano et al., 2004). Whether the CR glycoproteins of P. monodon fall into these 2 protein categories is still unknown. While SOP, an insect peritrophin-related protein, has been shown to possess a chitin-binding property and anti-microbial activity (Khayat et al., 2001), the function of shrimp TSP has not yet been discovered and has been proposed to act as a physical barrier to prevent polyspermy and egg damage (Yamano et al., 2004). As CRs serve as the precursors for egg jelly (Clark et al., 1990; Lynn and Clark, 1987; Yano, 1995), the aforementioned functions of SOP and the proposed function of TSP do not correspond to the fertilizationrelated function of the egg jelly. In this study, we have provided, for the first time, the fertilization-related function of the CR materials in shrimp sperm AR induction (Fig. 5A). Specifically, the wsCR components could generate a superior AR response compared to the corresponding concentration of the auCR components. In addition, this AR inducing ability of wsCR was comparable to that of EW. Taken together, these results implicated that shrimp sperm AR inducing elements were derived at least partly from the highly miscible components of CRs. This postulation was, in fact, supported by immunoblotting results demonstrating the positive immunoreactivity of some EW proteins with the anti-CR antibody (Fig. 4B).

Carbohydrates have been known to play significant roles in many steps of fertilization in invertebrates (Mengerink and Vacquier, 2001; Mulloy, 2005). The importance of the carbohydrate moieties for fertilization also holds true towards higher mammals including humans as was evident by the essence of carbohydrate moieties in the zona pellucida (ZP) glycoproteins in sperm-ZP binding (Shalgi and Raz, 1997; Wassarman, 2005; Zara and Naz, 1998). Using a number of lectins to analyze the specific sugar compositions of P. monodon CR glycoproteins, it was found that the reactivity of Con A to the isolated CR proteins was more predominant than the other lectins used in this study (Figs. 2 and 3). However, interpretation of Con A reactivity could be two fold: high-mannose or high-glucose CR glycoproteins. We substantiated the findings to explore that mannoses rather than glucoses were the enriched sugar termini in the CR's carbohydrates (Fig. 2B). In this regard, two well-characterized major CR proteins, SOP and CRP, have also been reported to be highly reactive with Con A (Khayat et al., 2001; Kim et al., 2004), and interpreted as the high-mannose type CR glycoproteins.

Apart from mannoses, a minor proportion of the CR carbohydrates also contained other sugars such as fucose (reactive with UEA-I), N-acetylglucosamine (GlcNAc) and sialic acid (both of which were reactive with WGA). Interestingly, the 36-kDa CR protein band reactive with UEA-I also developed a metachromatic reaction with toluidine blue staining, suggesting the presence of fucose and sulfated moieties in shrimp CR glycoproteins, although it is still unknown whether sulfation of CR glycoproteins takes place on carbohydrates or proteins and whether it is involved in the AR induction. In echinoderms, these fucose sulfate polymers (FSP) have been extensively studied in the egg jelly (Alves et al., 1998; Mulloy et al., 1994; Vilela-Silva et al., 1999) and reported to serve their pivotal role in the species-specific AR induction (Alves et al., 1997; Vacquier and Moy, 1997; Vilela-Silva et al., 2002). According to the glycoprotein rich property of the jelly materials in both sea urchins and shrimp, one would expect that shrimp's jelly substances, particularly sulfated glycans, may also be involved in the AR induction. We provided evidence herein that shrimp CRs, the jelly precursors, were involved in modulating the AR response. However, it was mannose rather than (sulfated) fucose residues that played a central role in the carbohydrate-mediated AR, which was a unique characteristic for this shrimp species. Further extensive experiments are required to address whether the carbohydrate termini or protein cores of the active CR glycoprotein(s) or both are responsible for modulating AR response in shrimp sperm.

Conclusively, we have shown in this study that CR materials in *P. monodon* are of high-mannose type glycoproteins. These CR glycoproteins also contain a minor proportion of GlcNAc, sialic acid and fucose residues, some of which are additionally sulfated. Upon solubilized into seawater, they form part of EW ingredients. These CR glycoproteins, especially their exposing mannose residues, play a key role in modulating shrimp sperm AR response. Our finding on the novel role of CR proteins in the AR induction may lead to an established method for detecting sperm quality which will be advantageous for improving artificial fertilization in the penaeid shrimp aquaculture.

### Acknowledgements

This work was supported by the National Science and Technology Development Agency of Thailand (to BW), Thailand Research Fund (to PS, WW and RV) and Commission of Higher Education (to HK). The authors would like to thank Ms. Chor Hoon Poh for her

thorough proof-reading of this manuscript and Dr. Boonyarath Pratoomchat, Department of Aquatic Science, Faculty of Science, Buraphar University for kindly providing shrimp samples.

### References

- Alfaro, J., Munoz, N., Vargas, M., Komen, J., 2003. Induction of sperm activation in open and closed thelycum penaeoid shrimps. Aquaculture 216, 371–381.
- Alves, A.P., Mulloy, B., Diniz, J.A., Mourao, P.A., 1997. Sulfated polysaccharides from the egg jelly layer are species-specific inducers of acrosomal reaction in sperms of sea urchins. J. Biol. Chem. 272, 6965–6971.
- Alves, A.P., Mulloy, B., Moy, G.W., Vacquier, V.D., Mourao, P.A., 1998. Females of the sea urchin *Strongylocentrotus purpuratus* differ in the structures of their egg jelly sulfated fucans. Glycobiology 8, 939–946.
- Anderson, S.L., Chang, E.S., Clark Jr., W.H., 1984. Timing of postvitellogenic ovarian changes in the ridgeback prawn *Sicyonia* ingentis (Penaeidae) determined by ovarian biopsy. Aquaculture 42, 257–271.
- Avarre, J.C., Khayat, M., Michelis, R., Nagasawa, H., Tietz, A., Lubzens, E., 2001. Inhibition of de novo synthesis of a jelly layer precursor protein by crustacean hyperglycemic hormone family peptides and posttranscriptional regulation by sinus gland extracts in *Penaeus semisulcatus* ovaries. Gen. Comp. Endocrinol. 124, 257–268
- Bar-Nun, S., Gershoni, J.M., 1998. Protein-blot analysis of glycoproteins and lectin overlays. Cell Biology: A Laboratory Handbook. Harcourt Publishers, New York, pp. 458–466.
- Bradford, M.M., 1976. A rapid and sensitive method for the quantitation of microgram quantities of protein utilizing the principle of protein-dye binding. Anal. Biochem. 72, 248–254.
- Clark Jr., W.H., Yudin, A.I., Lynn, J.W., Griffin, F.J., Pillai, M.C., 1990. Jelly layer formation in Penaeoidean shrimp eggs. Biol. Bull. 178, 295–299.
- Elvin, C.M., Vuocolo, T., Pearson, R.D., East, I.J., Riding, G.A., Eisemann, C.H., Tellam, R.L., 1996. Characterization of a major peritrophic membrane protein, peritrophin-44, from the larvae of *Lucilia cuprina*. cDNA and deduced amino acid sequences. J. Biol. Chem. 271, 8925–8935.
- Harlow, E., Lane, D., 1999. Using Antibodies: a Laboratory Manual. Cold Spring Harbor Laboratory Press, New York.
- Hirohashi, N., Lennarz, W.J., 2001. Role of a vitelline layer-associated 350 kDa glycoprotein in controlling species-specific gamete interaction in the sea urchin. Dev. Growth Differ. 43, 247–255.
- Hirohashi, N., Vacquier, V.D., 2002. Egg sialoglycans increase intracellular pH and potentiate the acrosome reaction of sea urchin sperm. J. Biol. Chem. 277, 8041–8047.
- Khayat, M., Babin, P.J., Funkenstein, B., Sammar, M., Nagasawa, H., Tietz, A., Lubzens, E., 2001. Molecular characterization and high expression during oocyte development of a shrimp ovarian cortical rod protein homologous to insect intestinal peritrophins. Biol. Reprod. 64, 1090–1099.
- Kim, Y.K., Kawazoe, I., Tsutsui, N., Jasmani, S., Wilder, M.N., Aida, K., 2004. Isolation and cDNA cloning of ovarian cortical rod protein in kuruma prawn *Marsupenaeus japonicus* (Crustacea: Decapoda: Penaeidae). Zool. Sci. 21, 1109–1119.
- Kim, Y.K., Tsutsui, N., Kawazoe, I., Okumura, T., Kaneko, T., Aida, K., 2005. Localization and developmental expression of mRNA

- for cortical rod protein in kuruma prawn *Marsupenaeus japonicus*. Zool. Sci. 22, 675–680.
- Laemmli, U.K., 1970. Cleavage of structural proteins during the assembly of the head of bacteriophage T4. Nature 227, 680-685.
- Lynn, J.W., Clark Jr., W.H., 1987. Physiological and biochemical investigations of the egg jelly release in *Penaeus aztecus*. Biol. Bull. 173, 451–460.
- Mengerink, K.J., Vacquier, V.D., 2001. Glycobiology of sperm–egg interactions in deuterostomes. Glycobiology 11, 37R–43R.
- Mulloy, B., 2005. The specificity of interactions between proteins and sulfated polysaccharides. An. Acad. Bras. Cienc. 77, 651–664.
- Mulloy, B., Ribeiro, A.C., Alves, A.P., Vieira, R.P., Mourao, P.A., 1994. Sulfated fucans from echinoderms have a regular tetra-saccharide repeating unit defined by specific patterns of sulfation at the 0–2 and 0–4 positions. J. Biol. Chem. 269, 22113–22123.
- Pillai, M.C., Clark Jr., W.H., 1990. Development of cortical vesicles in Sicyonia ingentis ova: their heterogeneity and role in elaboration of the hatching envelope. Mol. Reprod. Dev. 26, 78–89.
- Pongtippatee-Taweepreda, P., Chavadej, J., Plodpai, P., Pratoomchart, B., Sobhon, P., Weerachatyanukul, W., Withyachumnarnkul, B., 2004. Egg activation in the black tiger shrimp *Penaeus monodon*. Aquaculture 234, 183–198.
- Rankin, S.M., Davis, R.W., 1990. Ultrastructure of oocytes of the shrimp, *Penaeus vannamei*: cortical specialization formation. Tissue Cell 22, 879–893.
- Shalgi, R., Raz, T., 1997. The role of carbohydrate residues in mammalian fertilization. Histol. Histopath. 12, 813–822.
- Sun, Y.D., Zhao, X.F., Kang, C.J., Wang, J.X., 2006. Molecular cloning and characterization of Fc-TSP from the Chinese shrimp Fennerpenaeus chinensis. Mol. Immunol. 43, 1202–1210.
- Tan-Fermin, J.D., Pudadera, R.A., 1989. Ovarian maturation stages of the wild giant tiger prawn, *Penaeus monodon* Fabricius. Aquaculture 77, 229–242.
- Tellam, R.L., Wijffels, G., Willadsen, P., 1999. Peritrophic matrix proteins. Insect Biochem. Mol. Biol. 29, 87–101.
- Towbin, H., Staehelin, T., Gordon, J., 1979. Electrophoresis transfer of proteins from polyacrylamide gels to nitrocellulose sheets: procedures and some applications. Proc. Natl. Acad. Sci. U. S. A. 76, 4350.
- Vacquier, V.D., Moy, G.W., 1997. The fucose sulfate polymer of egg jelly binds to sperm REJ and is the inducer of the sea urchin sperm acrosome reaction. Dev. Biol. 192, 125–135.
- Vanichviriyakit, R., Kruevaisayawan, H., Weerachatyanukul, W., Tawipreeda, P., Withyachumnarnkul, B., Pratoomchat, B., Chavadej, J., Sobhon, P., 2004. Molecular modification of *Penaeus monodon* sperm in female thelycum and its consequent responses. Mol. Reprod. Dev. 69, 356–363.
- Vilela-Silva, A.C., Alves, A.P., Valente, A.P., Vacquier, V.D., Mourao, P.A., 1999. Structure of the sulfated alpha-L-fucan from the egg jelly coat of the sea urchin *Strongylocentrotus franciscanus*: patterns of preferential 2-O- and 4-O-sulfation determine sperm cell recognition. Glycobiology 9, 927–933.
- Vilela-Silva, A.C., Castro, M.O., Valente, A.P., Biermann, C.H., Mourao, P.A., 2002. Sulfated fucans from the egg jellies of the closely related sea urchins *Strongylocentrotus droebachiensis* and *Strongylocentrotus pallidus* ensure species-specific fertilization. J. Biol. Chem. 277, 379–387.
- Wassarman, P.M., 2005. Contribution of mouse egg zona pellucida glycoproteins to gamete recognition during fertilization. J. Cell. Physiol. 204, 388–391.
- Yamano, K., Seto, H., Qiu, G.F., Unuma, T., 2003. Immunological characterization of cortical rod proteins of kuruma prawn,

- *Marsupenaeus japonicus*. Comp. Biochem. Physiol., Part A Mol. Integr. Physiol. 136, 371–377.
- Yamano, K., Qiu, G.F., Unuma, T., 2004. Molecular cloning and ovarian expression profiles of thrombospondin, a major component of cortical rods in mature oocytes of penaeid shrimp, *Marsupenaeus japonicus*. Biol. Reprod. 70, 1670–1678.
- Yano, I., 1988. Oocyte development in the kuruma prawn *Penaeus japonicus*. Mar. Biol. 99, 547–553.
- Yano, I., 1995. Final oocyte maturation, spawning and mating in penaeid shrimp. J. Exp. Mar. Biol. Ecol. 193, 113–118.
- Zara, J., Naz, R.K., 1998. The role of carbohydrates in mammalian sperm-egg interactions: how important are carbohydrate epitopes? Front. Biosci. 3, D1028–D1038.

# Acrosome reaction in the sperm of the black tiger shrimp *Penaeus monodon* (Decapoda, Penaeidae)

Pattira Pongtippatee<sup>1</sup>, Rapeepan Vanichviriyakit<sup>2</sup>, Jittipan Chavadej<sup>2</sup>, Pornthep Plodpai<sup>3</sup>, Boonyarath Pratoomchart<sup>4</sup>, Prasert Sobhon<sup>2</sup> & Boonsirm Withyachumnarnkul<sup>2,5</sup>

Correspondence: B Withyachumnarnkul, Centex Shrimp, Chalerm Prakiat Building, 4th Floor, Faculty of Science, Mahidol University, 272 Rama 6 Rd., Bangkok 10400, Thailand. E-mail: boonsirm@yahoo.com

### **Abstract**

Owing to the problem of male infertility in the domesticated shrimp Penaeus monodon, this study was conducted to reveal the morphological events of an acrosome reaction (AR) of sperm of this highly valuable species. The AR observed in an in vitro incubation of sperm with egg water (EW) and that during actual spawning was compared. Under transmission and scanning electron microscopy, sperm taken from the female thelycum was composed of a posterior main body, a central cap and an anterior single spike. Upon contact with EW, the sperm underwent two phases of AR: acrosomal exocytosis and spherical mass formation. The former was composed of a degeneration of the spike, swelling of the cap region and rupture of the acrosomal pouch. The latter began with polymerization of materials within the subacrosomal region and ended with re-configuration of the subacrosomal region into an electron-dense spherical mass. The AR of the sperm observed during spawning revealed similar morphological events, with degeneration of the spike upon contact with the vitelline envelope and formation of the spherical mass while penetrating into jelly material produced by protruding cortical rods. The results suggest the presence of AR inducers derived from the vitelline envelope and cortical rods of the egg. This study forms the basis for an evaluation of infertility regarding to AR in the domesticated *P. monodon* male.

**Keywords:** acrosome reaction, sperm, thelycum, fertilization, *Penaeus monodon*, broodstock

### Introduction

The black tiger shrimp *Penaeus monodon* is one of the two most important cultured shrimp species in the world; the other one is the Pacific white shrimp Penaeus vannamei. In the cultivation of both species, the main problems being faced by the industry are disease outbreaks, slow growth and fluctuating shrimp price. One problem that has not been adequately addressed is male fertility. Hatchery operators know that, occasionally, male shrimp of both species have fertilization problems, especially the domesticated ones. The problem could be due to a low sperm count in the spermatophore (Pratoomchat, Piyatiratitivorakul & Menasveta 1993) or the low capacity of individual sperm to fertilize the eggs or both. At the time of fertilization, sperm of the penaeid shrimp need to undergo a morphological transformation termed an acrosome reaction (AR) before penetrating the eggs (Leung-Trujillo & Lawrence 1987; Griffin & Clark Jr. 1990). Because the AR process has never been explored in P. monodon, the purpose of this study was to study the morphological events of the sperm of P. monodon before and at the time of fertilization. The results of this study can serve as a basis for

<sup>&</sup>lt;sup>1</sup>Department of Anatomy, Faculty of Science, Prince of Songkla University, Songkla 90110, Thailand

 $<sup>^2</sup>$ Department of Anatomy, Faculty of Science, Mahidol University, Bangkok 10400, Thailand

<sup>&</sup>lt;sup>3</sup>Shrimp Culture Research Center, Charoen Pokphand Foods Company (Public), Nakorn Srithamaraj 80170, Thailand

 $<sup>^4</sup>$ Department of Marine Biology, Faculty of Science, Burapha University, Cholburi 20131, Thailand

<sup>&</sup>lt;sup>5</sup>Centex Shrimp, Faculty of Science, Mahidol University, Bangkok 10400, Thailand

future research on the problem of male infertility in this species.

Penaeus monodon is a closed thelycum species and the male inserts spermatophores or sperm sacs into the female thelycum during mating. After being inserted into the female thelycum, the sperm are stored for several weeks or longer, during which time they undergo morphological and biochemical changes that render them ready for fertilization (Clark Jr., Kleve & Yudin 1981; Hall, Young & Kenway 1999; Vanichviriyakit, Kruevaisayawan, Weerachatyanukul, Pongtippatee-Tawipreeda, Withyachumnarnkul, Pratoomchat, Chavadej & Sobhon 2004). It is generally believed that sperm are extruded from the thelycum to mix externally with the eggs that are released from gonopores during spawning. At spawning, the sperm undergoes AR, which is composed of two phases in most marine invertebrates: the acrosomal exocytosis, which is a release of the contents of the acrosomal vesicle onto the egg surface, and the acrosomal process formation (Colwin & Colwin 1963; Fa, Lin, Wei & Shuai 2004). The acrosomal process is a structure that extends from the sperm to make contact with the egg membrane and probably serves as a way to facilitate the entry of the sperm DNA into the egg. The mechanisms underlying the acrosomal exocytosis and acrosomal process formation are poorly understood. In the sea urchin Lytechinus pictus and Strongylocentrotus purpuratus, it has been known that acrosomal exocytosis requires a  $Ca^{2+}$  influx from the external environment (Collins & Epel 1977; SeGall & Lennarz 1979; Gonzalez-Martinez, Guerrero, Morales, de Ja Torre & Darszon 1992). In S. purpuratus, the acrosomal process formation is probably caused by polymerization of globular actin molecules in the subacrosomal region and depends on the release of hydrogen ions from the sperm head (Schackmann, Eddy & Shapiro 1978). In the marine shrimp Sicyonia ingentis, acrosomal exocytosis is induced when the sperm contact the vitelline envelope of the egg and the acrosomal process formation is induced by a proteolytic enzyme released from the egg (Clark Jr. et al. 1981; Griffin, Clark Jr., Crowe & Crowe 1987; Pillai & Clark Jr. 1987; Griffin & Clark Jr. 1990; Wikramanayake & Clark Jr. 1994).

In this study, the morphological events of *P. monodon* AR during an *in vitro* incubation with egg water (EW) and during spawning were examined under light microscopy (LM), transmission electron microscopy (TEM) and scanning electron microscopy (SEM). The study covered events from the beginning, or before

the sperm underwent morphological changes, to the end of AR.

#### **Materials and methods**

### **Animals and EW collection**

Wild-caught P. monodon broodstock (15 females and 15 males) from the Andaman Sea were kept in hatchery maturation tanks  $(4 \text{ m} \times 2 \text{ m})$ , and maintained under continuous darkness, 30 °C and 30 g L<sup>-1</sup> seawater, at 0.5 m depth. Mating usually occurred in the tank, and sperm were taken from the female thelycum for observation of AR upon contact with EW. One female was used for EW preparation and three females for AR observation of the sperm during spawning. The females were unilaterally eyestalk ablated and maintained in maturation tanks until their ovaries had become mature (Tan-Fermin & Pudadera 1989). To prepare EW, females that were ready to spawn were transferred to a 500 L tank and continuously observed for spawning behaviour, which was swimming in a circle on the water surface. Just before spawning, the shrimp was manually held and allowed to spawn into 200 mL artificial seawater (ASW) at 4 °C in a 500 mL bucket, and placed back in the 500 L tank. The eggs and ASW in the bucket were transferred to a 250 mL beaker.

The protocol for EW isolation was based on the original technique developed by Griffin  $et\ al.$  (1987). The eggs were allowed to settle to the bottom of the beaker, which was usually complete within 2 min. Water from the top devoid of eggs (ca. 200 mL) was drawn off and transferred to a new 250 mL beaker. It was then centrifuged at  $10\ 000\ g$  for  $15\ min$  at  $4\ ^\circ C$  and clear EW supernatant was prepared in  $1\ mL$  aliquots, and then stored in liquid nitrogen.

### Thelycal sperm collection, EW incubation and morphological observations

To extract sperm from the thelycum, the gelatinous sperm mass was gently withdrawn from the thelycum by a 1 mL syringe, placed in a tube containing 1 mL ASW, gently homogenized by a glass grinder to release the sperm and the tissue debris was allowed to settle. The supernatant was withdrawn and centrifuged at  $200\,g$  for 5 min to pellet the sperm. The supernatant was then removed and sperm were re-suspended by aspiration in 1 mL ASW. Five hundred microlitre of the sperm suspension was incubated

with 500  $\mu L$  of EW for 15, 30, 45, 60 s, 2, 5, 10 min and 1 h.

At each incubation period, 75 µL aliquot of the suspension was pipetted and fixed for 1h in ASW-buffered 2.5% glutaraldehyde. Then, 15 μL aliquot of the fixed sperm was also pipetted, placed on glass slides and viewed under differential interference contrast light microscopy (LM) (Nikon ECLIPSE E-600, Kanagawa, Japan). At the same time, the remaining fixed sperm were processed for TEM and SEM. For TEM, the sperm were washed in buffer, postfixed for  $30 \, min \, in \, 1\%$  buffered OsO<sub>4</sub>, rinsed in ASW and dehydrated through an ethanol series. The samples were embedded in a low-viscosity resin, thin sectioned on an ultramicrotome (MT-XL RMC, Boeckeler Instruments, Inc., Tucson, AZ, USA), stained with uranyl acetate and lead citrate and observed under TEM (JEOL, JEM-100 CXII, Tokyo, Japan).

For SEM, the fixed sperm were affixed to glass coverslips coated with 1% poly-L-lysine, washed in seawater, postfixed for 30 min in seawater-buffered 1% OsO<sub>4</sub>, critical-point dried, mounted on stubs and coated with 25 nm of gold and examined under SEM (Hitachi, S-2500, Tokyo, Japan).

### Observation of AR of the sperm in the spawning tank

The AR of the sperm that had been released from a female during spawning was also observed in a spawning tank under the hatchery conditions. The eggs and sperm released from the female broodstock at the time of spawning were immediately collected and fixed as soon as the eggs came out from the gonopores (approximately 5 s). The samples were fixed and processed for TEM and SEM as described above, and also for LM with haematoxylin and eosin and fluorescent chromosome staining. Bisbenzimide Hoechst 33258 (Sigma-Aldrich Pte., Ltd, Singapore) was used as a fluorescent chromosome stain to allow visualization of the sperm nucleus. A stock solution of Hoechst 33258 (0.005%), dissolved in sterile-distilled water containing 0.1% thimerosal, was filtered through 0.22 µm millipore membrane filters, protected from light and stored at 4 °C. The Hoechst stock solution was stirred for 30 min at room temperature and diluted 1:200 in sterile-distilled water, which was stirred for another 30 min at room temperature. Fertilized eggs were fixed for 10 min in 98% acetic acid and absolute methanol at 1:3 v/v, and air dried. Diluted Hoechst solution (50  $\mu L$ ) was added to fixed samples, which were incubated for

30 min in the dark at room temperature. After the incubation time had lapsed, the samples were rinsed three times with  $500\,\mu L$  distilled water, air dried and mounted for fluorescent microscopy.

Statistical analysis for numerical data was determined by Student's *t*-test.

#### Results

#### In vitro induction of AR

The AR took place within 1-2 min after incubation of the sperm with EW. Approximately  $82 \pm 12\%$  of sperm had undergone AR, while the other  $18 \pm 12\%$ remained unreacted (Fig. 1a); the percentage of reacted sperm was significantly higher than the unreacted ones (P < 0.01). The unreacted sperm were composed of a posterior spherical main body, a central cap and an anterior single spike extending from the cap (Fig. 1b). The main body contains a nucleus that houses a mixture of fibrous and globular chromatin, but the nuclear envelope was not observed (Fig. 1c). In contrast to mammalian sperm, which are highly motile, P. monodon sperm are non-motile and contain no mitochondria. The central cap region contains two main parts: the acrosome and subacrosome. The acrosome is composed of a high-density outer layer and a low-density inner layer (Fig. 1c). The subacrosomal region contains flocculent electron-lucent materials. The most anterior comprises a long single, electron-dense spike, which extends from its base located between the acrosome and subacrosomal region (Fig. 1c). The base of the spike extends into the central cap region and becomes a dense limiting membrane, separating the low-density inner layer of the acrosome and the subacrosomal region.

The AR began with curling, shortening and disappearance of the spike (Fig. 2a, b and c, respectively). The spike base existed for  $< 1 \, \text{min}$  after the onset of the AR and then disappeared (Fig. 2c and e). During the shortening and disappearance of the spike, the cap became markedly swollen (Fig. 2e), which was caused by the swelling of the acrosome (Fig. 2e and f). While the acrosome appeared to be swollen, the distinction between the high-density outer and lowdensity inner layers was not observed and the structures inside became flocculent (Fig. 2d and f). After complete disappearance of the spike, the outer limiting membrane of the acrosome was ruptured and the acrosomal content was released (Fig. 3a and b). The posterior part of the subacrosomal region began to condense, or polymerize, resulting in the subacrosomal region comprising the electron-dense and

1637

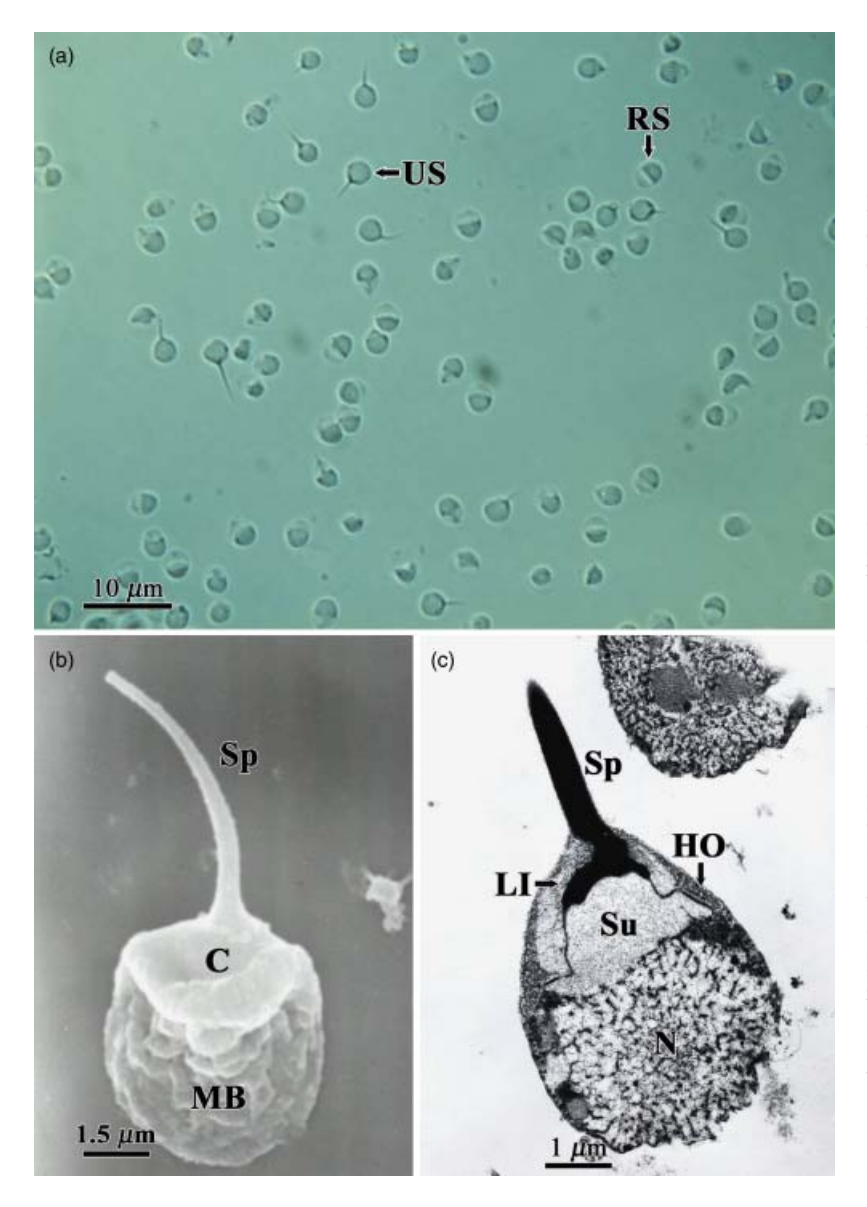


Figure 1 Light (a), scanning electron (b) and transmission electron (c) micrographs of P. monodon sperm. Using light microscopy, it was observed that most of the sperm become reactive after incubating with egg water, and few remain unreacted. Using scanning electron microscopy, it was observed that the unreacted sperm is composed of a posterior main body, a central cap region a and anterior spike. Using transmission electron microscopy, it was observed that the posterior main body contains a nucleus, the cap region consists of three parts: a high-density outer layer, a low-density inner layer and a subacrosomal region. The anterior spike extends its base towards an area between the low-density inner layer and the subacrosomal region. C, cap; HO, high-density outer layer; LI, low-density inner layer; MB, main body; N, nucleus; RS, reacted sperm; Sp, spike; Su, subacrosomal region; US, unreacted sperm.

electron-lucent areas when observed under TEM (Fig. 3a and c). Under SEM, the electron-lucent area appeared as a spherical knob at the anterior end of the sperm (Fig. 3d). Without the acrosome, the subacrosomal region became the most anterior part of the sperm, with the remaining outer limiting membrane of the acrosome hanging on the side of the subacrosomal region (Fig. 3c). Subsequently, the subacrosomal polymerization expanded throughout the region, and was re-configured to be a spherical mass on the anterior end of the sperm (Fig. 3e). These morphological changes made the sperm appear spherical, with a condensed knob at its anterior end when visualized under LM and SEM (Fig. 3e and f).

During morphological development of the AR, the ultrastructure of nucleoplasm, especially the ratio between the fibrous and globular chromatin that reflects the degree of chromatin decondensation, did not reveal any remarkable change (comparing Figs 1c–3e).

### AR in the spawning tank

Immediately after spawning, within 5 s, most of the sperm that contacted the eggs did not undergo AR (Fig. 4a). The sperm approached the egg by touching its spike on the egg surface (Fig. 4b), which was the

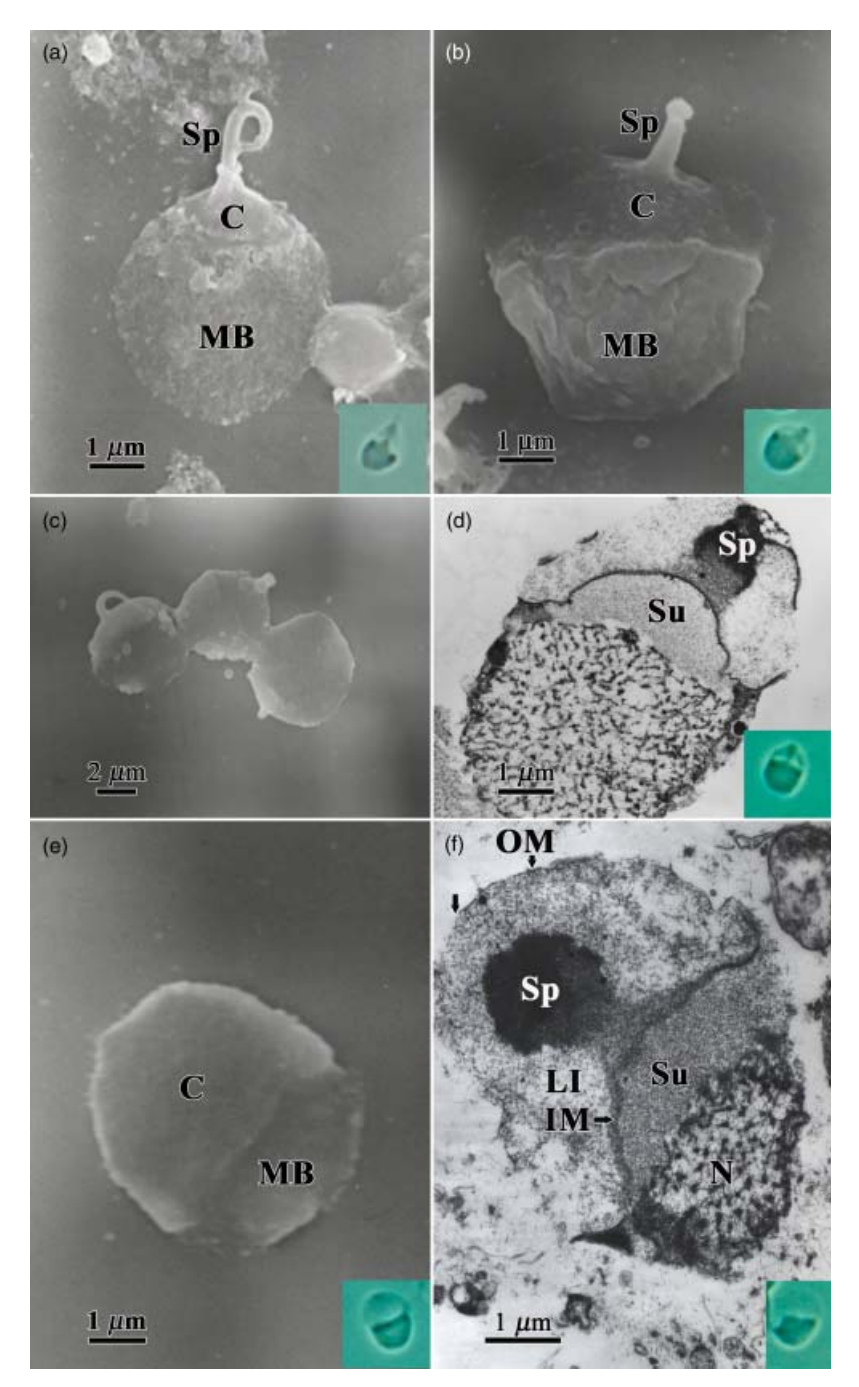


Figure 2 Scanning (a, b, c, e) and transmission (d, f) electron micrographs of the reacted sperm at 15 s after incubation with egg water. The insets correspond to LM pictures. The reaction begins with curling (a) and shortening (b, c, d) of the spike, followed by swelling of the cap (e). Using transmission electron microscopy, it was observed that the spike is reduced in length and shows only a stump in the cap region, which is markedly swollen (f). C, cap; IM, inner limiting membrane; LI, lowdensity inner layer; MB, main body; N, nucleus; OM, outer limiting membrane; Sp, spike; Su, subacrosomal region.

vitelline envelope. It then began the first phase of AR as it passed through the vitelline envelope (Fig. 4c and d) and was in contact with the cortical rod (Fig. 5a). Curling and degeneration of the sperm spike took place on the cortical rod surface (Fig. 5a), followed by penetration of the sperm into the substance of the cortical rod (Fig 5b). As the cortical rod was protruding, its content dispersed out and formed a jelly mate-

rial surrounding the egg surface (Fig. 5c). The reacted sperm on the surface of the jelly material developed the spherical mass only after being immersed in the jelly material (Fig. 5d). A clear zone was observed in the jelly material surrounding the spherical mass (Fig. 5e), which might suggest that the sperm excreted enzymes that digest its way through the jelly material. The ultrastructural features of this

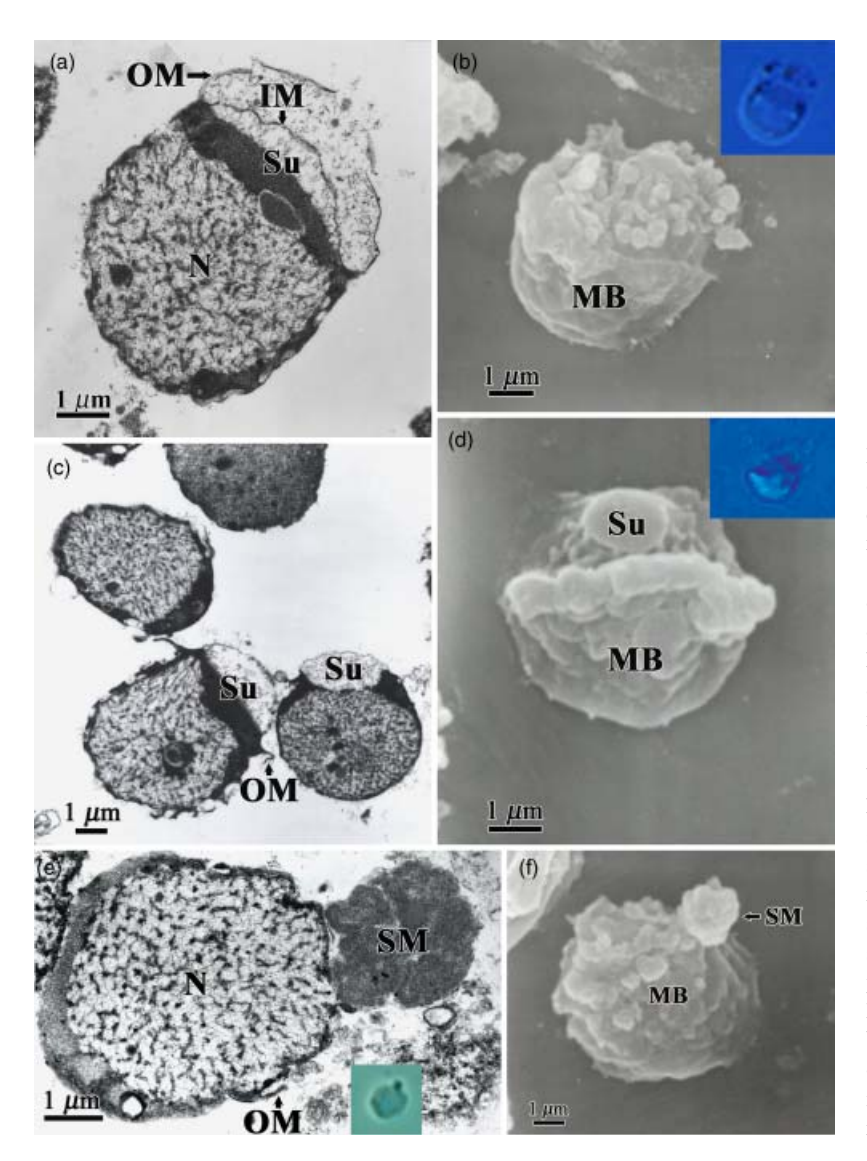


Figure 3 Transmission (a, c, e) and scanning (b, d, f) electron micrographs of the reacted sperm at exocytosis and formation of the spherical mass stage. The insets correspond to LM pictures. Following the disappearance of the spike, the outer limiting membrane is ruptured and the subacrosomal region begins to polymerize (a, b). Following the release of acrosomal content, the subacrosomal region becomes the most anterior part of the sperm (c, d) and becomes the spherical mass after complete polymerization (e, f). IM, inner limiting membrane; MB, main body; OM, outer limiting membrane; N, nucleus; Su, subacrosomal region; SM, spherical mass.

last stage of AR were identical to those of the in vitro sperm and the whole event was completed within 1 min post-spawning.

### **Discussion**

This study reveals that *P. monodon* sperm are a usual form of natantian sperm that have been reported in various shrimp species (Brown Jr., Kleve & Clark Jr. 1976; Kleve, Yudin & Clark Jr. 1980; Clark Jr. et al. 1981; Leung-Trujillo & Lawrence 1987; Pratoomchat et al. 1993; Rios & Barros 1997; Hall et al. 1999). They are non-motile, and composed of a single spike originating from the acrosomal region, a central cap with an acrosome and a subacrosomal region and a nucleus

of decondensed chromatin structures. In reptantian (crayfish, lobsters and crabs) sperm, the spikes are multiple, project from the nucleus and contain microtubules. The significant function of these nuclear extended spikes has not been explained, however (Yasuzumi 1960; Yasuzumi, Kaye, Pappas, Yamamoto & Tsubo 1961; Talbot & Summers 1978). The electrondense content of the spike may be a kind of contractile protein such as actin or other cytoskeletal proteins having depolymerizing or repolymerizing ability. The mechanism behind the curling and shortening of the spike is probably by depolarization of the cytoskeletal proteins.

In P. monodon sperm, the spherical main body contains the decondensed chromatin structure but the nuclear envelope was not observed. It is possible that

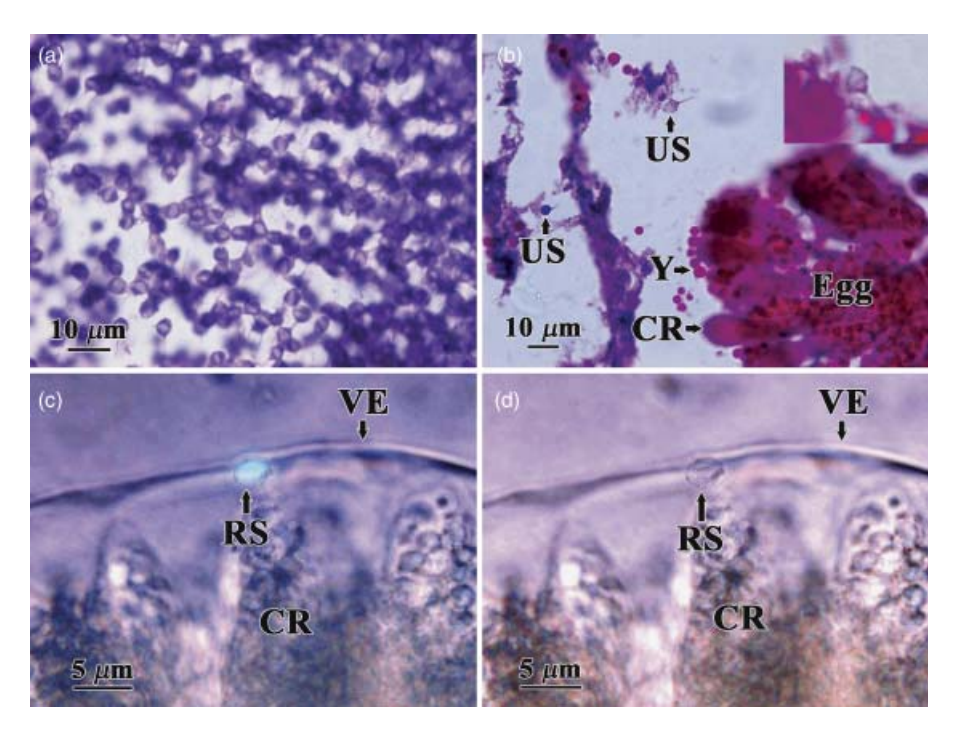


**Figure 4** Light micrographs of the ejected sperm in the water at spawning stained with haematoxylin and eosin (a, b) and with Hoechst staining observed under fluorescent (c) and differential interference contrast microscopy (d). Immediately after spawning, several unreacted sperm are observed (a) and some orient their spikes towards the egg surface (b, inset). Sperm located on the vitelline envelope (c, d) lacks a spike, suggesting that it could be a reacted one. CR, cortical rod; RS, reacted sperm; US, unreacted sperm; VE, vitelline envelope; Y, yolk granule.

breakdown of the nuclear envelope had occurred; the phenomenon was observed in natantian decapod crustaceans in concomitant with chromatin decondensation (Kleve *et al.* 1980). This phenomenon is believed to be important in preparing the sperm for fertilization.

The significance behind the different density layers (high and low) of the acrosome is not known at present. The low-density inner layer of the acrosomal content in *P. monodon* may be analogous to a similar structure of S. ingentis sperm that are in the AR process, which is arranged in a number of small pouches (Kleve et al. 1980). During exocytosis in P. monodon, the high-density outer and the low-density inner layers became enlarged, lightened and blended as a single layer. This phenomenon may be due to water influx from the external environment, which interacts with hydratable proteins, e.g. glycoproteins; the mechanism has been suggested for S. ingentis sperm and results in swelling and rupture of the pouch (Clark Jr. et al. 1981). In the lobster Homarus americanus, the acrosome contains a hydrolytic enzyme; the swelling of the cap is caused by this hydrolase and rapid hydration pulls the sperm forward to the

hatching envelope of the egg (Talbot & Chanmanon 1980). In mammals and sea urchins, the acrosomal exocytosis is usually accompanied by Ca<sup>2+</sup>-mediated fusion of membrane-enclosed acrosomal vesicle with the plasma membrane (Florman, Corron, Kim & Babcock 1992; Gonzalez-Martinez *et al.* 1992).

The subacrosomal region of P. monodon sperm taken from the female thelycum contained flocculent electron-lucent materials. These materials were found to be highly concentrated and more opaque than that of the subacrosomal region of sperm taken from the vas deferens and testes in the male (R. Vanichviriyakit, pers. comm.). The difference could be due to the higher degree of molecular cross linkages or molecular modifications of the subacrosomal contents, which is to prepare for the second phase of AR during fertilization. In S. ingentis and sea urchin, the formation of acrosomal process also originated from the subacrosomal region and, in sea urchin, the extension of the acrosomal process involves polymerization of subacrosome globular actin molecules (Schackmann et al. 1978; Tilney, Kiehart, Sardet & Tilney 1978; Griffin, Shigekawa & Clark Jr. 1988).

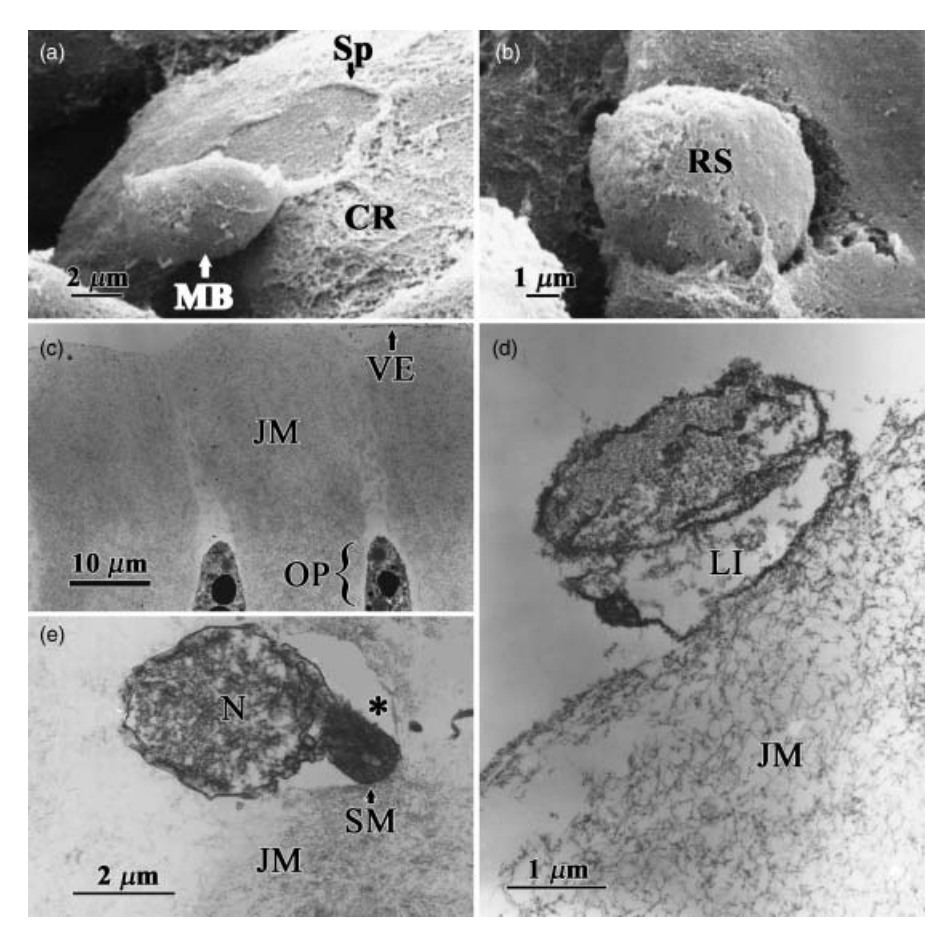


**Figure 5** Scanning (a, b) and transmission (c, d, e) electron micrographs of the sperm on the egg surface at actual spawning. A sperm on the surface of the protruding cortical rod shows a curled and degenerative spike (a) before sinking into the protruding cortical rod (b), which forms a jelly material surrounding the egg (c). The sperm attached to the jelly material shows a subacrosomal change (d) while penetrating into the material, with a clear space (\*) surrounding the spherical mass (e). CR, cortical rod; JM, jelly material; LI, low-density inner layer; MB, main body; N, nucleus; OP, ooplasm; RS, reacted sperm; Sp, spike; SM, spherical mass; VE, vitelline envelope.

This study shows that *P. monodon* sperm also has two phases of AR, similar to those of other marine species. The main point of interest here is what induces the first and the second phases of AR of the sperm. In *S. ingentis*, the first phase of AR occurs when the sperm is in contact the vitelline envelope of the egg (Wikramanayake & Clark Jr. 1994); a similar event occurs in *P. monodon* sperm as shown in this study. The acrosome of *P. monodon* sperm presumably contains enzymes that digest the vitelline envelope and allow the sperm to move forward; this mechanism has been shown in other species as well (Clark Jr. *et al.* 1981; Griffin *et al.* 1988; Wikramanayake & Clark Jr. 1994).

In the second phase, *P. monodon* sperm underwent this stage only after coming in contact with the jelly material released from the egg cortical rod. In sea urchin, AR occurs when the sperm contacts a jelly material surrounding the egg and causes an ion influx into the sperm (Neill & Vacquier 2004; Darszon, Nishigaki, Wood, Trevino, Felix & Beltran 2005). The substance in the jelly material of the sea urchin that could induce AR is sulfated fucan (Hirohashi, Ana-Cristina, Vilela-Silva, Mourao & Vacquier 2002). It is likely that similar substances in the jelly material of *P. monodon* egg induces AR of the sperm, probably with a similar mechanism; an ongoing study also suggests that the cortical rod of *P. monodon* contains sulphated fucan (Kruevaisayawan, pers. comm.).

Most of the *P. monodon* sperm under the *in vitro* and under actual spawning conditions had AR within 1–2 min upon contact with seawater, compared with

several minutes to more than an hour in other penaeoid shrimps, like *Trachypenaeus byrdi* and *Xiphopenaeus riveti* (Alfaro, Munoz, Vargas & Komen 2003). In those species, as well as in *P. monodon*, evidence has shown that capacitation of the sperm is accomplished while being in the thelycum (Alfaro *et al.* 2003; Vanichviriyakit *et al.* 2004). The fact that *P. monodon* sperm requires less time to complete AR suggests that their sperm is more reactive than sperm of other penaeids, which implies that the capacitation process in *P. monodon* may be more efficient than that of other species.

The results of this study form a basis for future evaluation of sperm quality in *P. monodon*, especially the domesticated ones. Besides the total sperm count, the ratio of reacted and unreacted sperm upon contacting EW and the morphological changes during AR could provide a reliable and better assessment of the sperm maturation in this highly economic species.

### **Acknowledgments**

This study was supported by the Center for Molecular Biology and Biotechnology of the National Science and Technology Development Agency (NSTDA), Thailand, Grant No. BT-B-06-SG-14-4505.

### References

- Alfaro J., Munoz N., Vargas M. & Komen J. (2003) Induction of sperm activation in open and closed thelycum penaeoid shrimps. Aquaculture 216, 371–381.
- Brown A. Jr., Kleve M.G. & Clark W.H. Jr. (1976) Evidence for the presence of actin in natantian sperm. American Zoology 16, 180.
- Clark W.H. Jr., Kleve M.G. & Yudin A.I. (1981) An acrosome reaction in natantian sperm. *Journal of Experimental Zool*ogy 218, 279–291.
- Collins F. & Epel D. (1977) The role of calcium ions in the acrosome reaction of sea urchin sperm. Experimental Cell Research 106, 211–222.
- Colwin A.L. & Colwin L.H. (1963) Role of the gamete membrane in fertilization in Saccoglossus kowalevskii (Enteropneustra) I. The acrosome reaction and its changes in early stages of fertilization. Journal of Cell Biology 19, 477–500.
- Darszon A., Nishigaki T., Wood C., Trevino C.L., Felix R. & Beltran C. (2005) Calcium channels and Ca<sup>2+</sup> fluctuations in sperm physiology. *International Review of Cytology* 243, 79–172.
- Fa Z.D., Lin W.G.C., Wei Y.H. & Shuai Z. (2004) Morphological and structural changes of sperm during the acrosome

- reaction in the swimming crab *Portunus trituberculatus*. *Acta Zoologica Sinica* **50**, 800–807.
- Florman H.M., Corron M.E., Kim T.D.-H. & Babcock D.F. (1992) Activation of voltage-dependent calcium channels of mammalian sperm in required for zona pellucida-induced acrosomal exocytosis. *Developmental Biology* 152, 304–314
- Gonzalez-Martinez M.T., Guerrero A., Morales E., de Ja Torre L. & Darszon A. (1992) A depolarization can trigger Ca<sup>2+</sup> uptake and the acrosome reaction when preceded by a hyperpolarization in *L. pictus* sea urchin sperm. *Developmental Biology* **150**, 193–202.
- Griffin F.J. & Clark W.H. Jr. (1990) Induction of acrosomal filament formation in the sperm of Sicyonia ingentis. Journal of Experimental Zoology 254, 296–304.
- Griffin F.J., Clark W.H. Jr., Crowe J.H. & Crowe L.M. (1987) Intracellular pH decrease during the in vitro induction of the acrosome reaction in the sperm of *Sicyonia ingentis*. *Biological Bulletin* 173, 311–323.
- Griffin F.J., Shigekawa K. & Clark W.H. Jr. (1988) Formation and structure of the acrosomal filament in the sperm of Sicyonia ingentis. Journal of Experimental Zoology 246, 94–102.
- Hall M.R., Young N. & Kenway M. (1999) Manual for the determination of egg fertility in Penaeus monodon. AIMS. Research. Australia, Available: http://www.aims.gov.au/pages/research/mdef/mdef-oo.html. [Accessed Aug 04 1999].
- Hirohashi N., Ana-Cristina E.S., Vilela-Silva P., Mourao A.S. & Vacquier V.D. (2002) Structural requirements for species-specific induction of the sperm acrosome reaction by sea urchin egg sulfated fucan. *Biochemical and Biophysical Research Communications* 298, 403–407.
- Kleve M.G., Yudin A.I. & Clark W.H. Jr. (1980) Fine structure of the unistellate sperm of the shrimp, Sicyonia ingentis (Natantia). Tissue and Cell 12, 29–45.
- Leung-Trujillo J.R. & Lawrence A.L. (1987) Observation on the decline in sperm quality of *Penaeus setiferus* under laboratory conditions. *Aquaculture* **65**, 363–370.
- Neill A.T. & Vacquier V.D. (2004) Ligands and receptors mediating signal transduction in sea urchin spermatozoa. *Reproduction* **127**, 141–149.
- Pillai M.C. & Clark W.H. Jr. (1987) Egg activation in the marine shrimp, Sicyonia ingentis. Journal of Experimental Zoology 244, 325–329.
- Pratoomchat B., Piyatiratitivorakul S. & Menasveta P. (1993) Sperm quality of pond-reared and wild-caught *Penaeus monodon* in Thailand. *Journal of World Aquaculture Society* **24**, 530–540.
- Rios M. & Barros C. (1997) Trypsin-like enzymes during fertilization in the shrimp Rhynchocinetes typus. Molecular Reproduction and Development 46, 581–586.
- Schackmann R.W., Eddy E.M. & Shapiro B.M. (1978) The acrosome reaction of *Strongylocentrotus purpuratus* sperm: ion requirements and movements. *Developmental Biology* 65, 483–495.

1643

- SeGall G.K. & Lennarz W.J. (1979) Chemical characterization of the component of the jelly coat from sea urchin eggs responsible for induction of the acrosome reaction. *Devel*opmental Biology 71, 33–48.
- Talbot P. & Chanmanon P. (1980) Morphological features of the acrosome reaction of lobster (*Homarus*) sperm and the role of the reaction in generating forward sperm movement. *Journal of Ultrastructure Research* 70, 287–297.
- Talbot P. & Summers R.G. (1978) The structure of sperm from *Panulirus*, the spiny lobster, with special regard to the acrosome. *Journal of Ultrastructure Research* 64, 341–351.
- Tan-Fermin J.D. & Pudadera R.A. (1989) Ovarian maturation stages of the wild giant tiger prawn *Penaeus monodon* Fabricius. *Aquaculture* **77**, 229–242.
- Tilney L.G., Kiehart D.P., Sardet C. & Tilney M. (1978) Polymerization of actin. IV. Role of  $Ca^{2+}$  and  $H^{+}$  in the assembly of actin and in membrane fusion in the acrosomal reaction of echinoderm sperm. *Journal of Cell Biology* **77**, 536–560.

- Vanichviriyakit R., Kruevaisayawan H., Weerachatyanukul W., Pongtippatee-Tawipreeda P., Withyachumnarnkul B., Pratoomchat B., Chavadej J. & Sobhon P. (2004) Molecular modification of *Penaeus monodon* sperm in female thelycum and its consequent responses. *Molecular Reproduction and Development* 69, 356–363.
- Wikramanayake A.H. & Clark W.H. Jr. (1994) Two extracellular matrices from oocytes of the marine shrimp Sicyonia ingentis that independently mediate only primary or secondary sperm binding. Development, Growth and Differentiation 36, 89–101.
- Yasuzumi G. (1960) Spermatogenesis in animals as revealed by electron microscopy. VII. Spermatid differentiation in the crab, *Eriocher japonicus*. *Journal of Biophysical and Biochemical Cytology* **7**, 73–78.
- Yasuzumi G., Kaye G.I., Pappas G.D., Yamamoto H. & Tsubo I. (1961) Nuclear and cytoplasmic differentiation in developing sperm of the crayfish *Cambaroides japonicus*. Zeitschrift fuer Zellforschung und Mikroskopische Anatomie **53**, 141–158.

### REGULAR ARTICLE

## Spermiogenesis and chromatin condensation in the common tree shrew, *Tupaia glis*

Worawit Suphamungmee • Chaitip Wanichanon • Rapeepun Vanichviriyakit • Prasert Sobhon

Received: 25 May 2007 / Accepted: 13 November 2007 / Published online: 19 December 2007 © Springer-Verlag 2007

Abstract We have investigated the cellular characteristics, especially chromatin condensation and the basic nuclear protein profile, during spermiogenesis in the common tree shrew, Tupaia glis. Spermatids could be classified into Golgi phase, cap phase, acrosome phase, and maturation phase. During the Golgi phase, chromatin was composed of 10-nm and 30-nm fibers with few 50-nm to 60-nm knobby fibers. The latter were then transformed into 70-nm knobby fibers during the cap phase. In the acrosome phase, all fibers were packed into the highest-order knobby fibers, each about 80-100 nm in width. These chromatin fibers became tightly packed in the maturation phase. In a mature spermatozoon, the discoid-shaped head was occupied by the acrosome and completely condensed chromatin. H3, the core histone, was detected by immunostaining in all nuclei of germ cell stages, except in spermatid steps 15-16 and spermatozoa. Protamine, the basic nuclear protein causing the tight packing of sperm chromatin, was detected by immunofluorescence in the nuclei of spermatids at steps 12-16 and spermatozoa. Cross-immunoreactivity of T. glis H3 and protamine to those of primates suggests the evolutionary resemblance of these nuclear basic proteins in primate germ cells.

**Keywords** Spermiogenesis · Sperm · Chromatin condensation · Histone · Protamine · Tree shrew, *Tupaia glis* (Scandentia)

This work was supported by the Thailand Research Fund (Senior Research Fellowship to Prof. Prasert Sobhon).

W. Suphamungmee · C. Wanichanon (⋈) ·

R. Vanichviriyakit · P. Sobhon

Department of Anatomy, Faculty of Science, Mahidol University, Rama VI Road.

Bangkok 10400, Thailand e-mail: sccwn@mahidol.ac.th

### Introduction

The process of spermatogenesis in mammals involves the mitotic division of spermatogonia; the first meiotic division yields spermatocytes, and the second meiotic division gives rise to spermatids that differentiate into spermatozoa (Clermont 1972; Kerr 1992; Johnson 1995; De Kretser et al. 1998; Lombardi 1998). During the last step, which is called spermiogenesis, unique events take place that comprise the condensation of the nuclear chromatin (Lalli and Clermont 1981), formation of the acrosome (Leblond and Clermont 1952a; Clermont and Leblond 1955; Bernstein and Teichman 1972), virtual elimination of the cytoplasm, and development of the tail with the arrangement of mitochondria into a helical formation in the midpiece (Oko and Clermont 1991; Turner 2006).

During spermiogenesis in mammals, the somatic-type basic nuclear proteins (histones) are partly replaced by testis-specific lysine-rich histones, which consist of H1t, TH2A, TH2B, and TH3 (Oko et al. 1996; Steger et al. 1998; Ausio 1999). These proteins are then replaced by the more basic nuclear proteins enriched in arginines, termed transitional proteins (Moneisi 1971; Martinage et al. 1990). Finally, transitional proteins are replaced by protamines, which are proteins relatively rich in arginine and cysteine (Balhorn 1982; Roux et al. 1988; Le Lannic et al. 1993; Kistler et al. 1996). Protamines are believed to be the major factor that results in the final condensation and tight packaging of the chromatin, events that partly lead to the formation of a variety of shapes of sperm heads in several mammalian species (Calvin and Bedford 1971; Calvin 1976; Chevaillier 1983; Dadoune and Alfonsi 1986; Auger and Dadoune 1993; Brewer et al. 1999). In human sperm, protamines induce the coiling of the DNA molecules into a doughnut structure called a toroid. Each toroidal loop



contains about 500 bp of DNA, and the torus grows in size as subsequent loops bind to previous loops (Balhorn et al. 1999). In addition to nucleoprotamines, approximately 15% of the DNA in human sperm is still packaged by histones in the form of nucleosomal type fibers (Tanphaichitr et al. 1978). Apart from the toroidal model, which is believed to occur in human sperm, other patterns of packaging are also possible in other mammalian species. For example, the nucleoprotamine fibers may be packed laterally into a bundle-type structure as appears in rat sperm (Wanichanon et al. 2001).

Evolutionarily, the common tree shrew (*Tupaia glis*) is considered to be a primitive primate with many similar characteristics to those possessed by the ancestor of the present day primates (Poonkhum et al. 2000). Spermatogenesis and the stages of seminiferous epithelium have been studied by Maeda et al. (1996). However, to date, no data are available concerning the ultrastructure of differentiating male germ cells of the common tree shrew, particularly during spermiogenesis. Therefore, the objectives of this work have been to study the ultrastructural characteristics of spermiogenic cells of the common tree shrew, especially with regard to their chromatin organization and the profile of their basic nuclear proteins.

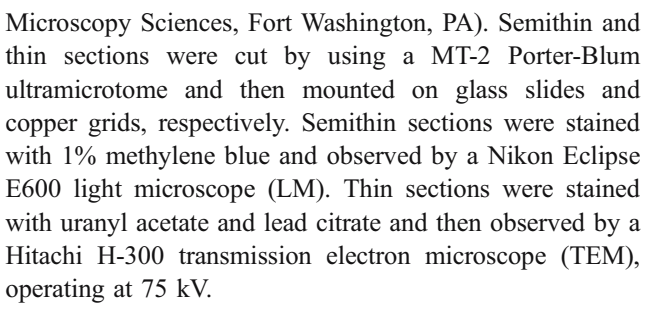
### Materials and methods

Specimen collection

Adult common tree shrews (*Tupaia glis*) were captured in a tropical forest area in Thailand. A total of 10 animals (120–180 g body weight) were studied. They were anesthetized with ether, and then their testes were removed, fixed, and prepared for light- and electron-microscopic observations. Alternatively, pieces of tissues were prepared for immunohistochemical localization and profiling of basic nuclear proteins.

Histological and ultrastructural observations

Testes were fixed in Bouin's fixative overnight, after which they were dehydrated in graded ethanol and embedded in paraffin blocks. Sections were cut at a thickness of 5 μm and stained with hematoxylin and eosin. In order to investigate the ultrastructure of the germ cells, pieces of testes were fixed immediately in 4% glutaraldehyde and 2% paraformaldehyde in 0.1 M phosphate-buffered saline (PBS), pH 7.4 at 4°C, overnight, and then washed several times with PBS. Specimens were postfixed in 1% osmium tetroxide in 0.1 M PBS, at 4°C for 1 h, washed with the same buffer, dehydrated in increasing concentrations of ethanol, and embedded in Araldite 502 resin (Electron



The size of the chromatin fibers in each step of germ cell development was measured from electron-microscopic negatives in a Nikon Profile Projector and compared with the lattice intervals (~0.232 Å) of catalase crystals (Agar Aids, Stansted, UK) at the same magnifications. At least 10 cells at each stage were used for chromatin fiber measurements.

Extraction of basic nuclear proteins from nuclei of testicular cells

Fresh testes from adult animals were dissected, and the basic nuclear proteins were extracted according to Suphamungmee et al. (2005). Briefly, testes were homogenized in cold incubation buffer consisting of 3 mM MgCl<sub>2</sub>, 0.31 M sucrose, 0.01% Triton X-100, 10 mM KH<sub>2</sub>PO<sub>4</sub>, pH 6.0, and 1 mM phenylmethane sulfonyl-fluoride (PMSF). The homogenate was centrifuged at 600g, at 4°C, for 10 min, and the supernatant was then discarded. The pellet was resuspended in a solution containing 0.15 M NaCl, 1% Triton X-100, 10 mM TRIS-HCl, pH 8.0, and 1 mM PMSF at 4°C. The suspension was placed on ice and sonicated six times for 15 s each, with a 15-s interval. Separation of the nuclei of the testicular cells from the tail debris was confirmed by viewing under a microscope. The nuclear suspension was washed twice in the washing buffer (5 mM MgCl<sub>2</sub>, 5 mM NaH<sub>2</sub>PO<sub>4</sub>, pH 6.5) followed by centrifugation at 8,000g, at 4°C. The pellet was treated in a reducing solution (0.15 M NaCl, 10 mM dithiothreitol, 50 mM TRIS-HCl, pH 8.0) at 4°C, for 1 h. Thereafter, the nuclei were dissolved in 0.4 N hydrochloric acid and maintained at 4°C, for 2 h. The supernatant was removed after centrifugation at 12,000g, at 4°C, for 10 min, and the basic nuclear proteins were precipitated by 20% trichloroacetic acid. The precipitated proteins were then centrifuged at 12,000g, at 4°C, for 10 min. The pellet was washed twice in cold acidified acetone and in several changes of cold acetone. Finally, the protein pellet was dried in vacuum desiccators for 1 h and stored at -20°C until used.

Acid-urea-Triton X-100 polyacrylamide gel electrophoresis

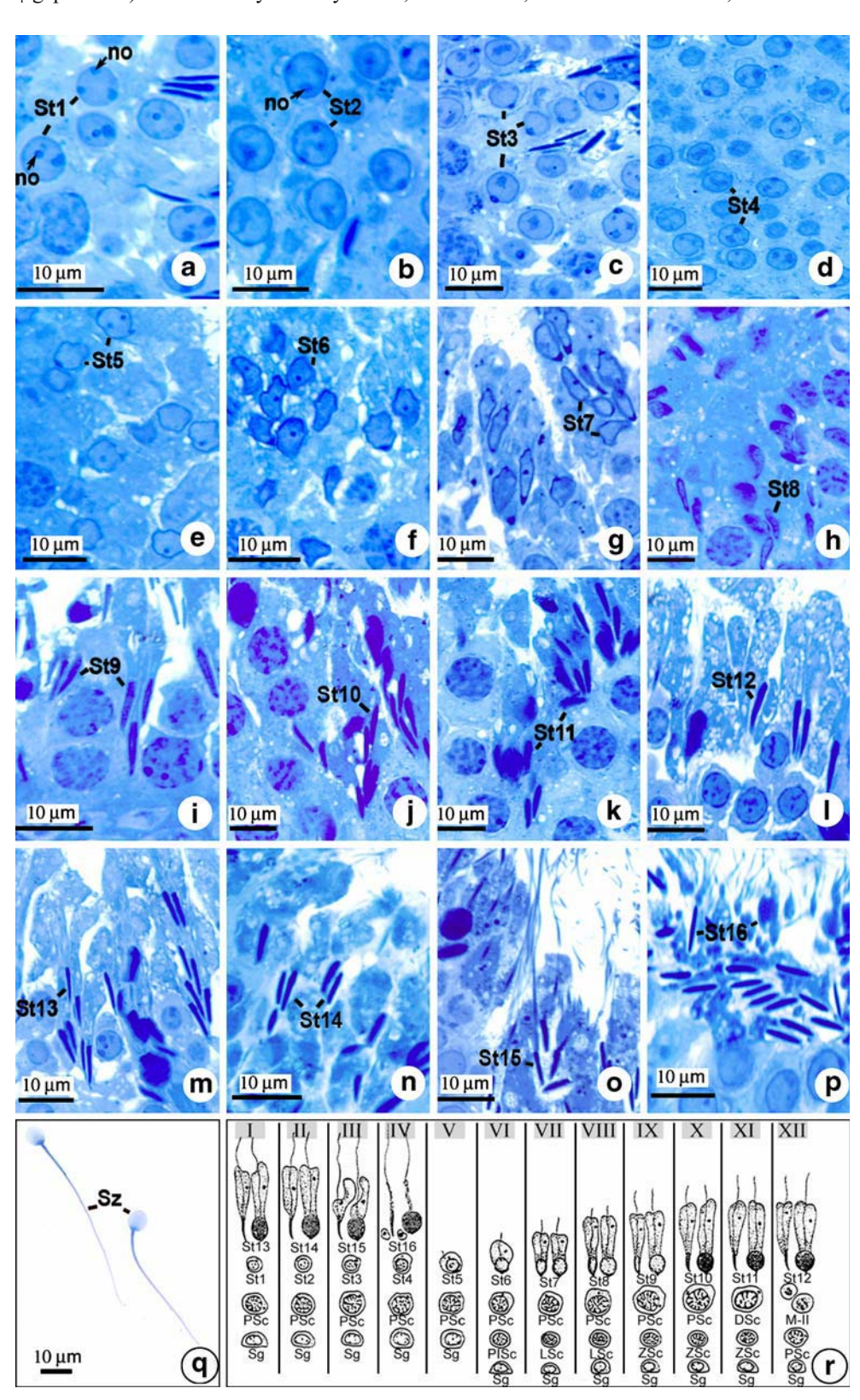
Extracted basic nuclear proteins from the testes were dissolved in sample buffer (1 ml glacial acetic acid, 5.4 g urea,



 $0.5 \text{ ml }\beta$ -mercaptoethanol, 0.1% pyronin-G in 4.5 ml deionized water). The protein concentration was determined by using bovine serum albumin as the standard (Lowry et al. 1951). The protein sample (15  $\mu$ g per well) was carefully

loaded onto acid-urea-Triton X-100 polyacrylamide gel (AUT gel; resolving gel: 15% acrylamide, 2.5 M urea, 6 mM Triton X-100, 5% acetic acid; stacking gel: 7.5% acrylamide, 2.5 M urea, 4 mM Triton X-100, 1.5% acetic

Fig. 1 Semithin sections stained with methylene blue showing the stages of seminiferous epithelium based on acrosome development and chromatin condensation during spermiogenesis. Developing spermatids (St) partly embedded in the cytoplasm of Sertoli cells are classified into the Golgi phase (St1-St2 in a, b), cap phase (St3-St5in c-e), early acrosome phase (St6-St8 in f-h), mid acrosome phase (St9-St11 in i-k), late acrosome phase (St12-St14 in I-n), and maturation phase (St15-St16 in  $\mathbf{o}$ ,  $\mathbf{p}$ ). Whole-mounts of mature spermatozoa (Sz in q) demonstrate the discoid shape of the head. The 12 stages of cellular association of seminiferous epithelium in the T. glis testis, as modified from Maeda et al. 1996, are also shown in r



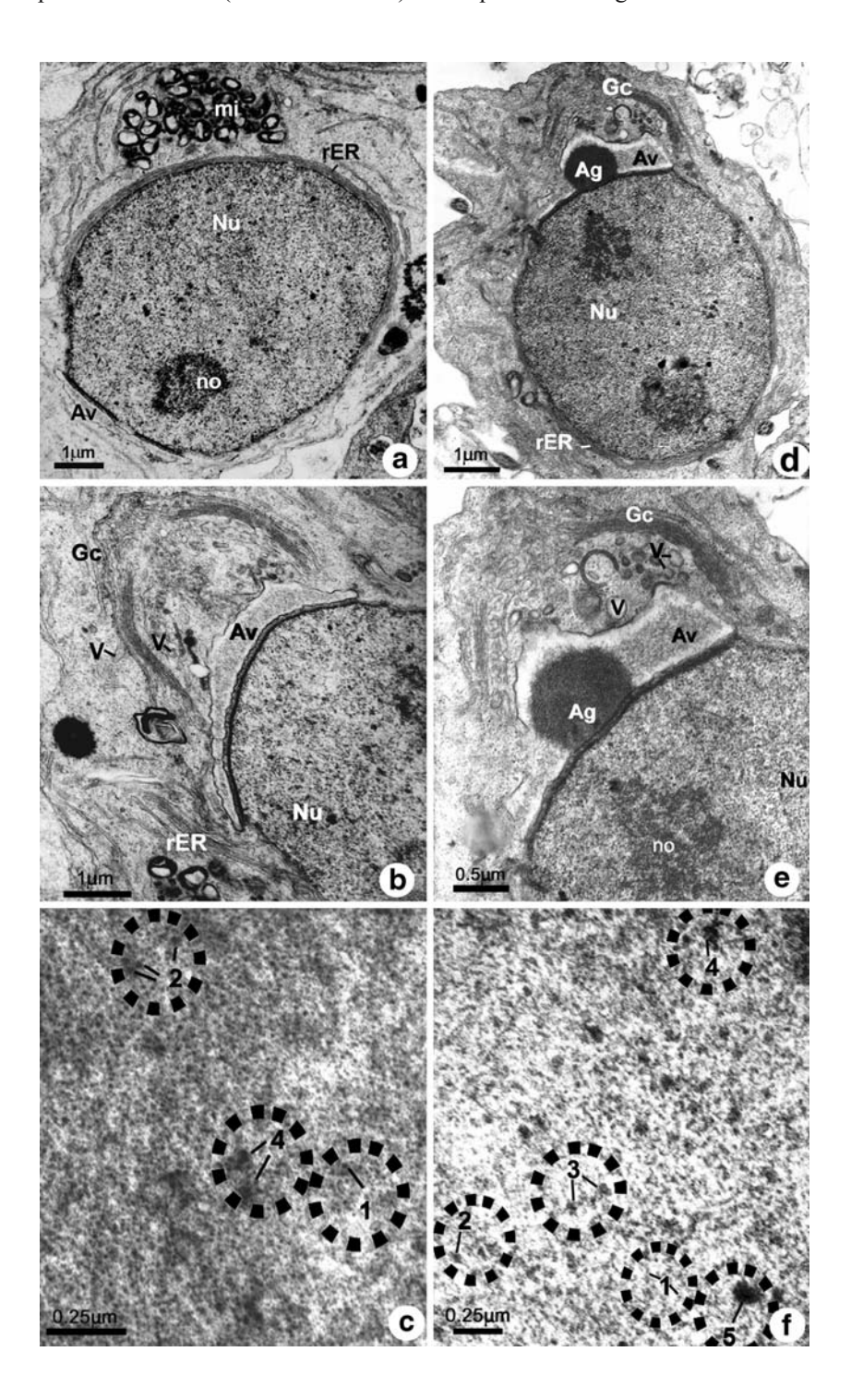


acid) in a 8×10 cm Hoefer vertical slab gel electrophoretic apparatus fitted with 0.75-mm spacers (Amersham Biosciences, USA; as modified from Panyim and Chalkley 1969). The separation was carried out in an electrophoretic buffer (0.9 N acetic acid) at 120 V, for 1.5 h. The bands of basic nuclear proteins were detected by Coomassie blue staining. Basic nuclear proteins similarly prepared from chick erythrocyte nuclei and human testicular nuclei were run under the same conditions and used for comparison.

Fig. 2 a-c Ultrastructure of the early round spermatids in the Golgi phase (steps 1-2) showing many mitochondria (mi) and the nucleus (Nu) with a prominent nucleolus (no). The Golgi complex (Gc) is a conspicuous structure in close association with proacrosomal vesicles (V). The nucleus contains chromatin fibers (c) with diameters of 10 nm (circle 1), 30 nm (circle 2), and 50-60 nm (circle 4). d-f Longitudinal sections of the cap phase spermatids (steps 3-5) showing the round nucleus (Nu) surrounded by rough endoplasmic reticulum (rER). The Golgi complex (Gc) is prominent and shows many proacrosomal vesicles (V). These vesicles fuse together to form the large cap of the acrosomal vesicle (Av), which contains a large acrosomal granule (Ag) attached to the inner acrosomal membrane. A higher magnification (f) shows five types (levels) of chromatin fibers dispersed throughout the nucleus: the 10-nm (circle 1) and the 30-nm (circle 2) fibers are most abundant, whereas fewer 40-45 nm (circle 3), 50-60 nm (circle 4), and 70-nm (circle 5) fibers

Western blot analysis of basic nuclear proteins

Basic nuclear proteins separated in AUT gel were electrophoretically transferred onto nitrocellulose membrane (Amersham Biosciences, Buckinghamshire, UK) in an electrophoretic transfer chamber (LKB Bromma, Hoefer Scientific Instruments, San Francisco, Calif.) with the current set at 400 mA, for 4 h, in cold transfer buffer (0.9 N acetic acid). Non-specific binding was blocked with





are seen

5% skim milk in 10 mM TRIS-buffered saline, pH 7.4, containing 0.1% Tween-20 (TBST), and then the membranes were incubated in mouse monoclonal antibody raised against human protamine P1N (1:500 dilution) or rabbit polyclonal antibody to chick-histone H3 (1:500 dilution) for 1 h at room temperature. For the negative control, the membrane strips were incubated with preimmune sera instead of the primary antibody. After being washed with TBST, the membranes were incubated in goat anti-mouse IgG or mouse anti-rabbit IgG conjugated to horseradish peroxidase (Zymed laboratories, San Francisco, Calif.) in TBST (1:2,000 dilution), for 30 min at room temperature. The color reaction was visualized by using diaminobenzidine as a chromogenic substrate (Sigma-Aldrich, Saint Louis, Mo.) and 0.013% H<sub>2</sub>O<sub>2</sub>.

Indirect immunofluorescence staining of basic nuclear proteins in testicular cells

Testes were dissected and fixed in a solution containing 0.5% glutaraldehyde, 4% paraformaldehyde in 0.1 M phosphate buffer, pH 7.4, at 4°C, for 2 h. Following a washing step in the same buffer, the specimens were dehydrated in an ethanol series and embedded in LR white resin (Electron Microscopy Sciences). Semithin sections were cut by using a MT-2 Porter-Blum ultramicrotome fitted with glass knives, picked up, and placed on the gelatin-coated glass slides. Non-specific binding was blocked by incubating the tissue sections with 0.15 M glycine and with 4% bovine serum albumin (Sigma-Aldrich). The sections were then incubated with rabbit polyclonal antibody against chicken-H3 (1:50 dilution) or mouse monoclonal antibody against human-protamine,

P1N fraction (1:100 dilution) for 1 h, at 37°C, and then treated with fluorescein-isothiocyanate (FITC)-conjugated goat anti-rabbit IgG or rabbit anti-mouse IgG (Zymed laboratories) as secondary antibodies, for 30 min, at 37°C, followed by observation under a fluorescence microscope. Negative control sections were processed similarly but were incubated with preimmune sera in place of the primary antibodies.

### Results

Testes of the common tree shrew were oval in shape and covered by a layer of tunica vaginalis on the anterior surface. The seminiferous tubules with the interstitial (Leydig's) cells were covered by a layer of tunica albuginea, a dense fibrous connective tissue capsule that was thickened on the posterior surface of the testes, whereas a layer of tunica vasculosa was not observed in any sections. In contrast to other mammals, the tunica albuginea did not extend inward to form the connective tissue septae dividing the testis into lobules.

The cycle of seminiferous epithelium in the common tree shrew was classified into 12 stages (Fig. 1r) as reported earlier by Maeda et al. (1996), and each cross section of the seminiferous tubule represented a single stage of cellular association. As in other mammals, the basal compartment of the epithelium contained the preleptotene and leptotene steps of primary spermatocytes, whereas the adluminal compartment contained the middle steps of differentiating cells from the zygotene and pachytene steps of primary spermatocytes up to spermatids.

**Table 1** Summary of six orders of chromatin organization (*Levels 1–6*), as appearing in various stages of spermatids of the common tree shrew (*SE* standard error of mean, – absent)

Spermiogenic cells	Chromatin fibers (diameter±SE)					
	Level 1 (10 nm)	Level 2 (30 nm)	Level 3 (40–45 nm)	Level 4 (50–60 nm)	Level 5 (70 nm)	Level 6 (80–100 nm)
Golgi phase spermatids (steps 1–2)	10.14±0.11	29.60±0.12	_	54.04±1.59	_	_
Cap phase spermatids (steps 3–5)	10.19±0.09	29.75±0.16	41.13±1.84	_	$70.02 \pm 0.08$	_
Early acrosome phase spermatids (steps 6–8)	10.03±0.07	29.60±0.31	_	56.97±2.95	69.92±0.11	_
Mid acrosome phase spermatids (steps 9–11)	-	_	41.12±2.31	_	69.65±0.18	-
Late acrosome phase spermatids (steps 12–14)	_	_	_	_	_	88.49±4.19
Maturation phase spermatids (steps 15–16)	Complete condensation					



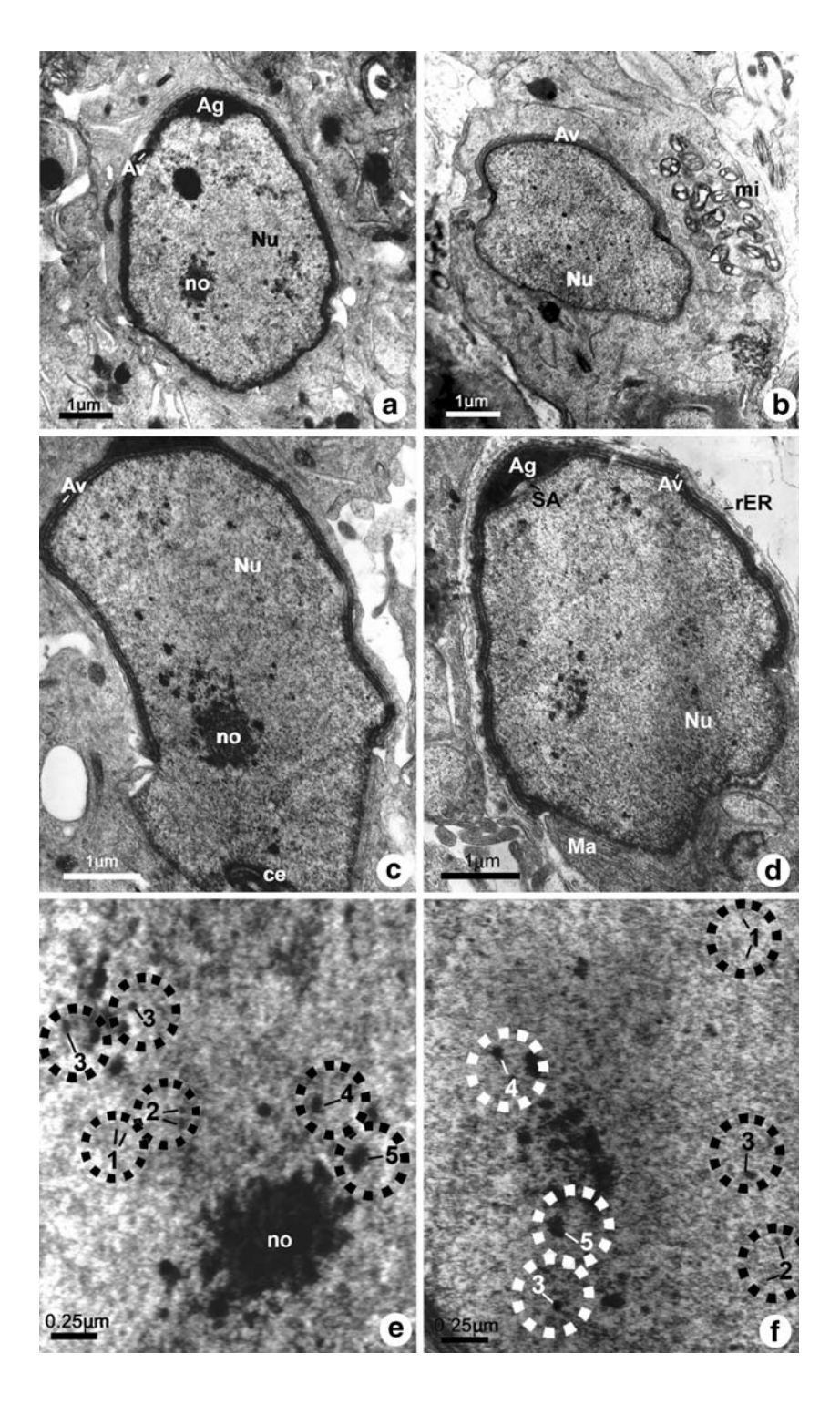
Histological and ultrastructural characteristics of spermiogenic cells

As in other mammals, four phases of spermatid differentiation could be distinguished according to acrosome development and the pattern of chromatin condensation in the nucleus, i.e., Golgi phase, cap phase, acrosome phase, and maturation phase. Based on observations at the LM and

TEM levels, these four phases of spermatids of the common tree shrew could be subdivided into 16 steps (Fig. 1).

Golgi phase (steps 1-2) These spermatids were characterized by the presence of spherical nuclei ( $\sim$ 7  $\mu$ m in diameter) with prominent nucleoli (Figs. 1a,b, 2a). Golgi apparatus was conspicuous and associated with small membrane-bound vesicles that were possible precursors of

Fig. 3 a, b Early acrosome phase spermatids (steps 6-8) demonstrating nuclear elongation (Nu). The acrosomal cap (Av) extends backward to the sides of the nucleus, and mitochondria (mi) still aggregate adjacent to one pole of the nucleus. c, d During caudal extension of the acrosomal cap, the subacrosomal space (SA) is observed beneath the entire acrosome. Microtubular manchettes (Ma) first appear at the caudal end of nucleus, and the proximal centriole (ce) is attached at the distal end of the nucleus. e, f The nuclear chromatin in this phase shows five levels of chromatin fibers: the 10-nm (circle 1) and 30-nm (circle 2) fibers are numerous, whereas the 40-nm to 45-nm (circle 3), 50-nm to 60-nm (circle 4), and 70-nm (circle 5) fibers are more sparse (no nucleolus)





the proacrosomal vesicles (Fig. 2b). Mitochondrial clusters were located near the Golgi apparatus. Rough endoplasmic reticulum was present throughout the cytoplasm (Fig. 2a,b). Within the nucleus, chromatin was dispersed homogeneously and showed dense circular masses possibly representing the reappearing nucleoli (Figs. 1a,b, 2a). The chromatin fibers could be classified into three groups (levels): (1) the fine 10-nm fibers that were the major component of euchromatin in the nucleus, (2) the 30-nm fibers, which were dispersed throughout the nucleoplasm and appeared in smaller quantities, amd (3) the largest fibers (50-60 nm in diameter) surrounding the heterochromatin mass, which was composed of clusters of the 30-nm fibers (Fig. 2c, Table 1). At step 2 of this phase, the membrane-bound vesicles from the Golgi apparatus began to fuse together forming a large acrosomal vesicle (Fig. 2b). The chromatin appeared denser, especially along the inner surface of the nuclear envelope, whereas the nucleolus became less prominent (Figs. 1b, 2b).

ized by the presence of acrosomal vesicles that increased further in size and covered the apical pole of their nuclei (Figs. 1c-e, 2d-f). A layer of electron-dense material was

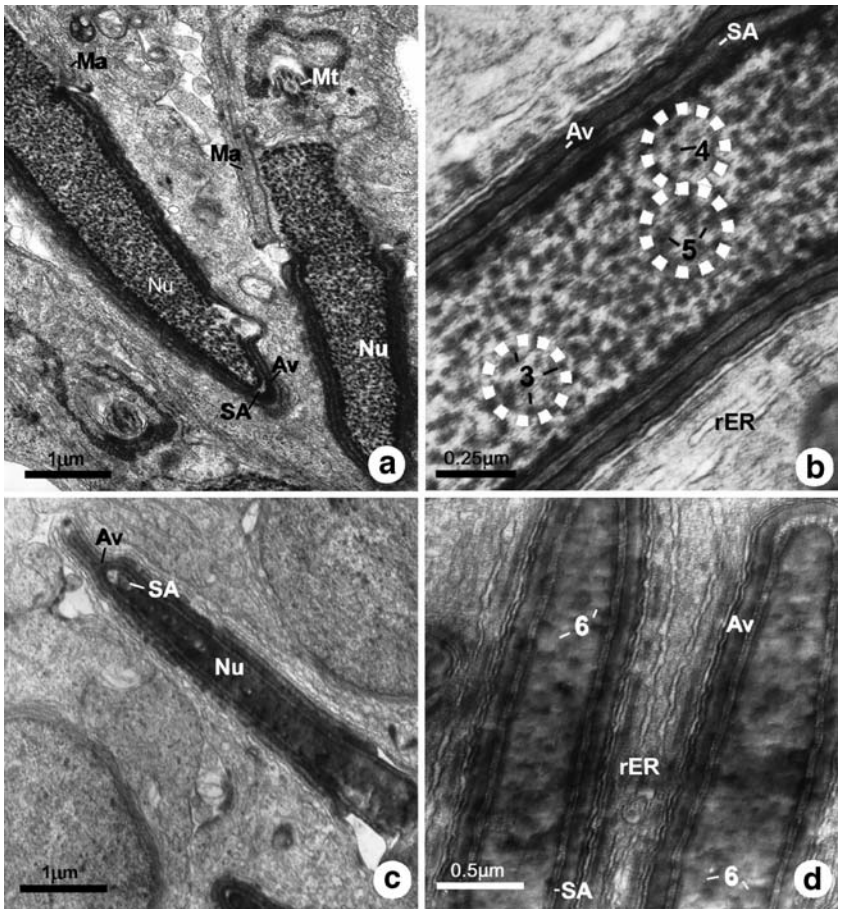
Cap phase (steps 3-5) Cells in this phase were character-Fig. 4 a, b Mid acrosome phase spermatids (steps 9–11) showing the acrosome (Av) covering the apical pole of the nucleus (Nu), which becomes progressively elongated and highly condensed. Microtubular manchettes (Ma)

bular axoneme, SA subacrosomal space). The nucleus contains chromatin fibers with thicknesses of 40-45 nm (circle 3), 50-60 nm (circle 4), and 70 nm (circle 5). c, d Longitudinal sections of late acrosome phase spermatids (steps 12-14) displaying the more elongating and condensing nucleus covered by an acrosome (Av). Chromatin fibers in the nucleus (Nu) become larger at 80-100 nm (6) in thickness. Rough endoplasmic reticulum (rER) still appears to surround

the acrosome and nucleus

are seen adjacent to the caudal half of the nucleus (Mt microtuattached to the inner surface of the acrosomal vesicle. An acrosomal granule was produced and appeared as a large dense body associated with the center of the inner acrosomal membrane (Fig. 2d-f). The enlarged acrosome with the acrosomal granule finally formed a cap-like structure covering the anterior pole of the nucleus, and only a narrow subacrosomal space was present between the inner acrosomal membrane and the nuclear membrane (Fig. 2f). The nucleus itself remained spherical (7–8 μm in diameter) and contained chromatin fibers that became thicker. The majority of fibers were at the levels of 10 nm and 30 nm and were dispersed throughout the nucleus (Fig. 2f). Thicker chromatin fibers with diameter of 40-45 nm and fewer fibers at 50-60 nm and 70 nm started to appear (Fig. 2f, Table 1).

Early acrosome phase (steps 6–8) The cell and nucleus began to elongate (Fig. 1f-h). The narrow electron-dense acrosome expanded over the anterior half of the nucleus (Fig. 3a-c). The proximal centriole was located in the depression at the caudal end of the nucleus (Fig. 3c). A microtubular manchette appeared in the cytoplasm adjacent to the nuclear membrane (Fig. 3d). The mass of cytoplasm, containing mitochondria, began to move caudally. At the





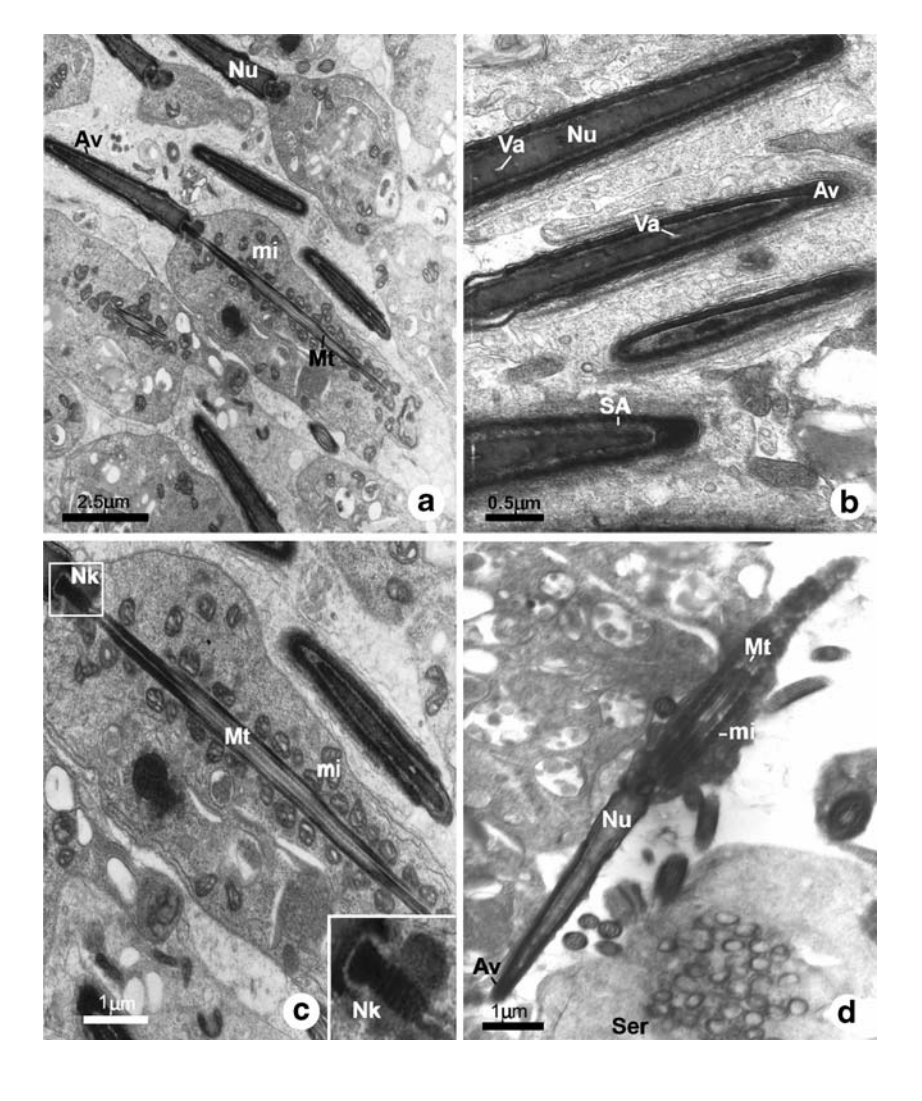
LM level, the nuclear material appeared to become increasingly denser (Fig. 1f–h); as revealed by TEM, the chromatin fibers appeared in five levels, i.e., with the majority still at 10 nm and 30 nm, but with thicker fibers at 50 nm, 60 nm, and 70 nm increasing in number (Fig. 3e,f, Table 1), and 40-nm to 45-nm fibers being present in smaller quantities.

Mid acrosome phase (steps 9–11) The nucleus and acrosome continued to elongate to such an extent that the nucleus assumed a distinctive wedge shape (Fig. 1i–k). The acrosome became condensed and assumed an arrow-shape that extended over the entire rostral end of the nucleus (Fig. 4a,b). At the last step of this phase, nuclear elongation reached its greatest length (Fig. 1k). At the LM level, the nuclear material appeared dense (Fig. 1i–k), and as revealed by TEM, the chromatin consisted of 70-nm knobby fibers disposed along the nuclear membrane, whereas the 10-nm and 30-nm fibers had disappeared. However, the majority of chromatin was made up of 40–45 nm fibers and a smaller amount of 50–60 nm fibers, most of which

appeared as dense cords distributed throughout the nucleus (Fig. 4b, Table 1). Some rough endoplasmic reticulum surrounded the acrosome and nuclear membrane (Fig. 4b). The microtubular manchette continued to extend from the posterior end of the acrosome to the caudal end of the nucleus (Fig. 4a). The cytoplasmic mass containing the mitochondria continued to move to the caudal end of the cell (Fig. 5a).

Late acrosome phase (steps 12–14) The spermatids in this phase were characterized by highly elongated heads that became slimmer than those of the earlier steps (Fig. 11–n, 4c,d). The cytoplasmic mass continued to move caudally, leaving only a small amount over the acrosome (Fig. 4c). The main body of the acrosome remained at the rostral end of the nucleus, but its lateral margins extended over the caudal end of the nucleus (Fig. 4c–d). At the LM level, the nuclear material appeared to be completely dense (Fig. 11–n); TEM revealed that most chromatin fibers occurred as large 80-nm to 100-nm knobby fibers that became closely packed (Fig. 4d, Table 1).

Fig. 5 a, b Maturation phase spermatids (steps 15-16) demonstrating the complete condensation of chromatin within the nucleus (Nu). The acrosome (Av) is clearly visible with its underlying subacrosomal space (SA). The nucleus contains a few vacuoles (Va). c Higher magnification of the tail showing the small amount of intact cytoplasm that moves caudally. The neck (Nk) is located at the caudal end of the nucleus and attached to the tail axoneme Numerous mitochondria (mi) are present around the microtubular axoneme (Mt)of the tail. Inset Detail of the neck region in the boxed area. d Longitudinal section of a spermatozoon released from the cytoplasm of a Sertoli cell (Ser). The head contains completely condensed chromatin and only a few vacuoles in the nucleus (Nu). At the midpiece, mitochondria (mi) are packed as a mitochondrial sheath around an axoneme (Mt)





Maturation phase (steps 15–16) The spermatids in this phase showed similar ultrastructural characteristics to those of mature spermatozoa (Figs. 1o-p, 5a-c). Chromatin fibers coalesced into a dense mass, but the nucleus still contained small electron-lucent vacuoles within the increasingly compact chromatin (Fig. 5b). All the cytoplasmic mass was relocated to the posterior end of the nucleus and became the residual body (Figs. 1o-p, 5a,c). The fully formed tail showed the helically arranged mitochondria surrounding a column of the outer dense fibers and an axoneme (Fig. 5a,c).

Mature spermatozoa The spermatozoa were freely distributed in the lumen of the seminiferous tubule after shedding their residual cytoplasm and being released from the apical cytoplasm of the Sertoli cells (Fig. 5d). In whole-mounts, the head had a discoidal shape of approximately 6×9 μm (Fig. 1q), whereas in side view, the head was a thin wedgeshaped structure (Fig. 5d). The nucleus contained electronopaque chromatin covered with the fully developed acrosome. Only a few small vacuoles remained in the completely condensed chromatin. The tail was approximately 95–98 µm in length (Fig. 1q) and comprised the neck with the proximal centriole, the connecting piece, and the midpiece containing a sheath of mitochondria surrounding the outer dense fibers and the 9+2 microtubular doublets (Fig. 5d). In the principal piece, the fibrous sheath, instead of the mitochondrial sheath, covered the outer dense fibers and the axoneme, whereas the end piece had the same structure as the principal piece but lacked the fibrous sheath.

### Characterization of the basic nuclear proteins

### Profile of basic nuclear proteins

Basic nuclear proteins from the nuclei of the testicular cells of the tree shrew were separated in 15% AUT gel (Fig. 6, lane 3). Most bands, i.e., H2A, H3, H2B, H4, and H1, exhibited identical mobilities to those from chick erythrocyte nuclei (Fig. 6, lane 1) and human testicular nuclei (Fig. 6, lane 2), which were used as references. No equivalent band to chick-H5 was present. However, a band with high basicity was seen at the bottom of the gel with slightly slower mobility than human protamine (Fig. 6, lane 3), implying that the protamines of the tree shrew had a smaller amount of basic amino acids.

### Western blotting of histone H3 and protamine

When tree shrew basic nuclear proteins from the nuclei of testicular cells were blotted and probed with anti-chick-H3, only the H3 band exhibited positive immunoreactivity

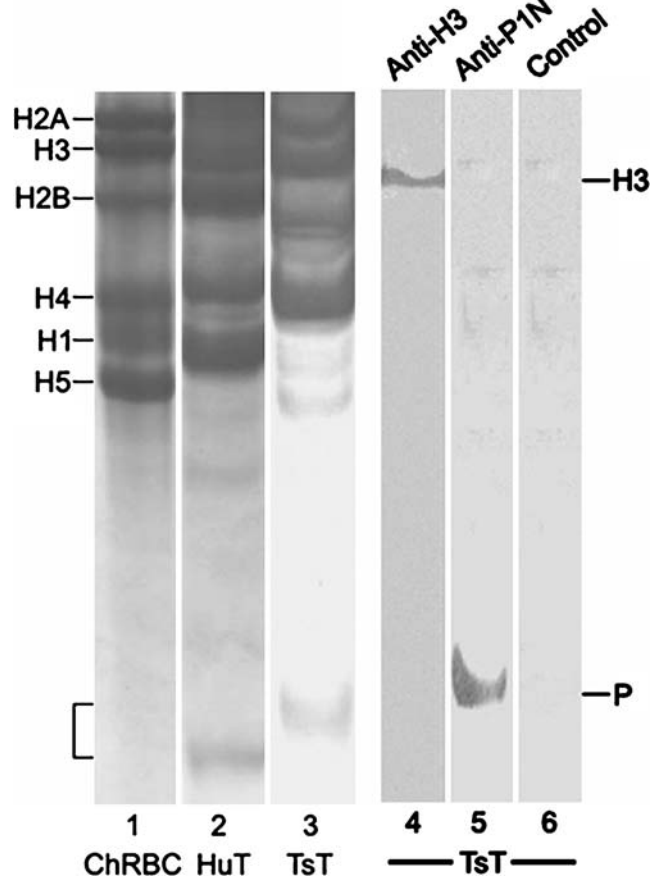


**Fig. 6** Acid-urea-Triton X-100 polyacrylamide gel electrophoresis (15%) of basic nuclear proteins: basic nuclear proteins extracted from chick erythrocyte nuclei (*ChRBC*, reference histones; *lane 1*), from human testis (*HuT*; *lane 2*), and *T. glis* testis (*TsT*; *lane 3*). *Lanes 4–6* Western blotting of extracted proteins from the tree shrew testis (*TsT*) probed with rabbit antiserum against chick H3 (*lane 4*) and mouse antiserum against human protamine P1N (*lane 5*). Strong reactions of the anti-H3 (*Anti-H3*) and anti-P1N (*Anti-P1N*) antibodies are detected at the *H3* and protamine (*P*) bands of the tree shrew testis, respectively. The negative control (*lane 6*) shows no immunoreactivity

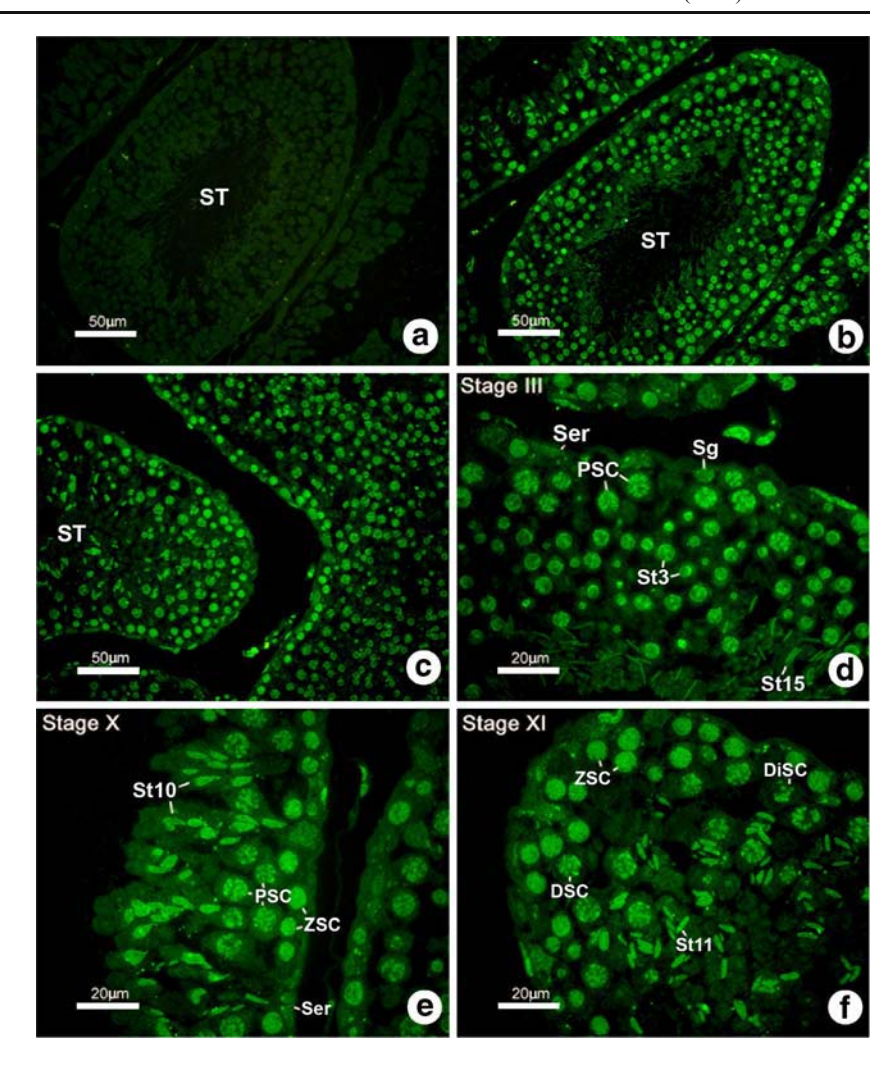
(Fig. 6, lane 4). The band at the bottom also showed positive immunoreactivity to the anti-human-protamine probe (Fig. 6, lane 5). In the negative control, no positive band was detected (Fig. 6, lane 6). These results indicated the presence of homologous basic nuclear proteins in human, chick, and tree shrew.

Immunofluorescence staining for histone-H3 and protamine in testicular cells

Immunostaining with the anti-H3 antiserum resulted in intense fluorescence in the nuclei of Sertoli cells and spermatogonia lining the basement membrane of the seminiferous tubules (Fig. 7b,c). Primary spermatocytes, especially those at the pachytene stage, also exhibited fluorescence in their nuclei (Fig. 7d–f). A uniformly intense immunofluorescence was present in the early round



Fig. 7 a-f Immunofluorescence images of T. glis seminiferous tubules (ST) stained with anti-H3 serum. a Negative control showing no immunoreactivity. b-f Immunoreactivity is found in all spermatogenic cells. Positive fluorescence decreases in the nuclei of mature spermatids (Ser Sertoli cell. Sg spermatogonia, ZSC zygotene spermatocyte, PSC pachytene spermatocyte, DSC diplotene spermatocyte, DiSC diakinetic spermatocyte, St spermatid, numbers steps)



spermatid nuclei (steps 1–5) and elongating spermatids (steps 6–14; Fig. 7e,f). In the late stages of spermatids (steps 15–16), anti-H3 immunofluorescence decreased (Fig. 7d) and almost disappeared in the last step of spermatids and mature spermatozoa. No immunofluorescence was found in the nuclei of any of the germ cells or Sertoli cells in the negative control (Fig. 7a).

When the anti-protamine antiserum was used for immunostaining, intense fluorescence was detected only in steps 12–16 of spermatids, whereas nuclei of all spermatogenic cells and early spermatids were not stained (Fig. 8b–f). In the negative control, no immunoreactivity was seen in the nuclei of any of the germ cells or somatic cells (Fig. 8a).

### Discussion

General histology of the testes of the common tree shrew

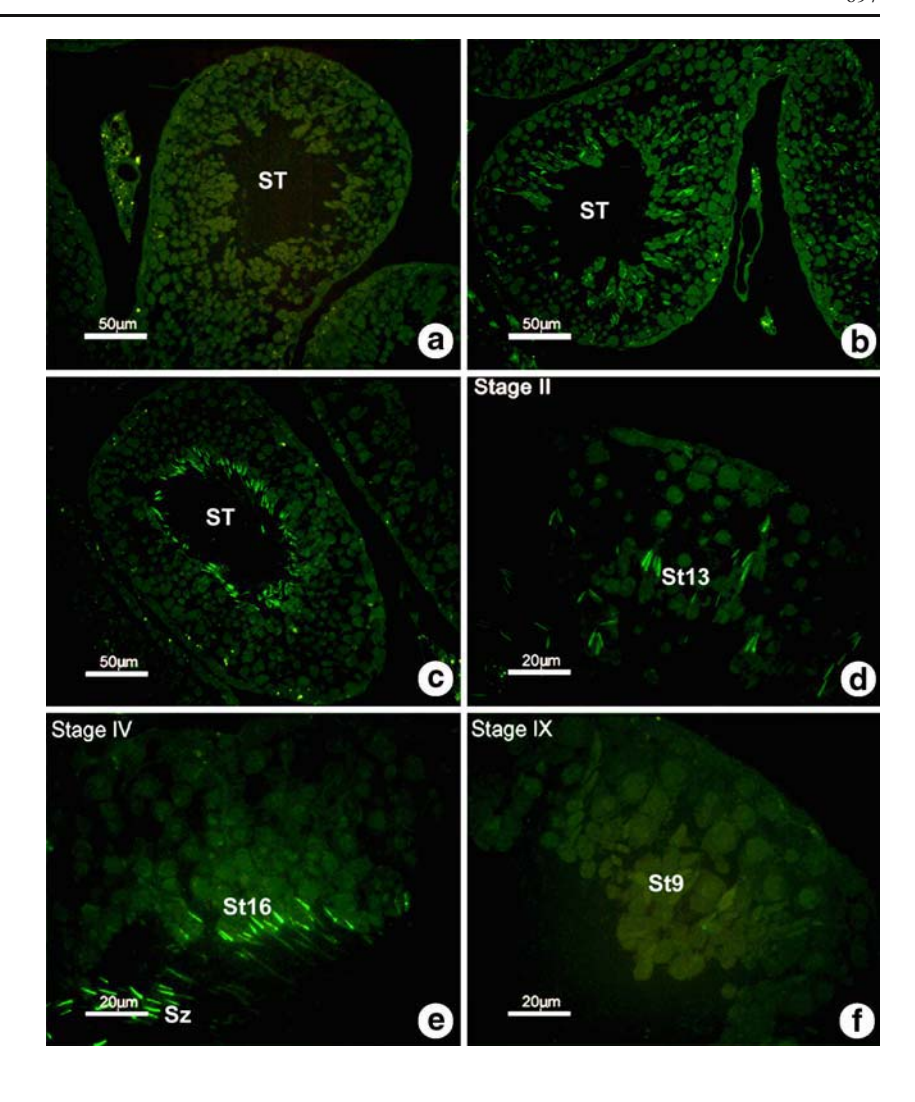
The testes of the tree shrew lie in a prepenial position, which differs from that of other primates whose testes are in

a postpenial position (Collins et al. 1982). The general histology of the tree shrew testes and stages of the cycle of seminiferous epithelium are similar to those described for other mammals (Kerr 1992). Each cross section of the seminiferous tubule shows only one stage of the cycle of seminiferous epithelium as found in the rat (Clermont 1972; Kerr 1992). However, the cycle is divided into 12 stages, whereas eight stages have been described in human (Clermont 1963), 14 stages in the rat (Leblond and Clermont 1952b), and 13 stages in the hamster (Mething 1998).

The process of spermiogenesis in the tree shrew is, in general, similar to that of other mammals (Clermont and Leblond 1955; Lalli and Clermont 1981). The four phases are based on acrosomal formation and the degree of chromatin condensation, i.e., Golgi, cap, acrosome, and maturation phases. The proacrosomal vesicles are synthesized and released from the Golgi complex in the Golgi phase spermatids and later fuse together to form a large acrosomal vesicle at the apical pole of the nucleus. Concurrent with the formation of the acrosomal vesicle,



Fig. 8 a-f Immunofluorescence staining in seminiferous tubules (ST) with the anti-protamine serum reveals intense immunoreactivities only in late spermatid steps (St spermatid, Sz spermatozoa, numbers steps). No immunoreactivity is observed in the negative control (a)



electron-dense materials inside the vesicle coalesce to form a large acrosomal granule, which is a characteristic of step 1 spermatids of the common tree shrew. The acrosomal vesicles then transform into a large cap that extends backward to cover the side of the nucleus; this characteristic is consistent with other mammalian sperm, including those of man, boar, and rabbit (Fawcett 1965). In the common tree shrew, early spermatids possess a small subacrosomal space, which lies between the inner acrosomal membrane and the outermost membrane of the nuclear envelope, as seen in the sperm of primates and human. In contrast, in rodents, a relatively large pyramidal subacrosomal space extends backward along the side of nucleus. This space contains perithecal materials that form a structure called the perforatorium (Lalli and Clermont 1981; Oko and Clermont 1990, 1991; Fornes and Bustos-Obregon 1994).

The nuclear chromatin in the spermatogonia and all spermatocytes of the common tree shrew exhibits fundamental fibers of 10 nm and 30 nm. Condensation into large heterochromatin blocks in these cellular stages is accom-

plished by the winding of the 30-nm fibers. This pattern of chromatin condensation appears to be universal in early germ cells of all mammalian species including the common tree shrew. In contrast, the patterns of chromatin organization and packaging during spermiogenesis are unique to each species (Chevaillier 1983). In T. glis, condensation starts by the transformation of the 10-nm and 30-nm fibers in the Golgi phase spermatid (steps 1) into the highly compact and knobby 50-nm to 60-nm fibers in the late Golgi phase (step 2). In the cap phase (steps 3-5), 10-nm and 30-nm fibers are still present, although most fibers have been transformed into higher ordered fibers of 40-45 nm and 50-60 nm, the larger knobby fibers being 70 nm (possibly transformed from the 50-nm to 60-nm fibers in earlier steps). The subsequent transformation of chromatin fibers continues in the early acrosome phase (steps 6-8) as is evident by both the presence of small 10-nm and 30-nm fibers and the increasing number of the larger sized 40-nm to 45-nm, 50-nm to 60-nm, and 70-nm fibers. Eventually, all chromatin appears in the form of the 40-nm to 45-nm, 50-nm to 60-nm, and 70-nm fibers in the mid acrosome



phase (steps 9-11). The 70-nm fibers might be transformed into the largest ordered fibers with a thickness about 80-100 nm in the late acrosome phase (steps 12-14). In addition, the condensation of the chromatin begins at the rim of the nuclear envelope and at the subacrosome region, later progressing toward the central part of the nucleus. In the maturation phase, especially the last two steps of spermatid development (steps 15-16), the highest ordered fibers (80-100 nm) become completely condensed and coalesce with each other, with only a few small vacuoles remaining in between them. These structures have also been observed in the nuclei of mature spermatozoa. The transformation from 30-nm to the multi-step, higher ordered, knobby fibers, which appear granulo-fibrillar in cross sections, is similar to that found in human spermatids in which toroids of 50-100 nm form after protamines replace histones in the 30-nm fibers (Brewer et al. 1999; Balhorn et al. 1999, 2000). These toroids are actually parts of the knobby fibers that become tightly packed in the maturation phase spermatids and spermatozoa (Holstein 1976). Whether the final higher order of chromatin in the spermatids and spermatozoa of the tree shew contain toroidal structures remains to be established.

Profiling and immunolocalization of the basic nuclear proteins

Analysis by AUT electrophoresis has shown that the histone-protamine compositions in the nuclei of the testicular cells of the tree shrew are similar to those of human (Prigent et al. 1996; Van Roijen et al. 1998) but probably with a smaller amount of protamines. Immunostaining with anti-H3 has revealed that H3 is present in the nuclei of spermatogonia, spermatocytes, most steps of spermatids, and Sertoli cells. Immunoblotting with antichick-H3 has detected immunoreactive H3 proteins in the tree shrew suggesting that H3, which is one of the nucleosomal core histones, is highly conserved. However, the amount of this histone, as reflected by the intensity of the fluorescence, decreases in the final steps of spermatids (steps 15–16) and almost completely disappears in spermatozoa. In contrast, immunostaining with anti-human protamine is intense in late spermatids and spermatozoa, whereas earlier stages of the germ cells are not stained. This result indicates the high degree of homology to human protamine; the presence of this protein in late stage spermatids and mature spermatozoa of the tree shrew is also similar to that reported in rat and human (Le Lannic et al. 1993; Kistler et al. 1996; Prigent et al. 1996; Steger 1999). Hence, in tree shrew, protamines are believed to be amongst the major nucleoproteins that play a role in the final condensation of chromatin in the nuclei from late spermatids to mature spermatozoa, as is the case in human and other mammals.

**Acknowledgements** We are grateful to Prof. Rod Balhorn, Lawrence Livermore National Laboratory, California, for kindly providing the monoclonal antibody against human-protamine, HuP1N fraction, and to Dr. Sirikul Manochantr, Thammasat University, Thailand, for providing the polyclonal antibody to chick-H3.

#### References

- Auger J, Dadoune JP (1993) Nuclear status of human sperm cells by transmission electron microscopy and image cytometry: changes in nuclear shape and chromatin texture during spermiogenesis and epididymal transit. Biol Reprod 49:166–175
- Ausio J (1999) Histone H1 and evolution of sperm nuclear basic proteins. J Biol Chem 274:31115–31118
- Balhorn R (1982) A model for the structure of chromatin in mammalian sperm. J Cell Biol 93:298–305
- Balhorn R, Cosman M, Thornton K, Krishnan VV, Corzett M, Bench G, Kramer C, Lee JD IV, Hud NV, Allen MJ, Prieto M, Meyer-Iese W, Brown JT, Kirz J, Zhang X, Bradbury EM, Maki G, Braun RE, Breed W (1999) Protamine mediated condensation of DNA in mammalian sperm. In: Gagnon C (ed) The male gamete: from basic science to clinical applications. Cache River, Vienna, pp 55–70
- Balhorn R, Brewer L, Corzett M (2000) DNA condensation by protamine and arginine-rich peptides: analysis of toroid stability using single DNA molecules. Mol Reprod Dev 56:230–234
- Bernstein MH, Teichman RJ (1972) Regional differentiation in the heads of spermatozoa of rabbit, man and bull. Am J Anat 133:165–178
- Brewer LR, Corzett M, Balhorn R (1999) Protamine-induced condensation and decondensation of the same DNA molecule. Science 286:120–123
- Calvin HI (1976) Comparative analysis of the nuclear basic proteins in rat, human, guinea pig, mouse and rabbit spermatozoa. Biochim Biophys Acta 434:377–389
- Calvin HI, Bedford JM (1971) Formation of disulfide bonds in the nucleus and accessory structures of mammalian spermatozoa during maturation in the epididymis. J Reprod Fertil 13:65–75
- Chevaillier P (1983) Some aspects of chromatin organization in sperm nuclei. In: Andre J (ed) The sperm cell: fertilizing power, surface properties, motility, nucleus and acrosome, evolutionary aspects. Nijhoff, London, pp 179–196
- Clermont Y (1963) The cycle of the seminiferous epithelium in man. Am J Anat 112:35–51
- Clermont Y (1972) Kinetics of spermatogenesis in mammals: seminiferous epithelium cycle and spermatogonial renewal. Physiol Rev 52:198–236
- Clermont Y, Leblond CP (1955) Spermiogenesis of man, monkey, ram and other mammals as shown by the periodic acid-Schiff technique. Am J Anat 96:229–253
- Collins PM, Thang WN, Lofts B (1982) Anatomy and function of the reproductive tract in the captive male tree shrew (*Tupaia belangeri*). Biol Reprod 26:169–182
- Dadoune JP, Alfonsi MF (1986) Ultrastructural and cytochemical changes of the head components of human spermatids and spermatozoa. Gamete Res 14:33–46
- De Kretser DM, Loveland KL, Meinhardt A, Simorangkir D, Wreford N (1998) Spermatogenesis. Hum Reprod 13:1–8
- Fawcett DW (1965) The anatomy of the mammalian spermatozoon with particular reference to the guinea pig. Z Zellforsch 67:279–296
- Fornes MW, Bustos-Obregon E (1994) Study of nuclear decondensation of the rat spermatozoa by reducing agents during epididymal transit. Andrologia 26:87–92



- Holstein AF (1976) Ultrastructural observations on the differentiation of spermatids in man. Andrologia 8:157–165
- Johnson L (1995) Efficiency of spermatogenesis. Microsc Res Tech 32:385–422
- Kerr JB (1992) Functional cytology of the human testis. Baillieres Clin Endocrinol Metab 6:235–250
- Kistler WS, Henriksen K, Mali P, Parvinen M (1996) Sequential expression of nucleoproteins during rat spermiogenesis. Exp Cell Res 225:374–381
- Lalli M, Clermont Y (1981) Structural changes of the head components on the rat spermatid during late spermiogenesis. Am J Anat 160:419–434
- Le Lannic G, Arkhis A, Vendrely E, Chevaillier P, Dadoune JP (1993) Production, characterization, and immunocytochemical applications of monoclonal antibodies to human sperm protamines. Mol Reprod Dev 36:106–112
- Leblond CP, Clermont Y (1952a) Spermiogenesis of rat, mouse, hamster and guinea pig as revealed by the "Periodic acid-Fuchsin sulfurous acid" technique. Am J Anat 90:167–206
- Leblond CP, Clermont Y (1952b) Definition of the stages of the cycle of seminiferous epithelium in the rat. Ann N Y Acad Sci 55:548–573
- Lombardi J (1998) Gamete and their reproduction. In: Lombardi J (ed) Comparative vertebrate reproduction. Kluwer Academic, London, pp 109–130
- Lowry OH, Rosebrough NJ, Farr AL, Randall RJ (1951) Protein measurement with the Folin phenol reagent. J Biol Chem 193:265–275
- Maeda S, Endo H, Kimura J, Rerkamnuaychoke W, Chungsamarnyart N, Yamada J, Kurohmarum, Hayashi Y, Nishida T (1996) Classification of the cycle of the seminiferous epithelium in the common tree shrew (*Tupaia glis*). J Vet Med Sci 58:481–484
- Martinage A, Arkhis A, Alimi E, Sautiere P, Chevaillier P (1990) Molecular characterization of nuclear basic protein HPI1, a putative precursor of human sperm protamines HP2 and HP3. Eur J Biochem 191:449–451
- Mething A (1998) The establishment of spermatogenesis in the seminiferous epithelium of the pubertal golden hamster (*Mesocricetus auratus*). Adv Anat Embryol Cell Biol 140:1–92
- Moneisi V (1971) Chromosome activities during meiosis and spermiogenesis. J Reprod Fertil 13:1–14
- Oko RJ, Clermont Y (1990) Mammalian spermatozoa: structure and assembly of the tail. In: Gagnon C (ed) Control of sperm mobility: biological and clinical aspects. CRC Press, Florida, pp 4–21

- Oko R, Clermont Y (1991) Origin and distribution of perforatorial proteins during spermatogenesis of the rat: an immunocytochemical study. Anat Rec 230:489–501
- Oko RJ, Jando V, Wagner CL, Kistler WS, Hermo LS (1996) Chromatin reorganization in rat spermatids during the disappearance of testis-specific histone, H1t, and the appearance of transition proteins TP1 and TP2. Biol Reprod 54:1141–1157
- Panyim S, Chalkley R (1969) High resolution acrylamide gel electrophoresis of histones. Arch Biochem Biophys 130:337
- Poonkhum R, Pongmayteegul S, Meeratana W, Pradidarcheep W, Thongpila S, Mingsakul T, Somana R (2000) Cerebral microvascular architecture in the common tree shrew (*Tupaia glis*) revealed by plastic corrosion casts. Microsc Res Tech 50:411– 418
- Prigent Y, Muller S, Dadoune JP (1996) Immunoelectron microscopical distribution of histones H2B and H3 and protamines during human spermiogenesis. Mol Hum Reprod 2:929–935
- Roux C, Gusse M, Chevaillier P, Dadoune JP (1988) An antiserum against protamines for immunohistochemical studies of histone to protamine transition during human spermiogenesis. J Reprod Fertil 82:35–42
- Steger K (1999) Transcriptional and translational regulation of gene expression in haploid spermatids. Anat Embryol (Berl) 199:471– 487
- Steger K, Klonisch T, Gavenis K, Drabent B, Doenecke D, Bergmann M (1998) Expression of mRNA and protein of nucleoproteins during human spermiogenesis. Mol Hum Reprod 4:939–945
- Suphamungmee W, Apisawetakan S, Weerachatyanukul W, Wanichanon C, Sretarugsa P, Poomtong T, Sobhon P (2005) Basic nuclear protein pattern and chromatin condensation in the male germ cells of a tropical abalone, *Haliotis asinina*. Mol Reprod Dev 70:211–221
- Tanphaichitr N, Sobhon P, Taluppeth N, Chalermisarachai P (1978) Basic nuclear proteins in testicular cells and ejaculated spermatozoa in man. Exp Cell Res 117:347–356
- Turner RM (2006) Moving to the beat: a review of mammalian sperm motility regulation. Reprod Fertil Dev 18:25–38
- Van Roijen JH, Ooms MP, Spaargaren MC, Baarends WM, Weber RFA, Grootegoed JA, Vreeburg JTM (1998) Immunoexpression of testis-specific histone2B in human spermatozoa and testis tissue. Hum Reprod 13:1559–1566
- Wanichanon C, Weerachatyanukul W, Suphamungmee W, Meepool A, Apisawetakan S, Linthong V, Sretarugsa P, Chavadej J, Sobhon P (2001) Chromatin condensation during spermiogenesis in rats. Sci Asia 27:211–220







GENERAL AND COMPARATIVE ENDOCRINOLOGY

General and Comparative Endocrinology 155 (2008) 613-622

www.elsevier.com/locate/ygcen

# The presence and distribution of gonadotropin-releasing hormone-liked factor in the central nervous system of the black tiger shrimp, *Penaeus monodon*

Piyada Ngernsoungnern <sup>a,b</sup>, Apichart Ngernsoungnern <sup>a,b</sup>, Scott Kavanaugh <sup>b</sup>, Prasert Sobhon <sup>a</sup>, Stacia A. Sower <sup>b</sup>, Prapee Sretarugsa <sup>a,\*</sup>

<sup>a</sup> Department of Anatomy, Faculty of Science, Mahidol University, Bangkok 10400, Thailand
<sup>b</sup> Department of Biochemistry and Molecular Biology, University of New Hampshire, Durham, NH 03824, USA

Received 4 April 2007; revised 5 July 2007; accepted 10 August 2007 Available online 26 August 2007

### **Abstract**

The distribution and presence of gonadotropin-releasing hormone (GnRH) in the central nervous system (CNS) of *Penaeus monodon* were examined by immunocytochemistry, high performance liquid chromatography (HPLC), and radioimmunoassay (RIA). We demonstrated the existence of octopus (oct)GnRH-liked immunoreactivity (ir-octGnRH) and lamprey (l)GnRH-III-liked immunoreactivity (ir-IGnRH-III) in cell bodies of medium-sized neurons of the anterior part (protocerebrum) of the supraesophageal ganglion (brain). In addition, only the ir-octGnRH was detected in the nerve fibers located in the brain and segmental ganglia (subesophageal, thoracic, and abdominal ganglia). Moreover, some branches of these fibers also innervated the neurons in the middle (deutrocerebrum), posterior (tritocerebrum) brain and segmental ganglia. There was no ir-IGnRH-I and ir-salmon (s)GnRH detected in the shrimp CNS. The results from HPLC and RIA showed ir-GnRH in the CNS using anti-IGnRH-III, but not with anti-mammalian (m)GnRH. The data from immunocytochemistry, HPLC and RIA suggest that ir-GnRH in shrimp may be more similar to octGnRH and IGnRH-III than the other forms. These findings support the hypothesis that GnRH-liked factor(s) may be an ancient peptide that also exists in this decapod crustacean.

© 2007 Elsevier Inc. All rights reserved.

Keywords: GnRH; Immunocytochemistry; Nervous system; Crustacean; Penaeus monodon

### 1. Introduction

GnRH is a well-known decapeptide that is a major mediator in the brain-pituitary-gonadal axis in vertebrates (Fernald and White, 1999; Morgan and Millar, 2004; Millar, 2005). Fourteen isoforms of GnRH have been reported in vertebrates and have been classified into three groups: GnRH1, 2, and 3 (Fernald and White, 1999; Tsai, 2006). Silver et al. (2004) proposed that there is the fourth group of vertebrate GnRH based on phylogenetic analysis, function, neuronal distribution, and developmental origin. In tetrapods, GnRH1 is synthesized in neurons of forebrain,

\* Corresponding author.

E-mail address: scpsr@mahidol.ac.th (P. Sretarugsa).

transported to median eminence, and finally released into hypothalamo-hypophyseal portal circulation to stimulate the release of gonadotropins, i.e., follicle stimulating hormone (FSH) and luteinizing hormone (LH) from the pituitary. GnRH2 is localized in the midbrain, and is speculated to serve as neurotransmitter/neuromodulator (Tsai, 2006). GnRH3 which is present in the telencephalon and the terminal nerves could be involved in sex-associated behaviors (Fernald and White, 1999). The lamprey GnRHs (IGnRH-I and -III) form the fourth group, GnRH4, which are both hypothalamic neurohormone and are derived from diencephalon/ventricular origin (Silver et al., 2004). In addition, GnRH is also detected in extra-pituitary tissues such as gonad, liver, kidney, placenta, breast, and prostate gland (González-Martínez et al., 2004).